Operator-Adapted Finite Element Wavelets: Theory and Applications to A Posteriori Error Estimation and Adaptive Computational Modeling

by

Raghunathan Sudarshan

Submitted to the Department of Civil and Environmental Engineering
in partial fulfillment of the requirements for the degree of

Doctor of Philosophy in the field of Computational Engineering

at the

MASSACHUSETTS INSTITUTE OF TECHNOLOGY

June 2005

Author .....
Department of Civil and Environmental Engineering
April 27, 2005

Certified by .....
Kevin S. Amaratunga
Associate Professor of Civil and Environmental Engineering
Thesis Supervisor

Accepted by .....
Andrew J. Whittle
Chairman, Department Committee for Graduate Students

Operator-Adapted Finite Element Wavelets: Theory and Applications to A Posteriori Error Estimation and Adaptive Computational Modeling

by

Raghunathan Sudarshan

Submitted to the Department of Civil and Environmental Engineering
on April 27, 2005, in partial fulfillment of the
requirements for the degree of
Doctor of Philosophy in the field of Computational Engineering

Abstract

We propose a simple and unified approach for *a posteriori* error estimation and adaptive mesh refinement in finite element analysis using multiresolution signal processing principles. Given a sequence of nested discretizations of a domain we begin by constructing approximation spaces at each level of discretization spanned by *conforming* finite element interpolation functions. The solution to the virtual work equation can then be expressed as a telescopic sum consisting of the solution on the coarsest mesh along with a sequence of error terms denoted as *two-level* errors. These error terms are the projections of the solution onto complementary spaces that are scale-orthogonal with respect to the inner product induced by the weak-form of the governing differential operator. The problem of generating a compact, yet accurate representation of the solution then reduces to that of generating a compact, yet accurate representation of each of these error components. This problem is solved in three steps: (a) we first efficiently construct a set of scale-orthogonal wavelets that form a Riesz stable basis (in the energy-norm) for the complementary spaces; (b) we then efficiently estimate the contribution of each wavelet to the two-level error and finally (c) we select a subset of the wavelets at each level to preserve and solve exactly for the corresponding coefficients.

Our approach has several advantages over *a posteriori* error estimation and adaptive refinement techniques in vogue in finite element analysis. First, in contrast to the true error, the two-level errors can be estimated very accurately even on coarse meshes. Second, mesh refinement is carried out by the addition of wavelets rather than element subdivision. This implies that the technique does not have to directly deal with the handling of irregular vertices. Third, the error estimation and adaptive refinement steps use the same basis. Therefore, the estimates accurately predict how much the error will reduce upon mesh refinement. Finally, the proposed approach naturally and easily accomodates error estimation and adaptive refinement based on both the energy norm as well any bounded linear functional of interest (i.e., goal-oriented error estimation and adaptivity).

We demonstrate the application of our approach to the adaptive solution of second and fourth-order problems such as heat transfer, linear elasticity and deformation of thin plates.

Thesis Supervisor: Kevin S. Amaratunga
Title: Associate Professor of Civil and Environmental Engineering

Für meine Eltern.

Acknowledgments

First and formost, I am very grateful to my advisor, Prof. K. Amaratunga for his help, encouragement and support throughout my stay at MIT. He also gave me the freedom to set and achieve my own targets and tempered my wildly ambitious and unrealistic goals with a healthy dose of pragmatism.

The distinguished members of my doctoral committee Prof. J. J. Connor and Prof. E. Kausel, successfully deciphered my hastily put together presentations full of obscure jargon and undefined terminology and offered valuable advice, guidance and feedback on my research. They also taught me all I know about dynamics of structures in general and that of ceramic coffee cups in particular :-)

Julio Castrillón-Candás, Stefan D'heedene and Thomas Grätsch graciously let me pick their brains, answered all my trivial questions and offered help and feedback on my research and writing. Mucho gracias, vele dank und danke schön für Alles :-)

My mother was a constant source of inspiration, courage and encouragement and goaded me along when the going was tough. My sisters, aunts, uncles, cousins, nephew, nieces and other family members showered me with their affection and words of encouragement.

I also owe my thanks to my long-suffering lab mates who bore the brunt of my eccentric behavior. Bharath, George, Ying-Jui, Scott and Sugata also offered valuable comments on my research and presentation. Joan McCusker constantly fussed over me and propped up my morale whenever it was low.

Finally, little of what I have accomplished would have been possible if not for that fateful year I spent under the tutelage of Prof. C. S. Krishnamoorthy at IIT Madras. To him I owe much gratitude and appreciation.

The material presented in this document is based on work supported by the National Science Foundation under Grant No. CCR 9984619. Any opinions, findings and conclusions or recomendations expressed in this material are those of the author(s) and do not necessarily reflect the views of the National Science Foundation (NSF).

Contents

List of Figures

List of Tables

Chapter 1

Wavelets in computational modeling

Think globally, act locally.
– Lloyd Trefethen, Spectral Methods in Matlab.

1.1 Chapter overview

In this introductory chapter, we provide a historical overview of the application of wavelets to the solution of partial differential and boundary integral equations. We then briefly define the goals and scope of our research and describe how it relates to (and differs from) the work of other researchers in the area. The final section of this chapter provides an overview of the contents of the rest of this document.

1.2 A bit of history

The basic principle behind multiresolution analysis is to decompose data sampled at a fine resolution into a low frequency component (the "average") that captures the global behavior of the signal and a set of high-frequency components (the "details") that capture local variations. In most cases of interest, multiresolution analyses possess the *perfect reconstruction* property [42]: on adding all the details to the coarse representation, one *exactly* recovers the original signal. The use of multiresolution techniques for the efficient representation of data stems from the fact that the detail coefficients are typically large

only near singularities in the signal such as such as edges (in the case of images) and shocks and transients (in the case of solutions to PDEs) and hence one can obtain a compact representation of the signal simply by preserving the subset of details that are large.

Although wavelets, filter banks and other concepts from multiresolution analysis have traditionally been the preserve of signal and image-processing applications, it is clear that their inherent hierarchical and adaptive nature also offers significant advantages in computational modeling. There have therefore been a number of efforts in recent years to harness the power of wavelets for the efficient solution of partial differential and boundary integral equations. For instance, Beylkin et al. [13] and Alpert et al. [3] proposed the use of compactly supported wavelet constructions such as those due to Daubechies [23] for the fast solution of first and second-kind boundary integral equations; Amaratunga et al. [6] developed several techniques based on the use of compactly supported wavelets for the efficient solution of one and two-dimensional boundary value problems. They also demonstrated the application of the adapted wavelet constructions of Dahlke and Weinreich [21] for the development of multilevel solvers of optimal storage and computational complexity [50] and proposed the *wavelet extrapolation* technique for the construction of orthogonal wavelets on bounded domains [5].

The primary disadvantage of many of the computational methods based on the use of classical wavelet constructions such as the orthogonal wavelet constructions due to Daubechies [23] or the biorthogonal constructions of Cohen et al. [19] is that these wavelets are invariant under translation and dilation. They are therefore best suited for the analysis of regularly-sampled one-dimensional signals or data which can be decomposed into a tensor product of several one-dimensional signals (such as images). Moreover, many of the classical wavelet basis functions used in signal processing applications do not have a closed-form representation and hence the accurate evaluation inner-products of these basis functions requires special tricks as described for instance in [34]. In summary therefore, the development of solution techniques for differential or integral equations over irregular discretizations of complex, bounded domains using the above-mentioned "first-generation" [45] wavelet constructions is an extremely challenging proposition.

Parallel to the advances in wavelet theory has been the development of *hierarchical ba-*

sis methods [46, 51, 52, 53] in finite element modeling. The basis functions in this framework span the same space of functions as traditional finite element interpolation functions (such as those described in Bathe [10]) except that they possess many desirable stability properties and have found several applications in finite element modeling, such as the development of fast iterative solvers [7, 8] and accurate *a posteriori* error estimators [9].

It may be shown (see Yserentant [51, 52]) that a hierarchical basis decomposition is an extremely elementary multiresolution analysis of the underlying Sobolev space of functions. In fact, hierarchical basis functions were termed by Sweldens as "lazy wavelets" [45] since they do not possess many of the desirable properties that characterize classical wavelet constructions such as vanishing polynomial moments or orthogonality. An advantage that they *do* possess however is that they can be constructed on complex geometries with relative ease and are piecewise polynomials and hence inner-products of hierarchical basis functions may be computed using simple quadrature rules.

It was shown recently that the dichotomy between wavelets possessing properties such as orthogonality and vanishing moments (but confined to regular, one-dimensional grids) and those that can be constructed on complex geometries (but without many desirable characteristics) can be bridged by the use of sophisticated construction techniques such as the *lifting scheme* of Sweldens [45], the *stable completion* technique of Carnicer, Dahmen and Peña [16] and their variations (such as the orthogonalization procedure of Lounsberry et al. [35] and the *wavelet-modified hierarchical basis* method of Vassilevski and Wang [48, 49]). These modern techniques have enabled the development of "second-generation" wavelets [45] that can be constructed on irregular discretizations, bounded intervals and over complex geometries but which at the same time are endowed with several desirable properties such as orthogonality, vanishing moments and regularity. The fundamental idea behind these methods is to start with a rudimentary multiresolution analysis (such as a hierarchical basis decomposition) and then *customize* the existing wavelets such that the resulting wavelets also form a valid multiresolution analysis and at the same time possess the properties desired.

In recent years second generation wavelets have found a multitude of applications in practical computational modeling. For example, Dahmen and collaborators (see for in-

stance the review by Dahmen [22] and references therein and Cohen, et al. [18]) have developed efficient techniques for the solution of partial differential and boundary integral equations using spline wavelets constructed on the unit interval. Similarly, the wavelet-modified hierarchical basis method of Vassilevski and Wang [48] has been used to develop fast iterative solvers for finite element systems. More recently, Amaratunga and Castrillón-Candás [4, 17] have developed sparsification techniques based on second-generation wavelets for boundary integral equations on complex geometries and D'Heedene et al. [25] have demonstrated the construction of operator-orthogonal wavelets using Lagrangian finite element interpolation functions for the case of second order operators in one and two dimensions.

1.3 Motivation and the big picture

With rapid increase in computing power it has become possible to solve large finite element problems with thousands or tens of thousands of unknowns in an extremely short period of time (of the order of a few minutes) even on inexpensive off-the-shelf workstations. One may therefore be tempted to conclude that adaptive techniques in practical finite element analysis may no longer be as relevant as they were a few years ago.

However, exactly the opposite is observed in practice: with enormous computational power at their disposal, finite element practitioners are now able to construct extremely large and highly accurate finite element models of physical systems with perhaps *millions* of unknowns. Even with so much computing power available, one is often very interested in getting the most "bang for the buck", i.e., how must one discretize the underlying mathematical model so that the resulting answer is most accurate for a given number of degrees of freedom? We believe that the only clear answer to this fundamental question is provided by the use of *efficient* and *accurate* error estimation and adaptive refinement techniques. It is further clear that the last word in this regard is yet to be written (see for example the concluding section of the review article by Grätsch and Bathe [33]). This is because *a posteriori* error estimators typically used in finite element analysis (such as the explicit, implicit and recovery-based estimators [1]) have several shortcomings; for example their accuracy often depends quite strongly on the quality of the initial mesh and the use of overly

coarse meshes can produce very misleading results. Moreover, many of the classical error estimation techniques were developed to estimate the error in the energy norm. Hence, these methods might not be ideally suited to more general problems, such as the problem of *goal-oriented* error estimation, where one interested in estimating the error in a given linear functional of the solution. Apart from the problem of estimating the error in a given mesh, techniques for adaptive mesh refinement used in contemporary finite element analysis themselves have several disadvantages. For example, adaptive mesh refinement based on the subdivision of elements leads to geometric artifacts known as irregular vertices that must be handled using procedures such as the imposition of multi-point constraints or green refinement [7]. These specialized techniques are typically formulated for a specific class of elements and can become extremely cumbersome to implement for several refinement levels and higher order interpolation functions such as those due to Bogner et al. [14]. We can therefore safely conclude that there is indeed a lot of scope for the development of efficient and reliable error estimation and adaptive refinement techniques that are, in addition, easy to implement and work across the board for a broad category of problems (including goal-oriented analysis) and finite element interpolation functions (i.e., not just piecewise linear Lagrangian finite elements). This, in essence, is the starting point of our investigations.

The primary message of this thesis is that adaptive finite element analysis is essentially a signal compression problem where the "signal" to be compressed is the solution to the underlying partial differential or boundary integral equation. The solution can then be decomposed using second-generation wavelets into a component on the coarsest level mesh (representing the average or global behavior) and a number of detail components (which are termed *two-level* errors and represent the local variations in the solution between two successive levels of refinement). The error estimation algorithm then computes efficient estimates of these two-level error components and the adaptive refinement process then constructs a compact representation of the same by retaining only those wavelets that contribute significantly to a given functional of interest.

There are several advantages to posing the problem of adaptive mesh refinement as a signal-compression problem as done above. For one, estimating the two-level error in a mesh is inherently much more accurate than estimating the true error (since the latter be-

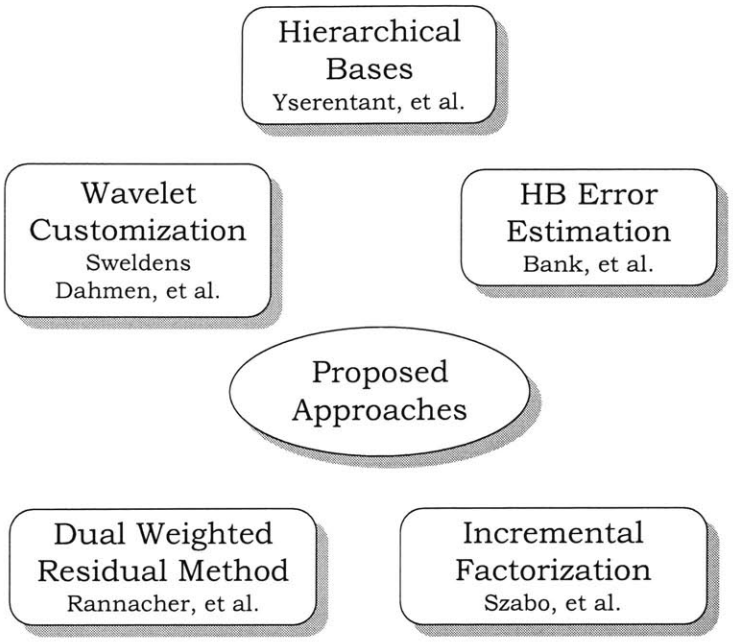

Figure 1-1: An overview of how our research relates to the work of other researchers.

longs to an infinite-dimensional Hilbert space and is hence very hard to estimate accurately on coarse meshes). Hence, the accuracy of our estimates does not depend to a large extent upon the resolution of the coarsest mesh. Further as we shall show in Chapter 6, the use of a scale-orthogonal basis that is also Riesz stable in the energy norm (as done in this investigation) provides a convenient, computationally efficient (and theoretically sound) framework for adaptive refinement. Finally, the mesh refinement process at each level itself involves the addition of a small subset of wavelet basis functions (this process is termed *space refinement* [18] in contrast to element refinement typically carried out in finite element practice) and does not have to explicitly handle hanging nodes.

The multiresolution error estimation and adaptive refinement techniques that we propose in this thesis do not stand isolated, but overlap with the work of a number of existing researchers in seeming disparate areas. A brief summary of this is provided in Figure 1-1 and further elaborated in the rest of the chapters of this thesis.

1.4 What lies ahead

In Chapter 2 we provide a brief overview of multiresolution analysis, wavelets and filter banks with particular emphasis on wavelets that are not scale and translation invariant and can hence be constructed with ease on complex geometries and bounded domains.

Chapter 3 focuses on the construction of a multiresolution analysis of a Sobolev space using finite element interpolation functions. While such constructions are well know for certain special cases (such as Lagrangian finite element shape functions [17]), we provide a condition that checks for the existence of a multiresolution analysis for the case of *general* finite element interpolation functions.

Chapter 4 introduces the *wavelet-Galerkin method*, which is the procedure for the solution of partial differential equations posed in terms of the virtual work equations. We discuss the structure of the stiffness matrices arising from this method and explain the significance behind coupling and quantify it in terms of the constants in the strengthened Cauchy-Schwarz inequality. Towards the end of this chapter, we make the case for the use of *scale-orthogonal* wavelets for the multilevel solution of linear partial differential equations.

In Chapter 5 we propose several techniques for the construction of scale-orthogonal wavelets from general finite element interpolation functions and characterize the stability propeties of the resulting scale-orthogonal wavelets. We also describe the trade-offs involved in the use of each of the proposed methods.

Chapter 6 presents our multiresolution (goal-oriented) error estimation and adaptive refinement method. As mentioned in the previous section, instead of estimating the true error at a certain level, our error-estimation procedure only determines an estimate for the two-level error in a mesh. The adaptive refinement algorithm then determines a compact representation for the two-level error by projecting the solution onto the that subspace of Riesz stable scale-orthogonal wavelets consisting only of basis functions that contribute significantly to a given quantity of interest. We also provide *a priori* error bounds that quantify the effect of several approximations made in the estimation and refinement steps.

In Chapter 7 we present several numerical experiments to validate the effectiveness of

our proposed error-estimation and adaptive refinement approach. The effectivity of the approach is measured using two quantities, the *compression ratio* and the *accuracy ratio* that illustrate the trade-off between the cost of computation and the accuracy of solution. The examples presented in the chapter are shown to have a low compression ratio (indicating fewer degrees of freedom vis-á-vis uniform refinement) and high accuracy ratio (indicating that the adaptive scheme converges at roughly the same rate as the uniform refinement scheme with increasing number of levels).

Finally, in Chapter 8 we conclude our presentation by summarizing the research proposed in this thesis and present several promising avenues for further research including the solution of problems such as two-field, non-linear and time-dependent problems.

Almost every chapter in this thesis begin follows the following model: The first section provides an overview of the contents of that chapter; the next few sections discuss the main material presented and the final section summarizes the key points laid out in the chapter.

Chapter 2

Multiresolution Analysis

"It is, of course, a trifle, but there is nothing so important as trifles."
– Sherlock Holmes in The Man with the Twisted Lip

2.1 Chapter overview

In this chapter, we describe some of the notational conventions used in the rest of this thesis. This will be followed by a brief exposition of the elements of multiresolution analysis and wavelet theory, where we derive the familiar expressions for the forward and inverse wavelet transforms in a simple fashion that differs from classical presentations such as in Strang and Nguyen [42]. In our derivations, we do not restrict ourselves to the traditional wavelet constructions based on scale and translation invariant wavelets; instead we focus our attention exclusively on the second-generation wavelet framework of Sweldens [45].

2.2 Notation

In this thesis, an expression of the form "$a \stackrel{\text{def}}{=} b$" must be interpreted as "a is defined as b". A *multi-index* is an n-tuple of non-negative integers, $\alpha = (\alpha_1, \alpha_2, \ldots, \alpha_n)$ with *magnitude*,

$$|\alpha| \stackrel{\text{def}}{=} \sum_{i=1}^{n} \alpha_i \tag{2.1}$$

For a smooth function $\phi : \mathbb{R}^n \rightarrow \mathbb{R}$, let

$$\partial^\alpha \phi(x) \stackrel{\text{def}}{=} \frac{\partial^{|\alpha|}\phi(x)}{\partial x_1^{\alpha_1} \cdots \partial x_n^{\alpha_n}} \tag{2.2}$$

Consider a subset Ω of $\mathbb{R}^n$ and let V be a Hilbert space on Ω. In particular we let V correspond to a subspace of the Sobolev space of functions $W^{s,2}(\Omega)$ $s \geq 0$ [15, 24], the space of functions with square-integrable derivatives of order s. Let $|\cdot|_t$, $t \leq s$ denote the Sobolev seminorm of order t, i.e., for any $v \in V$

$$|v|_t^2 \stackrel{\text{def}}{=} \int_\Omega \sum_{|\alpha|=t} (\partial^\alpha v)^2 \, \mathrm{d}\Omega \tag{2.3a}$$

and let $\|\cdot\|_t$ denote the corresponding Sobolev norm:

$$\|v\|_t^2 \stackrel{\text{def}}{=} \int_\Omega \sum_{|\alpha|\leq t} (\partial^\alpha v)^2 \, \mathrm{d}\Omega \tag{2.3b}$$

Finally, the norm on V, $\|\cdot\|$ will always refer to the Sobolev norm of order s.

Let the discretization of Ω at a certain level of resolution j be Ω_j. Let $\mathcal{K}(j) \subset \mathbb{N}$ be the index set of vertices or nodes in Ω_j such that $\mathcal{K}(j) \subset \mathcal{K}(j+1)$ and let
$\mathcal{M}(j) \stackrel{\text{def}}{=} \mathcal{K}(j+1) \setminus \mathcal{K}(j)$.

Letting N_j be the number of elements at level j, we define $\{S_{j,v}\}_{v=1}^{N_j}$ to be a dense collection of finite element partitions of Ω_j. The partitions are nested such that the ones are level $j+1$ are constructed by subdividing those at level j, cf. Figure 2-1.

Given a set of functions (resp. coefficients) $\{x_{j,k}\}$, we use x_j without the second index to denote a column vector of the set of functions (resp. coefficients). Given a function u_j expressed in terms of a basis ϕ_j as $u_j = \sum_k u_{j,k}^\mathsf{T} \phi_{j,k}$ we use the same symbol u_j to denote both the function as well as the vector of coefficients. This avoids a profusion of symbols and should not lead to confusion since the distinction between the function and the corresponding vector of coefficients is usually clear from the context.

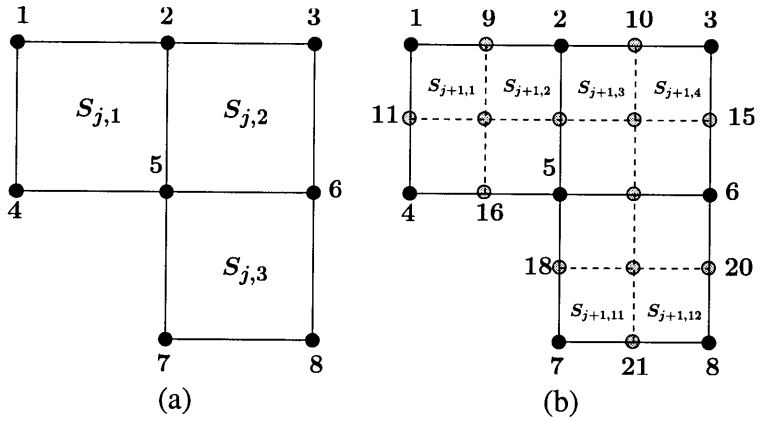

Figure 2-1: Multilevel discretization of a L-shaped domain. $\mathcal{K}(j) = \{1, 2, \ldots, 8\}$, $\mathcal{M}(j) = \{9, 10, \ldots, 21\}$, $\mathcal{K}(j+1) = \{1, 2, \ldots, 21\}$.

2.3 A Summary of Wavelet Theory

2.3.1 Multiresolution Analysis

We first consider a multiresolution analysis of V [16, 45, 42] consisting of

1. A ladder of nested approximation spaces $V_j \subset V$ such that

$$V_j \subset V_{j+1} \quad \text{and} \quad \text{clos} \bigcup_{j=0}^{\infty} V_j = V \tag{2.4a}$$

2. Complementary (wavelet) spaces $W_j \subset V$ such that

$$W_j \subset V_{j+1} \quad \text{and} \quad V_{j+1} = V_j \oplus W_j \tag{2.4b}$$

Eq (2.4a) and (2.4b) imply that each element in the finer approximation space V_{j+1} can be decomposed *uniquely* into an element lying in the coarser approximation space V_j and the corresponding details lying the in the complementary spaces W_j.

Let each approximation space V_j have a basis consisting of *scaling functions* $\varphi_{j,k}$ and each complementary space W_j have a basis consisting of *wavelets* $w_{j,m}$ such that

$$V_j = \text{clos span}\,\{\varphi_{j,k}\}_{k\in\mathcal{K}(j)} \tag{2.5a}$$

$$W_j = \text{clos span}\,\{w_{j,m}\}_{m\in\mathcal{M}(j)} \tag{2.5b}$$

From the nestedness relations Eqs (2.4a) and (2.4b) the scaling functions and wavelets can be seen to satisfy *refinement* and *wavelet* relations of the form

$$\varphi_{j,k} = \sum_{l\in\mathcal{K}(j+1)} h^0_{j,k,l}\,\varphi_{j+1,l} \quad (k \in \mathcal{K}(j)) \tag{2.6a}$$

$$w_{j,m} = \sum_{l\in\mathcal{K}(j+1)} h^1_{j,m,l}\,\varphi_{j+1,l} \quad (m \in \mathcal{M}(j)) \tag{2.6b}$$

where the coefficients h^0_j and h^1_j are referred to in wavelet literature [42] as the *primary low-pass* and *high-pass* filters respectively and in most cases of interest have only a small number of non-zero coefficients.

Note that the symbols $\varphi_{j,k}$ and $w_{j,m}$ may denote a vector of functions associated with a vertex in which case the filters h^0_j and h^1_j are matrices. Such basis functions are termed *multiscaling functions* and *multiwavelets* respectively [11, 30, 43].

Further, from the direct-sum decomposition property, Eq (2.4b) each scaling function φ_{j+1} can in turn be written in terms of scaling functions and wavelets at level j, or there exists an *unrefinement* equation of the form

$$\varphi_{j+1,l} = \sum_{k\in\mathcal{K}(j)} \left(\tilde{h}^0_{j,k,l}\right)^{\mathsf{T}} \varphi_{j,k} + \sum_{m\in\mathcal{M}(j)} \left(\tilde{h}^1_{j,k,l}\right)^{\mathsf{T}} w_{j,m} \tag{2.7}$$

where the coefficients $\tilde{h}^0_{j,k,l}$ and $\tilde{h}^1_{j,k,l}$ are referred to as the *dual low-pass* and *high-pass* filters respectively. Clearly, the primary and dual low-pass and high-pass filters are not completely independent of each other. For example, on substituting Eq (2.7) into Eqs

(2.6a) and (2.6b) and simplifying we obtain

$$\varphi_{j,k} = \sum_{\tilde{k}\in\mathcal{K}(j)} \sum_{l\in\mathcal{K}(j+1)} h^0_{j,k,l} \left(\tilde{h}^0_{j,\tilde{k},l}\right)^{\mathsf{T}} \varphi_{j,\tilde{k}} + \sum_{\tilde{m}\in\mathcal{M}(j)} \sum_{l\in\mathcal{K}(j+1)} h^0_{j,k,l} \left(\tilde{h}^1_{j,\tilde{m},l}\right)^{\mathsf{T}} w_{j,\tilde{m}} \quad (2.8a)$$

$$w_{j,m} = \sum_{\tilde{k}\in\mathcal{K}(j)} \sum_{l\in\mathcal{K}(j+1)} h^1_{j,m,l} \left(\tilde{h}^0_{j,\tilde{k},l}\right)^{\mathsf{T}} \varphi_{j,\tilde{k}} + \sum_{\tilde{m}\in\mathcal{M}(j)} \sum_{l\in\mathcal{K}(j+1)} h^1_{j,m,l} \left(\tilde{h}^1_{j,\tilde{m},l}\right)^{\mathsf{T}} w_{j,\tilde{m}} \quad (2.8b)$$

and hence the scaling functions and wavelets at each level are linearly independent if and only if the *biorthogonality* conditions [42]

$$\sum_{l\in\mathcal{K}(j+1)} h^0_{j,k,l} \left(\tilde{h}^0_{j,\tilde{k},l}\right)^{\mathsf{T}} = \delta_{k,\tilde{k}} \qquad \sum_{l\in\mathcal{K}(j+1)} h^0_{j,k,l} \left(\tilde{h}^1_{j,\tilde{m},l}\right)^{\mathsf{T}} = 0 \quad (2.9a)$$

$$\sum_{l\in\mathcal{K}(j+1)} h^1_{j,m,l} \left(\tilde{h}^0_{j,\tilde{k},l}\right)^{\mathsf{T}} = 0 \qquad \sum_{l\in\mathcal{K}(j+1)} h^1_{j,m,l} \left(\tilde{h}^1_{j,\tilde{m},l}\right)^{\mathsf{T}} = \delta_{m,\tilde{m}} \quad (2.9b)$$

are satisfied. Similarly, on substituting Eqs (2.6a) and (2.6b) into Eq (2.7), we obtain

$$\varphi_{j+1,l} = \sum_{\tilde{l}\in\mathcal{K}(j+1)} \left(\sum_{k\in\mathcal{K}(j)} \left(\tilde{h}^0_{j,\tilde{k},l}\right)^{\mathsf{T}} h^0_{j,k,l} + \sum_{m\in\mathcal{M}(j)} \left(\tilde{h}^1_{j,\tilde{m},l}\right)^{\mathsf{T}} h^1_{j,m,l} \right) \varphi_{j+1,\tilde{l}} \quad (2.10)$$

from which we obtain the *perfect reconstruction* conditions

$$\sum_{k\in\mathcal{K}(j)} \left(\tilde{h}^0_{j,\tilde{k},l}\right)^{\mathsf{T}} h^0_{j,k,l} + \sum_{m\in\mathcal{M}(j)} \left(\tilde{h}^1_{j,\tilde{m},l}\right)^{\mathsf{T}} h^1_{j,m,l} = \delta_{l,\tilde{l}} \quad (2.11)$$

which is clearly equivalent to Eqs (2.9a) and (2.9b), see Strang and Nguyen [42].

A multiresolution analysis (MRA) allows the representation of a function $f_{j+1} \in V_{j+1}$ in terms of its projection on a coarser approximation space along with multiple levels of

details, i.e.,

$$f_{j+1} = \sum_{l \in \mathcal{K}(j+1)} u_{j+1,l}^{\mathsf{T}} \varphi_{j+1,l} \tag{2.12a}$$

$$= \underbrace{\sum_{k \in \mathcal{K}(j)} u_{j,k}^{\mathsf{T}} \varphi_{j,k}}_{f_j} + \underbrace{\sum_{m \in \mathcal{M}(j)} r_{j,m}^{\mathsf{T}} w_{j,m}}_{g_j}$$

$$\vdots$$

$$= \underbrace{\sum_{k \in \mathcal{K}(0)} u_{0,k}^{\mathsf{T}} \varphi_{0,k}}_{f_0} + \sum_{i=0}^{j} \underbrace{\sum_{m \in \mathcal{M}(i)} r_{i,m}^{\mathsf{T}} w_{i,m}}_{g_i} \tag{2.12b}$$

where f_0 represents a coarse resolution version of f_{j+1} and g_i, $(i = 0, 1, \ldots, j)$ represent the details to be added to this coarse representation to arrive at the representation at level $j + 1$.

Using the unrefinement equation, Eq (2.7), and applying the linear independence of the scaling functions and wavelets at level j, we can express the approximation and detail coefficients at level j, resp. u_j and r_j in terms of the approximation coefficients at level $j + 1$, u_{j+1} as

$$u_{j,k} = \sum_{l \in \mathcal{K}(j+1)} \tilde{h}_{j,k,l}^{0} u_{j+1,l} \tag{2.13a}$$

$$r_{j,m} = \sum_{l \in \mathcal{K}(j+1)} \tilde{h}_{j,m,l}^{1} u_{j+1,l} \tag{2.13b}$$

Given the approximation coefficients u_j, one can recursively apply Eqs (2.13a) and (2.13b) to determine the approximation and wavelet coefficients at level $j - 1$ and so on. This is precisely the basis of the *pyramid decomposition algorithm* of Mallat [36, 42]. Conversely, given the approximation and detail coefficients at level j, we can reconstruct the approximation coefficients u_{j+1} using the refinement and wavelet equations Eqs (2.6a) and (2.6b) as:

$$u_{j+1,l} = \sum_{k \in \mathcal{K}(j)} \left(h_{j,k,l}^{0}\right)^{\mathsf{T}} u_{j,k} + \sum_{m \in \mathcal{M}(j)} \left(h_{j,m,l}^{1}\right)^{\mathsf{T}} r_{j,m} \tag{2.14}$$

It can be proved (see for instance, Strang and Nguyen [42] Section 7.1) that the detail coefficients in Eq (2.12a) are very small near regions where the solution is smooth and large in regions where the solution varies rapidly. We can therefore obtain a compact representation of the function by *adaptively* choosing the wavelets $w_{j,m}$ (or adding details) only near regions of rapid variation in the solution. Of course, when the function is known only indirectly via a governing PDE or BIE, one cannot resort to Eq (2.13b) to determine the details since the coefficients u_{j+1} at the final level are unknown. In Chapter 6 we discuss techniques by which the detail coefficients can be estimated in an efficient manner, based on which the wavelets to be retained can be determined.

2.4 Closure

In this chapter, we provided an overview of the most basic elements of multiresolution analysis. A major portion of this thesis will deal with the selection of the primary low and high-pass filters h_j^0 and h_j^1. As we shall see, the choice of the low-pass filters comes directly from the choice of the scaling functions, which in turn are assumed to be conforming finite element interpolation functions on nested discretizations. On the other hand, the filters h_j^1 will be constructed such that the wavelets span the space of orthogonal complements to the approximation spaces V_j with respect to the inner product induced by the weak-form of a differential operator.

Chapter 3

Construction of Scaling Functions

All truths are easy to understand once they are discovered; the point is to discover them.
– Galileo Galilei

3.1 Motivation and chapter overview

As mentioned in Chapter 1, this thesis concerns itself primarily with the development and application of wavelet-based multiresolution methods to the the fast solution of partial differential equations defined on general domains. One of the main reasons why multiresolution methods based on classical wavelet constructions such as those due to Daubechies [23] or Cohen, et al. [19] have not been widely used in adaptive computational modeling is that the basis functions in such constructions are normally constructed on regular, unbounded, one-dimensional grids. Therefore, in approximating solutions to differential equations defined on more general meshes, one must develop constructions such as wavelet-extrapolation [5] to handle bounded domains. Even so, many of these constructions become rather complicated on irregular meshes in higher dimensions. An additional disadvantage of the classical wavelets constructions is that many cases, the basis functions do not have a closed-form expression and are defined only recursively. Therefore, computing inner-products of these basis functions is not very straightforward and special techniques must be devised to evaluate inner-products accurately, see for example Latto, et

al. [34].

In contrast to classical wavelet basis functions, finite element interpolation functions have a number of advantages such as piecewise polynomial representation and ease of construction on complex geometries. Therefore, the two fundamental questions that need to be asked are (a) under what conditions is it possible to construct scaling functions (and hence wavelets) from finite element interpolation functions and (b) what is the corresponding refinement relation?

The main purpose of this chapter is to provide an answer for both the questions posed above; we first define the conditions under which scaling functions may be constructed from finite element interpolation functions and then go on to derive the refinement equation for such piecewise-polynomial interpolating scaling functions. We finally provide a number of examples for the construction of scaling functions from finite element interpolation functions.

It must be noted that while the construction of scaling functions and the derivation of the associated refinement equation is rather well-established in the existing literature for the case of Lagrange interpolating functions (see for instance Zienkiewicz, et al. [53] and Yserentant [51, 52] for piecewise linear interpolating functions and Castrillón-Candás and Amaratunga [17] for higher-order interpolating functions on unstructured grids), the conditions under which more general finite element interpolating functions (that interpolate displacements and rotations) give rise to scaling functions is not very well established except for a few simple cases [11, 43].

3.2 Scaling functions from finite element interpolation functions

Definition 3.1. Given a collection $\mathcal{D}$ of multi-indices representing nodal degrees of freedom, a set of functions $\left\{\phi^{\alpha}_{j,k}\right\}_{\alpha\in\mathcal{D},\ k\in\mathcal{K}(j)}$ is defined to be *$\mathcal{D}$-interpolating* if

$$\partial^{\beta}\phi^{\alpha}_{j,k}(x_{k'}) = \delta_{\alpha,\beta}\delta_{k,k'} \quad k,k' \in \mathcal{K}(j) \quad \text{and} \quad \alpha,\beta \in \mathcal{D}. \tag{3.1}$$

Let $\phi_{j,k} \stackrel{\text{def}}{=} \left\{\phi_{j,k}^{\alpha}\right\}_{\alpha\in\mathcal{D}}$ be the column vector of all $\mathcal{D}$-interpolating functions associated with a vertex $k \in \mathcal{K}(j)$. For example, in $\mathbb{R}^1$, the interpolation functions for truss and beam elements are $\mathcal{D}$-interpolating with $\mathcal{D} = \{0\}$ and $\mathcal{D} = \{0, 1\}$ respectively, see Figure 3-1.

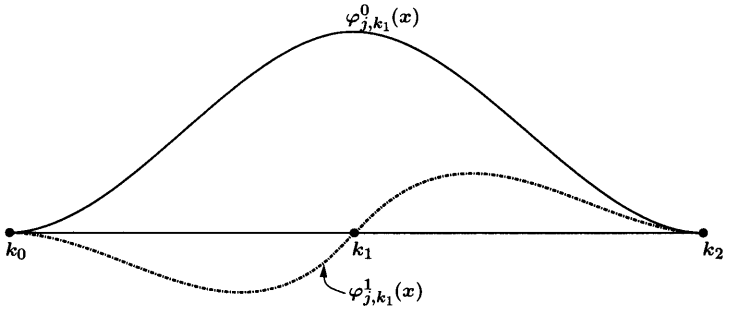

Figure 3-1: Illustration of Eq (3.1) in $\mathbb{R}^1$ for beam elements which have $\mathcal{D} = \{0, 1\}$

Let $\mathcal{P}_\kappa$, $\kappa \geq 0$ be some multi-index collection containing all multi-indices with magnitude less than or equal to κ. For example in $\mathbb{R}^2$, the multi-index collections $\{(0,0),(0,1),(1,0)\}$ and $\{(0,0),(1,0),(0,1),(1,1)\}$ are valid examples of $\mathcal{P}_1$ whereas $\{(0,0),(1,0),(0,1),(1,1),(2,0),(0,2)\}$ is a valid example of $\mathcal{P}_2$. Given such a multi-index collection, $\mathcal{P}_\kappa$, let

$$\mathcal{P}_{\kappa,j} \stackrel{\text{def}}{=} \left\{u : \Omega_j \to \mathbb{R} \text{ s.t. } u|_{S_{j,v}} \in \text{span}\{x_1^{\alpha_1} x_2^{\alpha_2} \cdots x_n^{\alpha_n}\}_{\alpha\in\mathcal{P}_\kappa}\right\} \tag{3.2}$$

denote piecewise polynomials at level j whose exact form is determined by $\mathcal{P}_\kappa$. Observe that since the mesh at a level $j+1$ is constructed by uniformly subdividing all the elements in the mesh at level j, we have,

$$\mathcal{P}_{\kappa,j} \subset \mathcal{P}_{\kappa,j+1} \tag{3.3}$$

Given a set of partitions $\{S_{j,v}\}_{v=1}^{N_j}$, suppose that the nodal degrees of freedom $\mathcal{D}$ and the polynomial set $\mathcal{P}_\kappa$ are chosen such that we have a unique set $\{\phi_{j,k}\}_{k\in\mathcal{K}(j)}$ of $\mathcal{D}$-interpolating polynomials in $\mathcal{P}_{\kappa,j}$. Further define $V_j \stackrel{\text{def}}{=} \text{span}\,\{\phi_{j,k}\}_{k\in\mathcal{K}(j)}$.

Now, if the approximation spaces, V_j, and the Hilbert space, V, are such that

$$V_j = \mathcal{P}_{\kappa,j} \cap V, \tag{3.4}$$

i.e., the $\mathcal{D}$-interpolating functions are *conforming*, then we have

$$\begin{aligned} V_j &= \mathcal{P}_{\kappa,j} \cap V \\ &\subset \mathcal{P}_{\kappa,j+1} \cap V \\ &= V_{j+1} \end{aligned} \tag{3.5}$$

or $V_j \subset V_{j+1}$. We can then simply choose the scaling functions $\{\varphi_{j,k}\}_{k\in\mathcal{K}(j)}$ to be the interpolating basis functions, $\{\phi_{j,k}\}_{k\in\mathcal{K}(j)}$ and can write a refinement equation as in Eq (2.6a). Moreover, the density condition, $\operatorname{clos} \bigcup_{j=0}^{\infty} V_j = V$ follows from standard *a priori* convergence arguments for conforming shape functions (see for example, Bathe [10] Section 4.3 or Brenner and Scott [15] Section 4.4).

Note that non-conforming interpolating basis functions such as the ones due to Melosh [37] do not lead to nested approximation spaces even though they may be constructed on nested meshes.

3.3 Refinement relation for interpolating scaling functions

If nestedness of the approximation spaces is established, we can express the scaling functions at level j in terms of the scaling functions at level $j+1$ as:

$$\varphi_{j,k} = \sum_{l\in\mathcal{K}(j+1)} h_{j,k,l}\, \varphi_{j+1,l} \tag{3.6}$$

Since the scaling functions at each level are compactly supported and $\mathcal{D}$-interpolating, we have

$$h_{j,k,l}^{\alpha,\beta} = \partial^\beta \varphi_{j,k}^\alpha(x_l) = \begin{cases} \delta_{\alpha,\beta}\delta_{k,l} & l \in \mathcal{K}(j) \\ \partial^\beta \varphi_{j,k}^\alpha(x_l) & l \in n(j,k) \stackrel{\text{def}}{=} \{m \in \mathcal{M}(j) \text{ s.t. } x_m \in \operatorname{supp}(\varphi_{j,k})\} \\ 0 & \text{otherwise} \end{cases} \tag{3.7}$$

and therefore the refinement relation for $\mathcal{D}$-interpolating scaling functions can be simplified as

$$\varphi_{j,k} = \varphi_{j+1,k} + \sum_{m \in n(j,k)} h_{j,k,m}\, \varphi_{j+1,m} \tag{3.8}$$

Observe that for the case of Lagrange interpolating functions, the filters $h_{j,k,m}$ turn out to be scalars rather than matrices and correspond exactly to the filters derived by Castrillón-Candás and Amaratunga [17] using interpolating subdivision arguments. Moreover, observe that for higher-order basis functions, the filters are natural generalizations of those derived for regular, one dimensional grids by Strela and Strang [43] and Beam and Warming [11].

3.4 Examples of interpolating scaling functions

In this section, we give a few examples of finite element interpolation functions that satisfy a refinement relation of the form given in Eq (3.8). Even though the refinement relation is valid for non-uniform meshes, we assume a uniform discretization in the examples to keep the expressions for the filters simple.

3.4.1 Refinement for discontinuous piecewise linear basis functions

We first consider the refinement relation for the case of discontinuous, piecewise polynomial interpolation functions that are used, for instance, in discontinuous Galerkin methods. These functions are in fact a generalization of the Haar basis functions [42, 45] commonly used in wavelet applications and can be used to generate a MRA of $L^2(\Omega)$. Defining the two discontinuous segments of a basis function at a vertex $k \in \mathcal{K}(j)$ as $\varphi^{\mathrm{L}}_{j,k}$ and $\varphi^{\mathrm{R}}_{j,k}$ we can write the refinement equation for the basis function φ_{j,k_1} shown in Figure 3-2 as

$$\begin{bmatrix} \varphi^{\mathrm{L}}_{j,k_1} \\ \varphi^{\mathrm{R}}_{j,k_1} \end{bmatrix} = \begin{bmatrix} \varphi^{\mathrm{L}}_{j+1,k_1} \\ \varphi^{\mathrm{R}}_{j+1,k_1} \end{bmatrix} + \begin{bmatrix} \frac{1}{2} & \frac{1}{2} \\ 0 & 0 \end{bmatrix} \begin{bmatrix} \varphi^{\mathrm{L}}_{j+1,m_0} \\ \varphi^{\mathrm{R}}_{j+1,m_0} \end{bmatrix} + \begin{bmatrix} 0 & 0 \\ \frac{1}{2} & \frac{1}{2} \end{bmatrix} \begin{bmatrix} \varphi^{\mathrm{L}}_{j+1,m_1} \\ \varphi^{\mathrm{R}}_{j+1,m_1} \end{bmatrix} \tag{3.9a}$$

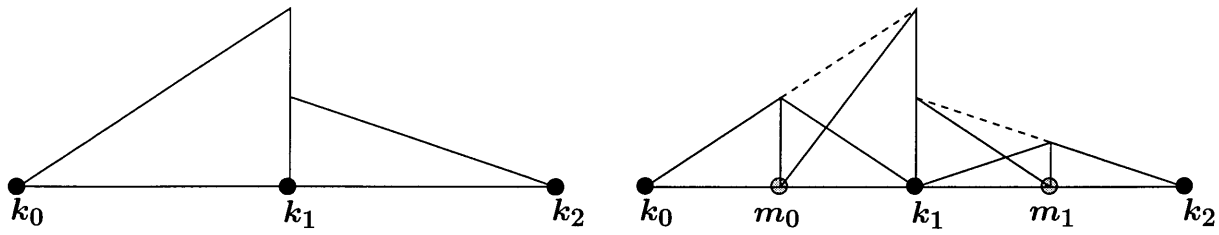

Figure 3-2: Refinement relation for discontiuous piecewise-linear interpolation functions

or, by grouping the two discontinuous segments into a column vector,

$$\varphi_{j,k_1} = \varphi_{j+1,k_1} + \begin{bmatrix} \frac{1}{2} & \frac{1}{2} \\ 0 & 0 \end{bmatrix} \varphi_{j+1,m_0} + \begin{bmatrix} 0 & 0 \\ \frac{1}{2} & \frac{1}{2} \end{bmatrix} \varphi_{j+1,m_1} \tag{3.9b}$$

3.4.2 Lagrange interpolating functions in $\mathbb{R}^1$

Figures 3-3 and 3-4 respectively illustrate the refinement relations for one-dimensional piecewise linear and quadratic finite element interpolation functions.

For the piecewise linear case, the refinement relation for the interpolating function at node k_0 in Figure 3-3 can be written as:

$$\varphi_{j,k_0} = \varphi_{j+1,k_0} + \frac{1}{2} \left(\varphi_{j+1,m_0} + \varphi_{j+1,m_1}\right) \tag{3.10}$$

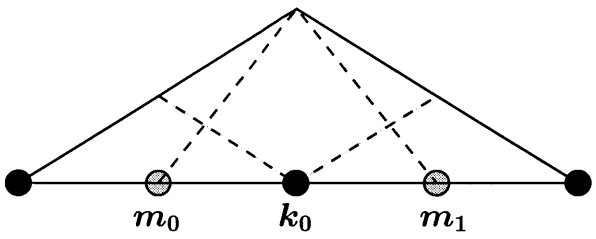

Figure 3-3: Refinement relation for piecewise-linear interpolating function

For the piecewise quadratic case, there are two types of basis functions (denoted in [17] as φ_j^{odd} and φ_j^{even}), with supports spanning one and two elements respectively. The corresponding refinement equations can be written as:

$$\varphi_{j,k_1} = \varphi_{j+1,k_1} + \frac{3}{4}\left(\varphi_{j+1,m_0} + \varphi_{j+1,m_1}\right) \tag{3.11}$$

$$\varphi_{j,k_2} = \varphi_{j+1,k_2} - \frac{1}{8}\left(\varphi_{j+1,m_0} + \varphi_{j+1,m_3}\right) + \frac{3}{8}\left(\varphi_{j+1,m_1} + \varphi_{j+1,m_2}\right) \tag{3.12}$$

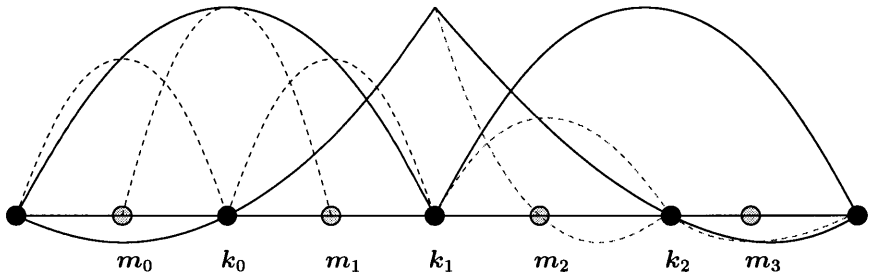

Figure 3-4: Illustration of the refinement relation for piecewise-quadratic interpolating function

3.4.3 Piecewise cubic Hermite interpolating functions in $\mathbb{R}^1$

Figure 3-5 illustrates the refinement relation for the interpolation functions for the beam element. The corresponding refinement relation, assuming a mesh width at level j to be h can be written as:

$$\varphi_{j,k_2} = \varphi_{j+1,k_2} + \begin{bmatrix} \frac{1}{2} & \frac{h}{8} \\ -\frac{3}{2h} & -\frac{1}{4} \end{bmatrix} \varphi_{j+1,m_1} + \begin{bmatrix} \frac{1}{2} & -\frac{h}{8} \\ \frac{3}{2h} & -\frac{1}{4} \end{bmatrix} \varphi_{j+1,m_2} \tag{3.13}$$

Note that for the uniform refinement case considered here, Eq (3.13) corresponds exactly to the refinement relations derived by Strela and Strang [43] and Beam and Warming [11].

3.4.4 Piecewise bilinear Lagrange interpolating functions in $\mathbb{R}^2$

Figure 3-6 illustrates the support of the bilinear scaling function, φ_{j,k_0} and also indicates the vertices in the set $n(j,k_0)$, see Eq (3.7). The refinement relation can be written as:

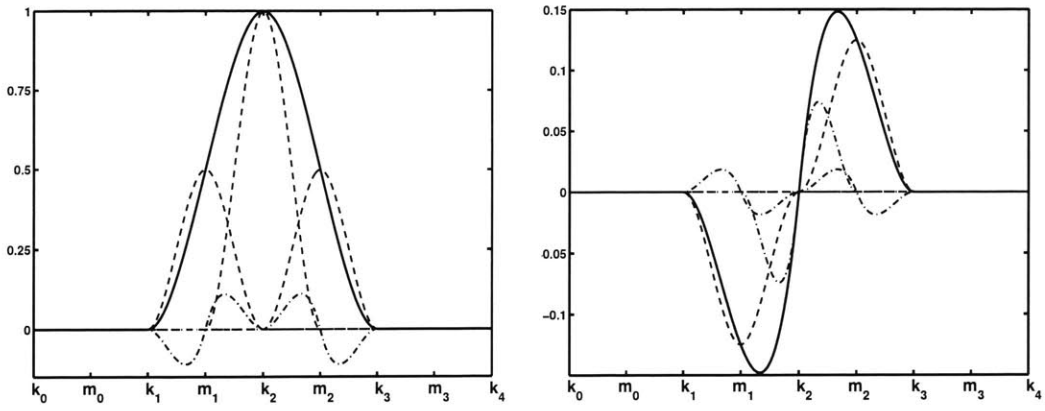

Figure 3-5: Illustration of the refinement relation for piecewise cubic Hermite interpolating scaling functions

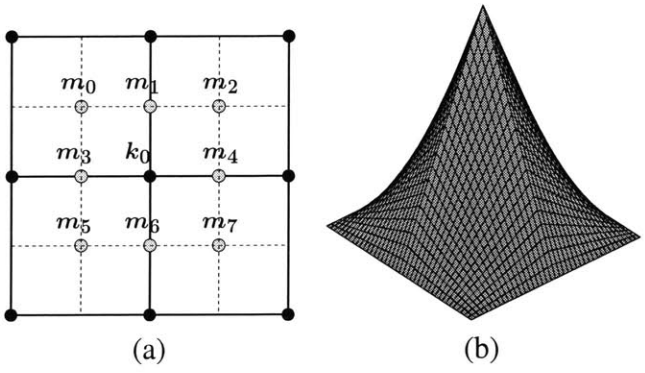

Figure 3-6: (a) Piecewise bilinear Lagrange interpolating scaling function at node k_0 (a) The refinement set $n(j, k_0)$ and (b) φ_{j,k_0}

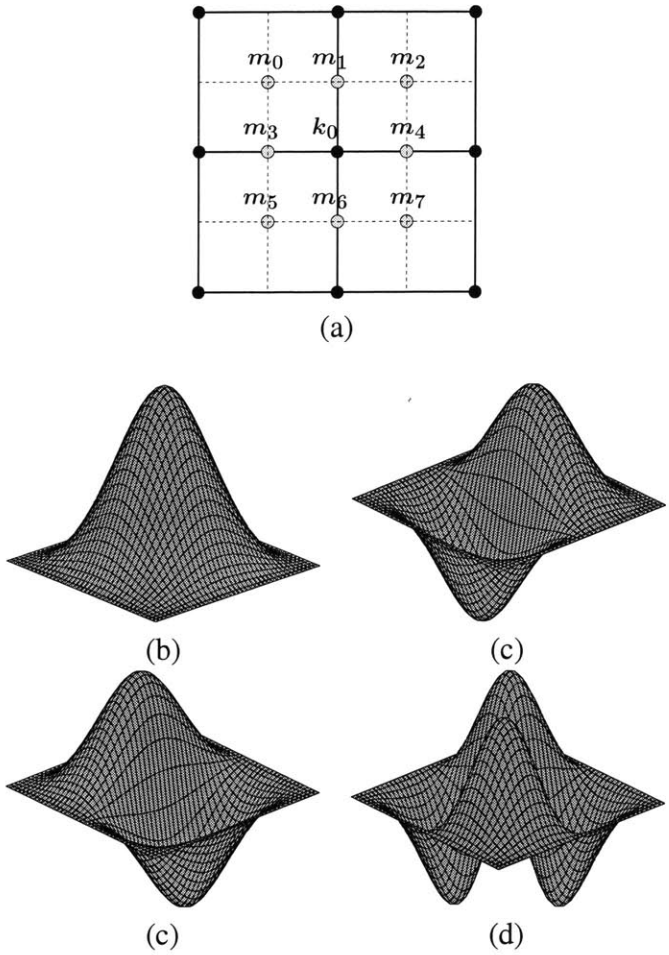

Figure 3-7: Bogner-Fox-Schmit scaling functions at node k_0: (a) The refinement set $n(j, k_0)$; (b) $\varphi_{j,k_0}^{(0,0)}$; (c) $\varphi_{j,k_0}^{(1,0)}$; (d) $\varphi_{j,k_0}^{(0,1)}$ and (e) $\varphi_{j,k_0}^{(1,1)}$

$$\varphi_{j,k_0} = \varphi_{j+1,k_0} + \frac{1}{2}\left(\varphi_{j+1,m_1} + \varphi_{j+1,m_3} + \varphi_{j+1,m_4} + \varphi_{j+1,m_6}\right) + \frac{1}{4}\left(\varphi_{j+1,m_0} + \varphi_{j+1,m_2} + \varphi_{j+1,m_5} + \varphi_{j+1,m_7}\right) \tag{3.14}$$

3.4.5 Piecewise bicubic Bogner-Fox-Schmidt interpolating functions in $\mathbb{R}^2$

Finally, in Figure 3-7 we illustrate the four piecewise bi-cubic Bogner-Fox-Schmidt interpolation functions [14] at vertex k_0 over a square grid along with the refinement set $n(j, k_0)$.

Recall that the Bogner-Fox-Schmidt elements have four degrees of freedom at each vertex corresponding to $\mathcal{D} = \{(0,0),(1,0),(0,1),(1,1)\}$. The filters for the refinement equations corresponding to the newly introduced vertices at the element faces are given as:

$$h_{j,k_0,m_1} = \begin{bmatrix} 1/2 & 0 & -3/2\,h & 0 \\ 0 & 1/2 & 0 & -3/2\,h \\ 1/8\,h^{-1} & 0 & -1/4 & 0 \\ 0 & 1/8\,h^{-1} & 0 & -1/4 \end{bmatrix} \tag{3.15a}$$

$$h_{j,k_0,m_3} = \begin{bmatrix} 1/2 & 3/2\,h & 0 & 0 \\ -1/8\,h^{-1} & -1/4 & 0 & 0 \\ 0 & 0 & 1/2 & 3/2\,h \\ 0 & 0 & -1/8\,h^{-1} & -1/4 \end{bmatrix} \tag{3.15b}$$

$$h_{j,k_0,m_4} = \begin{bmatrix} 1/2 & -3/2\,h & 0 & 0 \\ 1/8\,h^{-1} & -1/4 & 0 & 0 \\ 0 & 0 & 1/2 & -3/2\,h \\ 0 & 0 & 1/8\,h^{-1} & -1/4 \end{bmatrix} \tag{3.15c}$$

$$h_{j,k_0,m_6} = \begin{bmatrix} 1/2 & 0 & 3/2\,h & 0 \\ 0 & 1/2 & 0 & 3/2\,h \\ -1/8\,h^{-1} & 0 & -1/4 & 0 \\ 0 & -1/8\,h^{-1} & 0 & -1/4 \end{bmatrix} \tag{3.15d}$$

and the filters corresponding to newly introduced vertices at the edges are given as:

$$h_{j,k_0,m_0} = \begin{bmatrix} 1/4 & 3/4\,h & -3/4\,h & -9/4\,h^2 \\ -1/16\,h^{-1} & -1/8 & 3/16 & 3/8\,h \\ 1/16\,h^{-1} & 3/16 & -1/8 & -3/8\,h \\ -\frac{1}{64}\,h^{-2} & -1/32\,h^{-1} & 1/32\,h^{-1} & 1/16 \end{bmatrix} \tag{3.15e}$$

$$h_{j,k_0,m_2} = \begin{bmatrix} 1/4 & -3/4\,h & -3/4\,h & 9/4\,h^2 \\ 1/16\,h^{-1} & -1/8 & -3/16 & 3/8\,h \\ 1/16\,h^{-1} & -3/16 & -1/8 & 3/8\,h \\ \frac{1}{64}\,h^{-2} & -1/32\,h^{-1} & -1/32\,h^{-1} & 1/16 \end{bmatrix} \tag{3.15f}$$

$$h_{j,k_0,m_5} = \begin{bmatrix} 1/4 & 3/4\,h & 3/4\,h & 9/4\,h^2 \\ -1/16\,h^{-1} & -1/8 & -3/16 & -3/8\,h \\ -1/16\,h^{-1} & -3/16 & -1/8 & -3/8\,h \\ \frac{1}{64}\,h^{-2} & 1/32\,h^{-1} & 1/32\,h^{-1} & 1/16 \end{bmatrix} \tag{3.15g}$$

$$h_{j,k_0,m_7} = \begin{bmatrix} 1/4 & -3/4\,h & 3/4\,h & -9/4\,h^2 \\ 1/16\,h^{-1} & -1/8 & 3/16 & -3/8\,h \\ -1/16\,h^{-1} & 3/16 & -1/8 & 3/8\,h \\ -\frac{1}{64}\,h^{-2} & 1/32\,h^{-1} & -1/32\,h^{-1} & 1/16 \end{bmatrix} \tag{3.15h}$$

3.5 Closure

In this chapter we summarized the conditions under which general finite element interpolation functions give rise to nested approximation spaces, Eq (3.4) and derived the refinement relation for scaling functions constructed out of such interpolating functions, Eq (3.8). While we considered only square meshes for simplicity, we must emphasize the fact that Eq (3.8) is valid even on unstructured meshes as long as the set of finite element interpolation functions satisfy the conditions given by Eq (3.4).

Chapter 4

The Wavelet-Galerkin Method

Ut Tensio, Sic Vis.
– Robert Hooke

4.1 Chapter overview

In this chapter we discuss the approximation of solutions to linear partial differential equations posed in terms of the corresponding virtual-work equations using wavelet basis functions. This technique is often referred to in literature as the *wavelet-Galerkin* method [5, 6].

One of the main goals of this chapter is to rigorously quantify the role of the *interaction* or *coupling* matrices that contain inner-products of basis functions at different resolutions using the strengthened Cauchy-Schwarz inequality [51]. We illustrate how the norms of these matrices directly influence the extent of coupling errors produced on mesh refinement. To keep the discussion as general as possible, we do not specify *a priori* the choice of wavelet basis functions; instead in the final section of this chapter, we discuss the motivation for constructing the wavelet spaces, W_j such that the interaction matrices at each level are identically zero.

4.2 Problem definition

Let $a : V \times V \rightarrow \mathbb{R}$ be a symmetric bilinear form on V satisfying the continuity and coercivity conditions [10, 15, 24]:

$$\begin{array}{lllll} \text{(continuity)} & \exists \alpha \text{ s.t.} & |a(v,w)| & \leq & \alpha \|v\| \|w\| \quad (v,w \in V) \\ \text{(coercivity)} & \exists M \text{ s.t.} & a(v,v) & \geq & M \|v\|^2 \quad (v \in V) \end{array} \tag{4.1}$$

We can therefore define the *energy norm* of a vector $v \in V$, denoted as $\|v\|_{\mathrm{E}}$ as:

$$\|v\|_{\mathrm{E}}^2 = a(v,v) \tag{4.2}$$

which, from Eq (4.1), is equivalent to the (Sobolev) norm on V.

If $l : V \rightarrow \mathbb{R}$ is a bounded linear functional on V, i.e.,

$$\exists K \geq 0 \text{ s.t. } |l(v)| \leq K \|v\| \quad (v \in V) \tag{4.3}$$

then by the Lax-Milgram Lemma [15, 24] there exists a unique solution, $u \in V$, to the primal problem:

$$a(u,v) = l(v) \quad (v \in V) \tag{4.4}$$

Moreover, by the symmetry and coercivity of $a(\cdot,\cdot)$ we have [10, 15]:

$$u = \arg\min_{w \in V} \frac{1}{2} a(w,w) - l(w) \tag{4.5}$$

4.3 The wavelet-Galerkin method

We consider the projection u_j of the solution u onto the space V_j satisfying the virtual work equation:

$$a(u_j, v_j) = l(v_j) \quad (v_j \in V_j) \tag{4.6}$$

or equivalently,

$$u_j = \arg\min_{v_j \in V_j} \|u - v_j\|_{\mathrm{E}} \tag{4.7}$$

From Eq (4.4) and Eq (4.6) we have that the solution error $u - u_j$ satisfies the Galerkin orthogonality condition:

$$a\left(u - u_j, v_j\right) = 0 \quad \left(v_j \in V_j\right) \tag{4.8}$$

and from the continuity and coercivity conditions, Eq (4.1) we have:

$$\|u - u_j\| \leq \sqrt{\frac{\alpha}{M}} \inf_{v_j \in V_j} \|u - v_j\| \tag{4.9}$$

Recall that Cea's Lemma, Eq (4.9) is one of the key results for establishing the *a priori* convergence rate of the Galerkin finite element method based on results from interpolation theory [10, 15, 41].

On expanding u_j and v_j in terms of only the scaling functions (i.e., the finite element interpolation functions) at level j, we arrive at the system of equations corresponding to a nodal finite element discretization at level j:

$$\mathbf{K}_j \, u_j = f_j \tag{4.10}$$

where $\mathbf{K}_j = a\left(\varphi_j, \varphi_j^{\mathsf{T}}\right)$ is the nodal finite element stiffness matrix. On the other hand, on expanding u_j and v_j in terms of the scaling functions at level 0 and wavelets at levels $0, 1, \ldots, j-1$, we arrive at a *multilevel* system of equations:

$$\hat{\mathbf{K}}_j \hat{u}_j = \hat{f}_j \tag{4.11}$$

where the multilevel stiffness matrix $\hat{\mathbf{K}}_j$ is composed of block matrices of the form:

$$\hat{\mathbf{K}}_j = \begin{bmatrix} \mathbf{K}_0 & \mathbf{B}_{0,1} & \cdots & \mathbf{B}_{0,j} \\ \mathbf{B}_{0,1}^{\mathsf{T}} & \mathbf{C}_1 & \cdots & \mathbf{B}_{1,j} \\ \vdots & \vdots & \ddots & \vdots \\ \mathbf{B}_{0,j}^{\mathsf{T}} & \mathbf{B}_{1,j}^{\mathsf{T}} & \cdots & \mathbf{C}_j \end{bmatrix} \tag{4.12}$$

where $\mathbf{K}_0 = a\left(\varphi_0, \varphi_0^{\mathsf{T}}\right)$ is simply the nodal finite element stiffness matrix at level 0, $\mathbf{B}_{0,i} = a\left(\varphi_0, w_{i-1}^{\mathsf{T}}\right)$, $1 \leq i \leq j$ and $\mathbf{B}_{i,k} = a\left(w_{i-1}, w_{k-1}^{\mathsf{T}}\right)$, $1 \leq i < k \leq j$ are referred to as

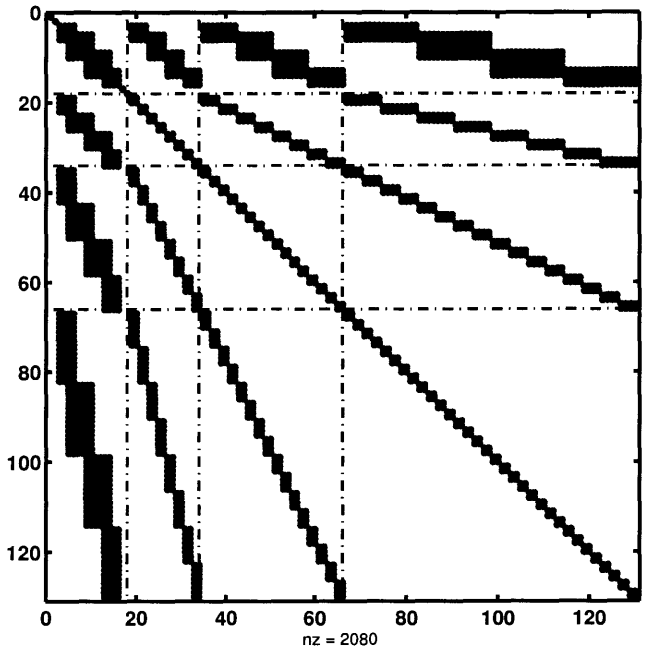

Figure 4-1: Sparsity pattern for a four-level stiffness matrix. The dotted lines seperate the interaction and detail matrices at each scale.

interaction matrices and $\mathrm{C}_i = a\left(w_{i-1}, w_{i-1}^{\mathsf{T}}\right)$, $1 \leq i \leq j$ are referred to as *detail* matrices. Figure 4-1 illustrates the sparsity pattern for a typical multilevel stiffness matrix. Similarly, the right-hand side $\hat{f}_j$ can be written as:

$$\hat{f}_j = \begin{bmatrix} f_0 \\ g_0 \\ \vdots \\ g_{j-1} \end{bmatrix} \tag{4.13}$$

where $f_0 = l\left(\varphi_0\right)$ and $g_i = l\left(w_i\right)$, $0 \leq i < j$.

4.3.1 Single-level vs. multilevel approaches

While Eq (4.10) and Eq (4.12) give rise to exactly the same solution, u_j (albeit expressed in a different basis), the multilevel system of equations has several advantages over the single-level system of equations, particularly for applications such as preconditioning and

adaptive mesh refinement.

Recall that the nodal finite element interpolation functions, upon suitable normalization are Riesz stable in the L^2 norm [15, 29, 51]. That is, there exist two constants c_1 and c_2 independent of the level of discretization j such that for an element $v_j \in V_j$ written as $v_j = \sum_{k \in \mathcal{K}(j)} v_{j,k}^{\mathsf{T}} \varphi_{j,k}$,

$$c_1 \sum_{k \in \mathcal{K}(j)} \left\| v_{j,k}^{\mathsf{T}} \varphi_{j,k} \right\|_{L^2}^2 \leq \|v_j\|_{L^2}^2 \leq c_2 \sum_{k \in \mathcal{K}(j)} \left\| v_{j,k}^{\mathsf{T}} \varphi_{j,k} \right\|_{L^2}^2 \tag{4.14}$$

The practical consequence of this of course is that the nodal finite element mass matrix upon normalization of the basis is always well-conditioned. However, in case of the energy norm, we have from the inverse inequality [15] and equivalence between the Sobolev norm in V and the energy norm that in two dimensions

$$c_1 4^{-sj} \sum_{k \in \mathcal{K}(j)} \left\| v_{j,k}^{\mathsf{T}} \varphi_{j,k} \right\|_{\mathrm{E}}^2 \leq \|v_j\|_{\mathrm{E}}^2 \leq c_2 \sum_{k \in \mathcal{K}(j)} \left\| v_{j,k}^{\mathsf{T}} \varphi_{j,k} \right\|_{\mathrm{E}}^2 \tag{4.15}$$

and hence the condition number of the nodal finite element stiffness matrix normalized with respect to its diagonal grows as 4^{sj} which makes the use of iterative solvers extremely uneconomical especially for higher-order partial differential equations.

In contrast, it is possible to construct wavelet basis functions that are Riesz stable in the energy norm, i.e., there exist two constants c_1 and c_2 independent of j such that on writing an element $v_j \in V_j$ in terms of scaling functions and wavelets as $v_j = \sum_{k \in \mathcal{K}(0)} v_{0,k}^{\mathsf{T}} \varphi_{0,k} + \sum_{i=0}^{j-1} \sum_{m \in \mathcal{M}(i)} v_{i,m}^{\mathsf{T}} w_{i,m}$ we have

$$c_1 \sum_{k \in \mathcal{K}(0)} \left\| v_{0,k}^{\mathsf{T}} \varphi_{0,k} \right\|_{\mathrm{E}}^2 + \sum_{i=0}^{j-1} \sum_{m \in \mathcal{M}(i)} \left\| v_{i,m}^{\mathsf{T}} w_{i,m} \right\|_{\mathrm{E}}^2 \leq \|v_j\|_{\mathrm{E}}^2 \leq c_2 \sum_{k \in \mathcal{K}(0)} \left\| v_{0,k}^{\mathsf{T}} \varphi_{0,k} \right\|_{\mathrm{E}}^2 + \sum_{i=0}^{j-1} \sum_{m \in \mathcal{M}(i)} \left\| v_{i,m}^{\mathsf{T}} w_{i,m} \right\|_{\mathrm{E}}^2 \tag{4.16}$$

The construction of multilevel solvers based on the use of Riesz stable bases satisfying Eq (4.16) has been discussed by a number of authors, for instance Dahmen and collaborators [16, 18], Vassilevski and Wang [48] and Aksoylu and Holst [2].

Multiresolution solvers based on the wavelet-Galerkin method also offer several advan-

tages over nodal finite element interpolation functions for applications requiring adaptive mesh refinement. We recall that adaptive refinement using classical finite element analysis typically proceeds by element subdivision: the error-estimation step determines the elements that have large contributions to the error on a particular mesh and one then proceeds to refine the mesh by subdividing only these elements by quadrisection in two dimensions and octasection in three dimensions. The main disadvantage of the approach based on element subdivision is that it creates geometric artifacts termed *irregular* or *hanging* vertices (see also Chapter 6) that need to be handled appropriately. The methods currently used for handling hanging nodes (such as imposition of multipoint constraints, green refinement or the use of transition elements) have several drawbacks. For example, the imposition of multipoint constraints becomes extremely cumbersome over several levels of refinement and for higher-order interpolation functions such as the Bogner-Fox-Schmidt shape functions [14] whereas closing irregular vertices often leads to meshes with poor aspect ratios over several levels of refinement. While special techniques (such as permitting only one hanging vertex per edge) can be formulated, they are normally very specific to the type of mesh and do not in general extend in a robust manner to higher-order finite element interpolations.

In contrast, mesh refinement in the wavelet-Galerkin method is achieved by the addition of wavelet basis functions over several refinement levels (the process is termed *space refinement* [18] in contrast to *element refinement*) and the implementation does not directly have to contend with hanging nodes as in the classical finite element method. In this sense therefore, the wavelet-Galerkin method resembles several meshless methods where the role of the finite element mesh is simply to serve as a convenient means for computing the inner-products required for the assembly of the stiffness matrix.

4.4 Interaction matrices and the strengthened Cauchy-Schwarz inequality

In this section, we analyze the role of the interaction matrices $\mathbf{B}_{i,j}$ in Eq (4.12) in the wavelet-Galerkin method. As will be evident, the interaction matrices govern how much the details at the finer levels are influenced by the coarse solution and vice-versa and hence it is important to first rigorously characterize this influence before developing error estimation and adaptive refinement procedures based on the multiresolution technique.

Before considering the case of a general Hilbert space, it is instructive to first consider the influence of non-zero interaction matrices for a two-dimensional Euclidean setting; the results derived in this case can be easily and naturally generalized to more general (albeit, finite dimensional) approximation and wavelet spaces using matrix norms as shown in Section 4.4.2.

4.4.1 A two-dimensional analogy

Consider the two-dimensional Euclidean setting shown in Figure 4-2 where $V_{j+1} \subset \mathbb{R}^2$, $V_j, W_j \subset \mathbb{R}^1$ and $a(\cdot,\cdot)$ is simply the dot product. Let θ be the angle between V_j and W_j and let $\gamma = \cos(\theta)$. The scaling function and wavelet can then be taken to be:

$$\varphi_j = \hat{e}_1 \tag{4.17a}$$

$$w_j = \gamma\, \hat{e}_1 + \sqrt{1-\gamma^2}\, \hat{e}_2 \tag{4.17b}$$

Let the vectors u_j and u_{j+1} correspond to the Galerkin projection of the true solution onto the spaces V_j and V_{j+1} and let $g_j = l(w_j)$. Then, the multilevel system of equations to

determine the solution u_{j+1} can be written as:

$$\begin{bmatrix} a(\varphi_j,\varphi_j) & a(\varphi_j,w_j) \\ a(w_j,\varphi_j) & a(w_j,w_j) \end{bmatrix} \begin{bmatrix} \tilde{u}_j \\ r_j \end{bmatrix} = \begin{bmatrix} l(\varphi_j) \\ l(w_j) \end{bmatrix} \quad \text{or,} \tag{4.18a}$$

$$\begin{bmatrix} 1 & \gamma \\ \gamma & 1 \end{bmatrix} \begin{bmatrix} \tilde{u}_j \\ r_j \end{bmatrix} = \begin{bmatrix} u_j \\ g_j \end{bmatrix} \tag{4.18b}$$

from which we obtain,

$$|\tilde{u}_j - u_j| \leq \gamma \ |r_j| \tag{4.19}$$

Therefore, *the magnitude of the interaction matrix (which coincides with the cosine of the angle between the spaces V_j and W_j) detemines how much the solution at the coarser level mesh changes upon the addition of details.*

A related interpretation may be obtained by writing the solution at level $j+1$ as:

$$u_{j+1} = \underbrace{\tilde{u}_j}_{\in V_j} + \underbrace{r_j}_{\in W_j} \tag{4.20}$$

from which we obtain the two-level error, $e_j \overset{\text{def}}{=} u_{j+1} - u_j$ as

$$e_j = \underbrace{r_j}_{\in W_j} + \underbrace{(\tilde{u}_j - u_j)}_{\in V_j} \tag{4.21}$$

Hence, we conclude that the two-level error may be decomposed into two constituents: the first consists solely of the details that are added at each resolution; the second component (which we denote as the "coupling error") on the other hand reflects the extent of interaction between the scales, since from Eq (4.19), the lesser the interaction (the smaller the value of γ), the lower the coupling error.

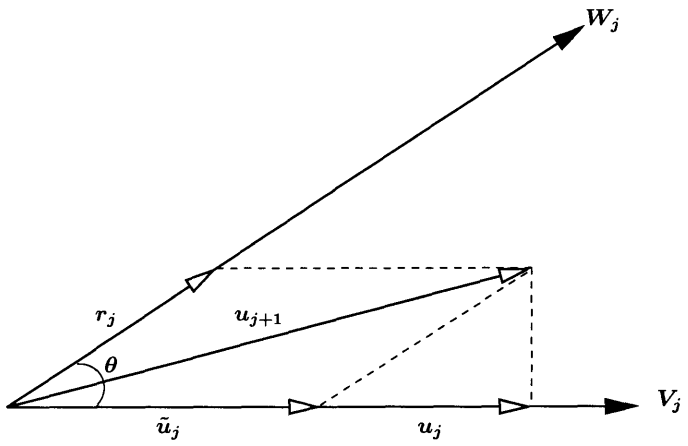

Figure 4-2: Physical interpretation of the constant in strengthened Cauchy-Schwarz inequality for a two-dimensional setting; $\gamma = \cos(\theta)$

The two-dimensional analogy may be extended in a natural manner to higher dimensional Hilbert spaces satisfying the direct-sum property. The fundamental result for general approximation and wavelet spaces, referred to by Yserentant [51] as the *strengthened Cauchy-Schwarz inequality* may be stated as follows:

Lemma 4.1 (Strenghened Cauchy-Schwarz Inequality). *There exists a constant* $\gamma \in [0, 1)$ *independent of* j *such that*

$$|a(v, w)| \leq \gamma \ \|v\|_{\mathrm{E}} \|w\|_{\mathrm{E}} \quad v \in V_j \text{ and } w \in W_j \tag{4.22}$$

Proof. See Yserentant [51]. □

Lemma 4.2. *For any element* $v_{j+1} \in V_{j+1}$ *such that* $v_{j+1} = v_j + r_j$ *where* $v_j \in V_j$ *and* $r_j \in W_j$

$$\|r_j\|_E \leq \frac{1}{\sqrt{1-\gamma^2}} \|v_{j+1}\|_E \tag{4.23}$$

Proof. From Lemma 4.1,

$$\begin{aligned}
\|v_{j+1}\|_{\mathrm{E}} &= a(v_j, v_j) + 2a(v_j, r_j) + a(r_j, r_j) \\
&= \|v_j\|_{\mathrm{E}}^2 + 2a(v_j, r_j) + \|r_j\|_{\mathrm{E}}^2 \\
&\geq \|v_j\|_{\mathrm{E}}^2 - 2\gamma \|v_j\|_{\mathrm{E}} \|r_j\|_{\mathrm{E}} + \|r_j\|_{\mathrm{E}}^2 \quad \text{(Lemma 4.1)} \\
&\geq \|v_j\|_{\mathrm{E}}^2 - \|v_j\|_{\mathrm{E}}^2 - \gamma^2 \|r_j\|_{\mathrm{E}}^2 + \|r_j\|_{\mathrm{E}}^2 \quad \text{(AM-GM inequality)} \\
&= \left(1 - \gamma^2\right) \|r_j\|_{\mathrm{E}}^2
\end{aligned} \tag{4.24}$$

from which the desired result follows immediately. □

As we shall see in the subsequent discussion, the constant γ in the more general setting can be used to prove bounds on the magnitude of coupling errors due to refinement. In deriving these bounds, it is often convenient to use matrix notation and therefore in the next section, we provide a matrix characterization of γ in Eq (4.22).

4.4.2 Matrix characterization of the strengthened Cauchy-Schwarz inequality

In the two-dimensional setting considered in the previous section, the constant γ simply corresponded to the magnitude of the coupling term in the multilevel stiffness matrix. Not surprisingly, in the more general case, the constant may be related to the norm of the interaction matrix at each level provided that the scaling functions and wavelets are suitably normalized. This relation is provided by the following lemma.

Lemma 4.3. *Let* $\mathbf{B}_{j+1} = a\left(\varphi_j, w_j^{\mathsf{T}}\right)$, $\mathbf{C}_{j+1} = a\left(w_j, w_j^{\mathsf{T}}\right)$ *and* $\mathbf{X}_{j+1} = \mathbf{K}_j^{-\frac{1}{2}}\mathbf{B}_{j+1}\mathbf{C}_{j+1}^{-\frac{1}{2}}$. *If* γ *is the constant in the strengthened Cauchy-Schwarz inequality, Eq (4.22) then* $\gamma = \|\mathbf{X}_{j+1}\|$ *where* $\mathbf{K}_j^{\frac{1}{2}}$ *(resp.* $\mathbf{C}_{j+1}^{\frac{1}{2}}$*) is the principal square root of* $\mathbf{K}_j$ *(resp.* $\mathbf{C}_{j+1}$*).*

Proof. By definition,

$$\begin{aligned}
\gamma &= \sup_{v\in V_j, w\in W_j} \frac{|a(v,w)|}{\|v\|_{\mathrm{E}}\,\|w\|_{\mathrm{E}}} \\
&= \sup_{v,w} \frac{\left|v^{\mathsf{T}}\mathbf{B}_{j+1}w\right|}{\sqrt{v^{\mathsf{T}}\mathbf{K}_j v}\,\sqrt{w^{\mathsf{T}}\mathbf{C}_{j+1}w}} \\
&= \sup_{v',w'} \frac{\left|v'\mathbf{K}_j^{-\frac{1}{2}}\mathbf{B}_{j+1}\mathbf{C}_{j+1}^{-\frac{1}{2}}w'\right|}{\|v'\|\,\|w'\|} \quad \text{where } v' = \mathbf{K}_j^{\frac{1}{2}}v,\ w' = \mathbf{C}_{j+1}^{\frac{1}{2}}w \\
&= \|\mathbf{X}_{j+1}\| \qquad (4.25)
\end{aligned}$$

□

Remark. Evidently, in the above lemma, we can replace the principal square root of a matrix with its Cholesky factor.

The next result is an extension of Lemma 4.3 and is used in proving certain estimates about the the accuracy of the error-estimation and adaptive refinement schemes that we propose in Chapter 6.

Lemma 4.4. *If* $\mathbf{X}_{j+1}$ *is as defined in Lemma 4.3 then* $\left\|\mathbf{I} - \mathbf{X}_{j+1}^{\mathsf{T}}\mathbf{X}_{j+1}\right\| \leq 1$ *and* $\left\|\left(\mathbf{I} - \mathbf{X}_{j+1}^{\mathsf{T}}\mathbf{X}_{j+1}\right)^{-1}\right\| = \frac{1}{1-\gamma^2}$.

Proof. Let $\mathbf{X}_{j+1}$ have a singular-value decomposition of the form $\mathbf{X}_{j+1} = \mathbf{U}\boldsymbol{\Sigma}\mathbf{V}^{\mathsf{T}}$ where $\sigma_{\max}(\mathbf{X}_{j+1}) = \gamma$. Hence, the matrix $\mathbf{I} - \mathbf{X}_{j+1}^{\mathsf{T}}\mathbf{X}_{j+1}$ has an eigenvalue decomposition of the form $\mathbf{V}\left(\mathbf{I} - \Lambda\right)\mathbf{V}^{\mathsf{T}}$ with $\lambda_{\min} \geq 0$ and $\lambda_{\max} = \gamma^2 < 1$. Hence,

$$\left\|\mathbf{I} - \mathbf{X}_{j+1}^{\mathsf{T}}\mathbf{X}_{j+1}\right\| = 1 - \lambda_{\min}^2 \qquad \leq 1 \text{ and} \tag{4.26a}$$

$$\left\|\left(\mathbf{I} - \mathbf{X}_{j+1}^{\mathsf{T}}\mathbf{X}_{j+1}\right)^{-1}\right\| = \frac{1}{(1 - \lambda_{\max}^2)} \qquad = \frac{1}{1 - \gamma^2} \tag{4.26b}$$

exactly as desired. □

While Lemma 4.3 suggests a convenient numerical procedure to compute the value of γ, it is possible to arrive at upper-bounds without having to actually assemble the global stiffness, interaction and detail matrices. Instead, as discussed in the monograph by Ainsworth and Oden [1], we can compute an upper-bound for γ using computations performed at the element level. Considering two elements $v \in V_j$ and $w \in W_j$ we have:

$$\begin{aligned}
|a(v,w)| &\leq \sum_{Q \in S_{j,v}} |a(v,w)_Q| \\
&\leq \sum_{Q \in S_{j,v}} \gamma_Q \left\|v\right\|_{E;Q} \left\|w\right\|_{E;Q} \\
&\leq \max_{Q \in S_{j,v}} \gamma_Q \left(\sum_{Q \in S_{j,v}} \left\|v\right\|_{E;Q} \left\|w\right\|_{E;Q}\right) \\
&\leq \max_{Q \in S_{j,v}} \gamma_Q \left(\sum_{Q \in S_{j,v}} \left\|v\right\|_{E;Q}^2\right)^{\frac{1}{2}} \left(\sum_{Q \in S_{j,v}} \left\|w\right\|_{E;Q}^2\right)^{\frac{1}{2}} \text{ (Cauchy-Schwarz Inequality)} \\
&= \max_{Q \in S_{j,v}} \gamma_Q \left\|v\right\|_{\mathrm{E}} \left\|w\right\|_{\mathrm{E}}
\end{aligned} \tag{4.27}$$

Therefore, assuming a regular grid, one can arrive at an upper-bound for the value of γ by applying Lemma 4.3 to a reference element that is properly supported against all rigid-body motion. In practice however, these bounds tend to be quite conservative while the estimate for γ derived directly by applying Lemma 4.3 at each level are in general more accurate.

4.4.3 Coupling errors and the strengthened Cauchy-Schwarz inequality

In this section, we extend the results for the two-dimensional Euclidean space and analyze the influence of the constant γ on the coupling errors for the general case. First, we decompose the finite element solution, $u_{j+1} \in V_{j+1}$ into two components, $\tilde{u}_j \in V_j$ and $v_j \in W_j$. The system of equations for determining these components is given as:

$$\begin{bmatrix} \mathbf{K}_j & \mathbf{B}_{j+1} \\ \mathbf{B}_{j+1}^{\mathsf{T}} & \mathbf{C}_{j+1} \end{bmatrix} \begin{bmatrix} \tilde{u}_j \\ r_j \end{bmatrix} = \begin{bmatrix} f_j \\ g_j \end{bmatrix} = \begin{bmatrix} \mathbf{K}_j u_j \\ g_j \end{bmatrix} \tag{4.28}$$

Observe that for any element v_j in V_j written as $v_j = \sum_{k \in \mathcal{K}(j)} v_{j,k}^{\mathsf{T}} \varphi_{j,k}$ we have,

$$\|v_j\|_{\mathrm{E}}^2 = a(v_j, v_j) = v_j^{\mathsf{T}} \mathbf{K}_j v_j \tag{4.29}$$

From Eq (4.28) we have

$$\mathbf{K}_j (\tilde{u}_j - u_j) = -\mathbf{B}_{j+1} r_j \tag{4.30}$$

and hence

$$\begin{aligned} \frac{\|\tilde{u}_j - u_j\|_{\mathrm{E}}^2}{\|r_j\|_{\mathrm{E}}} &= \frac{r_j^{\mathsf{T}} \mathbf{B}_{j+1}^{\mathsf{T}} \mathbf{K}_j^{-1} \mathbf{B}_{j+1} r_j}{r_j^{\mathsf{T}} \mathbf{C}_{j+1} r_j} \\ &= \frac{r_j^{\mathsf{T}} \mathbf{C}_{j+1}^{-\frac{1}{2}} \mathbf{B}_{j+1}^{\mathsf{T}} \mathbf{K}_j^{-1} \mathbf{B}_{j+1} \mathbf{C}_{j+1}^{-\frac{1}{2}} r_j}{r_j^{\mathsf{T}} r_j} \quad (\text{setting } r_j = \mathbf{C}_{j+1}^{\frac{1}{2}} r_j) \\ &= \frac{r_j^{\mathsf{T}} \mathbf{X}_{j+1}^{\mathsf{T}} \mathbf{X}_{j+1} r_j}{r_j^{\mathsf{T}} r_j} \\ &\leq \gamma^2 \end{aligned} \tag{4.31}$$

Therefore,

$$\|\tilde{u}_j - u_j\|_{\mathrm{E}} \leq \gamma \|r_j\|_{\mathrm{E}} \tag{4.32}$$

which has the same form as Eq (4.19). Further, by Lemma 4.2, we can bound the energy-norm of the coupling error in terms of the energy-norm of the solution at the next level,

u_{j+1} as:

$$\|\tilde{u}_j - u_j\|_{\mathrm{E}} \leq \frac{\gamma}{\sqrt{1-\gamma^2}} \|u_{j+1}\|_{\mathrm{E}} \tag{4.33}$$

4.5 Closure

4.5.1 The case for the use of scale-orthogonal wavelets

As evident from the discussion in Section 4.4, a desirable property in the design of fast adaptive multiresolution solvers it to have no interaction between basis functions at different levels of resolution, i.e., we design the wavelet spaces W_j such that the constant γ in the strengthened Cauchy-Schwarz inequality is 0 over all levels j. To determine the solution at a level $j+1$, we therefore arrive at a system of equations of the form:

$$\begin{aligned} \mathbf{K}_0\, u_0 &= f_0 \text{ and} \\ \mathbf{C}_{i+1}\, r_i &= g_i \; i = 0, 1, \ldots, j \end{aligned} \tag{4.34}$$

which permits the computation of the solution at each level of resolution in an entirely scale-independent manner, that is, once the solution at a particular level has been computed, it does not have to be modified on adding details at a finer level. Moreover, in computing the detail at a certain level j, one needs to factor the detail matrix $\mathbf{C}_{j+1}$ corresponding *only* to that level.

In order to arrive at a decoupled system of equations, it suffices for the scaling functions and wavelets at a certain level j to be a-orthogonal, i.e.,

$$a\left(\varphi_j, w_j^{\mathsf{T}}\right) = 0 \tag{4.35}$$

Since the scaling functions and wavelets at any level $i < j$ can be expressed solely in terms of scaling functions at level j, satisfying the one-level scale-orthogonality condition

therefore also leads to the following orthogonality conditions to hold

$$\mathbf{B}_{0,j+1} = a\left(\varphi_0, w_j^{\mathsf{T}}\right) = 0 \tag{4.36a}$$

$$\mathbf{B}_{i+1,j+1} = a\left(w_i, w_j^{\mathsf{T}}\right) = 0, \quad i < j \tag{4.36b}$$

which in turn leads to a decoupled system of equations, Eq (4.34).

In the next chapter, we describe how it is possible to construct the wavelet basis functions such that the conditions Eq (4.36a) and Eq (4.36b) are satisfied over all levels j leading to a block-diagonal multilevel system of equations.

Chapter 5

Construction and Properties of Scale-Orthogonal Wavelets

It is by logic that we prove, but by intuition that we discover.
– Henri Poincaré

5.1 Chapter overview

As concluded in Chapter 4, for the design of fast adaptive multiresolution solvers we desire that the approximation and wavelet spaces be orthogonal with respect to the bilinear form $a(\cdot,\cdot)$. In this chapter we describe several techniques for the construction of scale-orthogonal wavelets for general operators that span precisely such complementary spaces. In constructing these wavelets, the essential tasks are ensuring that (a) they can be constructed in an efficient manner (ideally, the wavelets must have a local support) and (b) they form a Riesz stable basis in the energy norm for the wavelet spaces. As we shall see in Chapter 6, the second property is of *utmost* importance in the development of fast and accurate multilevel error estimation and adaptive refinement procedures.

The outline for the rest of the chapter is as follows: we begin in Section 5.2 by deriving the condition necessary for the linear independence of scaling functions and wavelets using the polyphase representation. We then describe the most straightforward approach (directly

using the wavelet equation, Eq (2.6b)) for the construction of scale-orthogonal wavelets. As will be evident from the discussion, the main disadvantage of this approach is that ensuring the linear independence of scaling functions and wavelets using the conditions described in Section 5.2 is extremely cumbersome. Therefore, in Sections 5.5 and 5.6 we describe two approaches for the construction of scale-orthogonal wavelets by *customizing* an existing (non-scale-orthogonal) wavelet basis such that the resulting wavelets are scale-orthogonal. The first procedure considered (*stable completion,* due to Carnier, et al. [16]) ensures that most of the wavelets are locally supported, but does not guarantee *a priori* that the wavelets are also Riesz stable. On the other hand, the second procedure (Gram-Schmit orthogonalization) ensures that the wavelets are Riesz stable, but often leads to globally supported, albeit rapidly decaying wavelets. We then propose a third approach in Section 5.7 based on *partial* Gram-Schmidt orthogonalization that leads to the efficient construction of scale-orthogonal wavelets in an adaptive refinement setting and at the same time guarantees *a priori* that the resulting wavelets are also Riesz stable. We also propose (and derive the operation cost estimates for) a class of simple and efficient algorithms for the fast assembly and factorization of the stiffness matrices resulting from these wavelets.

In the rest of the chapter, we analyze some of the key properties of the wavelets constructed in the previous sections (particularly those constructed via Gram-Schmidt orthogonalization and its variations). In Section 5.8 we analyze the decay of these wavelets by deriving bounds for their point-wise values in terms of the Green's function of the underlying operator. Then, in Section 5.9 we prove *a priori* Riesz stability of the wavelets in the energy norm using many of the results from Chapter 4 and demonstrate the validity of the derived bounds for a model fourth-order problem. We do not completely analyze the influence of partial orthogonalization of the wavelets upon the accuracy of the solution in this chapter; a thorough analysis of this approximation is instead provided at the end of Chapter 6.

5.2 The polyphase representation

When constructing wavelets that are not scale and shift invariant, one is concerned with, at the very minimum, ensuring linear independence between scaling functions and wavelets. A convenient method to ensure that the scaling functions and wavelets are linearly independent is to use the polyphase or operator notation [16, 42, 45]. In this section, we give a brief overiew of this technique and derive an *a posteriori* test that determines if the scaling functions and wavelets are independent.

Let φ_j and w_j denote the column vector of scaling functions and wavelets at level j. The refinement and wavelet relations, Eq (2.6a) may be cast in matrix notation as:

$$\begin{bmatrix} \varphi_j \\ w_j \end{bmatrix} = \begin{bmatrix} \mathbf{H}_j^0 \\ \mathbf{H}_j^1 \end{bmatrix} \varphi_{j+1} \tag{5.1}$$

We now define the *even* and *odd permutation matrices*, $\mathbf{P}_{\mathrm{E},j}$ and $\mathbf{P}_{\mathrm{O},j}$ as:

$$\mathbf{P}_{\mathrm{E},j,k,l} \stackrel{\text{def}}{=} \delta_{k,l} \quad (k \in \mathcal{K}(j),\ l \in \mathcal{K}(j+1)) \quad \text{and} \tag{5.2a}$$

$$\mathbf{P}_{\mathrm{O},j,m,l} \stackrel{\text{def}}{=} \delta_{m,l} \quad (m \in \mathcal{M}(j),\ l \in \mathcal{K}(j+1))\,, \tag{5.2b}$$

which satisfy the following *perfect reconstruction* conditions:

$$\begin{bmatrix} \mathbf{P}_{\mathrm{E},j}^{\mathsf{T}} & \mathbf{P}_{\mathrm{O},j}^{\mathsf{T}} \end{bmatrix} \begin{bmatrix} \mathbf{P}_{\mathrm{E},j} \\ \mathbf{P}_{\mathrm{O},j} \end{bmatrix} = \mathbf{I} \quad \text{and} \tag{5.3a}$$

$$\begin{bmatrix} \mathbf{P}_{\mathrm{E},j} \\ \mathbf{P}_{\mathrm{O},j} \end{bmatrix} \begin{bmatrix} \mathbf{P}_{\mathrm{E},j}^{\mathsf{T}} & \mathbf{P}_{\mathrm{O},j}^{\mathsf{T}} \end{bmatrix} = \mathbf{I} \tag{5.3b}$$

Eq (5.1) may then be recast as:

$$\begin{bmatrix} \varphi_j \\ w_j \end{bmatrix} = \begin{bmatrix} \mathbf{H}_j^0 \\ \mathbf{H}_j^1 \end{bmatrix} \begin{bmatrix} \mathbf{P}_{\mathrm{E},j}^{\mathsf{T}} & \mathbf{P}_{\mathrm{O},j}^{\mathsf{T}} \end{bmatrix} \begin{bmatrix} \mathbf{P}_{\mathrm{E},j} \\ \mathbf{P}_{\mathrm{O},j} \end{bmatrix} \varphi_{j+1} = \begin{bmatrix} \mathbf{H}_j^0 \mathbf{P}_{\mathrm{E},j}^{\mathsf{T}} & \mathbf{H}_j^0 \mathbf{P}_{\mathrm{O},j}^{\mathsf{T}} \\ \mathbf{H}_j^1 \mathbf{P}_{\mathrm{E},j}^{\mathsf{T}} & \mathbf{H}_j^1 \mathbf{P}_{\mathrm{O},j}^{\mathsf{T}} \end{bmatrix} \begin{bmatrix} \mathbf{P}_{\mathrm{E},j} \\ \mathbf{P}_{\mathrm{O},j} \end{bmatrix} \varphi_{j+1}. \tag{5.4}$$

In the case of interpolating scaling functions, which satisfy a refinement relation shown in

Eq (3.8), the matrix represenation takes on the following form:

$$\begin{bmatrix} \varphi_j \\ w_j \end{bmatrix} = \begin{bmatrix} \mathbf{I} & \mathbf{H}_j \\ \mathbf{H}_j^1 \mathbf{P}_{\mathrm{E},j}^{\mathsf{T}} & \mathbf{H}_j^1 \mathbf{P}_{\mathrm{O},j}^{\mathsf{T}} \end{bmatrix} \begin{bmatrix} \mathbf{P}_{\mathrm{E},j} \\ \mathbf{P}_{\mathrm{O},j} \end{bmatrix} \varphi_{j+1} \tag{5.5}$$

where the entries in the matrix $\mathbf{H}_j$ correspond to the filters h_j in Eq (3.8).

5.2.1 Linear independence of scaling functions and wavelets

To test for the linear independence of scaling functions and wavelets in Eq (5.5), we consider the homogeneous system of equations:

$$\begin{bmatrix} \varphi_j^{\mathsf{T}} & w_j^{\mathsf{T}} \end{bmatrix} \begin{bmatrix} u_j \\ r_j \end{bmatrix} = 0 \tag{5.6}$$

Substituting Eq (5.5) into Eq (5.5) and using the linear independence of scaling functions at level $j+1$ we have:

$$\begin{bmatrix} \mathbf{I} & 0 \\ \mathbf{H}_j^{\mathsf{T}} & \mathbf{I} \end{bmatrix} \begin{bmatrix} \mathbf{I} & \mathbf{P}_{\mathrm{E},j} \left(\mathbf{H}_j^1\right)^{\mathsf{T}} \\ 0 & \mathbf{P}_{\mathrm{O},j} \left(\mathbf{H}_j^1\right)^{\mathsf{T}} - \mathbf{H}_j^{\mathsf{T}} \mathbf{P}_{\mathrm{E},j} \left(\mathbf{H}_j^1\right)^{\mathsf{T}} \end{bmatrix} \begin{bmatrix} u_j \\ r_j \end{bmatrix} = 0 \tag{5.7a}$$

$$\iff \left(\mathbf{P}_{\mathrm{O},j} \left(\mathbf{H}_j^1\right)^{\mathsf{T}} - \mathbf{H}_j^{\mathsf{T}} \mathbf{P}_{\mathrm{E},j} \left(\mathbf{H}_j^1\right)^{\mathsf{T}}\right) r_j = 0 \tag{5.7b}$$

or, the scaling functions and wavelets are linearly independent if and only if the matrix $\mathbf{P}_{\mathrm{O},j} \left(\mathbf{H}_j^1\right)^{\mathsf{T}} - \mathbf{H}_j^{\mathsf{T}} \mathbf{P}_{\mathrm{E},j} \left(\mathbf{H}_j^1\right)^{\mathsf{T}}$ is non-singular.

5.3 Construction of scale-orthogonal wavelets using the wavelet equation

To construct wavelets satisfying Eq (4.35) we start by assuming a wavelet equation of the form:

$$w_{j,m} = \sum_{l \in \mathcal{M}(j,m)} h_{j,m,l}^1 \varphi_{j+1,l} \tag{5.8}$$

where $\mathcal{M}(j,m) \subset \mathcal{K}(j+1)$. The support of the wavelet can therefore be determined as:

$$\text{supp}\,(w_{j,m}) \subseteq \bigcup_{l \in \mathcal{M}(j,m)} \text{supp}\,(\varphi_{j+1,l}) \tag{5.9}$$

Substituting Eq (5.8) into Eq (4.35) we have the following constraint on the high-pass filters:

$$\sum_{l \in \mathcal{M}(j,m)} a\left(\varphi_{j,k}, \varphi_{j+1,l}^{\mathsf{T}}\right)\left(h_{j,m,l}^{1}\right)^{\mathsf{T}} = 0 \quad (k \in \mathcal{K}(j)), \quad \text{or} \tag{5.10a}$$

$$\mathbf{B}_{j+1}^{\text{loc}}\left(h_{j}^{1}\right)^{\mathsf{T}} = 0. \tag{5.10b}$$

We therefore conclude that the wavelets with the assumed support are scale-orthogonal to the scaling function filters *if and only if* the high-pass filters h_j^1 lie in the null space of the matrix $\mathbf{B}_{j+1}^{\text{loc}}$. Moreover, the dimension of the nullspace of $\mathbf{B}_{j+1}^{\text{loc}}$ gives the number of linearly independent scale-orthogonal wavelets with their support governed by the set $\mathcal{M}(j,m)$ in Eq (5.8). As an example of constructing scale-orthogonal wavelets directly from the refinement relation, we consider piecewise cubic Hermite interpolating scaling functions, see Figure 3-5 and construct wavelets that are orthogonal to the scaling functions with respect to the L^2 inner-product. The resulting wavelets in the interior and the left boundary are shown in Figure 5-1. Note that over regular grids, the wavelets shown in Figure 5-1 (a) and (b) correspond to the ones derived by Strela and Strang [43].

While directly constructing wavelets using Eqs (5.8) and (5.10b) is a valid approach, it is necessary to verify that the condition for linear independence, Eq (5.7b) holds true after constructing the filters h_j^1. It is therefore more convenient in practice to start with an existing multiresolution analysis and then customize the wavelets such that they satisfy the desired properties (such as scale-orthogonality). The most natural choice for such an elementary MRA is the hierarchical finite element basis framework [51, 52, 53], which is briefly described in the next section.

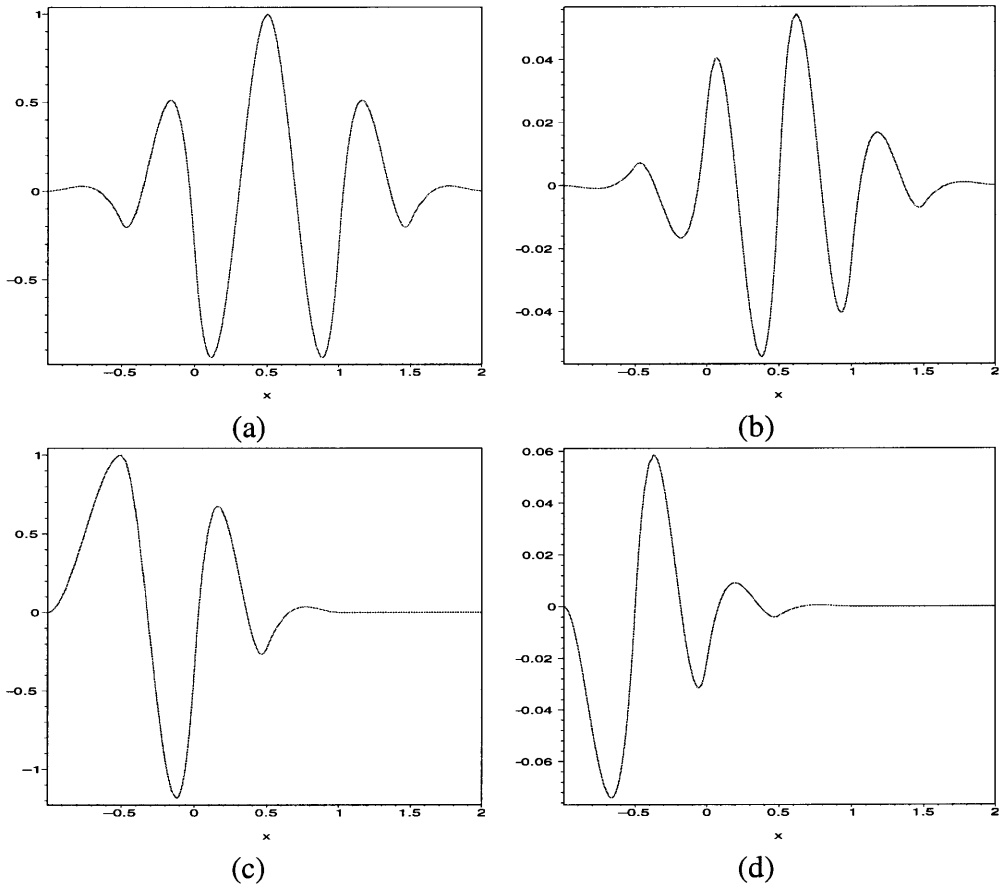

Figure 5-1: Scale-orthogonal multiwavelets: (a) and (b) in the interior and (c) and (d) next to the left boundary.

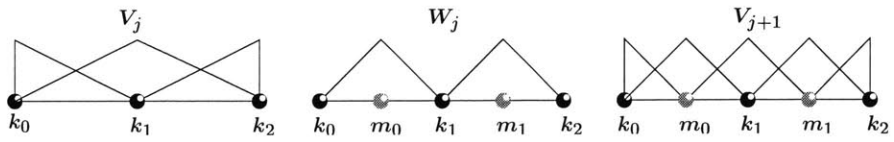

Figure 5-2: A multiresolution analysis of a piecewise linear finite element approximation space brought about using hierarchical basis functions,$V_j \oplus W_j = V_{j+1}$.

5.4 Hierarchical basis functions

In the hierarchical basis framework, the wavelets are assumed to be the interpolating basis functions associated with the newly introduced vertices, x_m, $m \in \mathcal{M}(j)$:

$$w_{j,m}^{\mathrm{HB}} \stackrel{\mathrm{def}}{=} \varphi_{j+1,m} \tag{5.11}$$

corresponding to $h_{j,m,l}^{1} = \delta_{m,l}$, see Figures 5-2 and 5-3. It is easy to see that the complementary space, $W_j^{\mathrm{HB}} = \text{clos span}\left\{w_{j,m}^{\mathrm{HB}}\right\}_{m\in\mathcal{M}(j)}$ satisfies the the nestedness ($W_j^{\mathrm{HB}} \subset V_{j+1}$) and direct-sum conditions ($W_j^{\mathrm{HB}} \oplus V_j = V_{j+1}$) and therefore hierarchical bases lead to a valid (albeit trivial) multiresolution analysis of the space V. For this reason, hierarchical basis functions are often referred to in wavelet literature as *lazy wavelets* [42, 45].

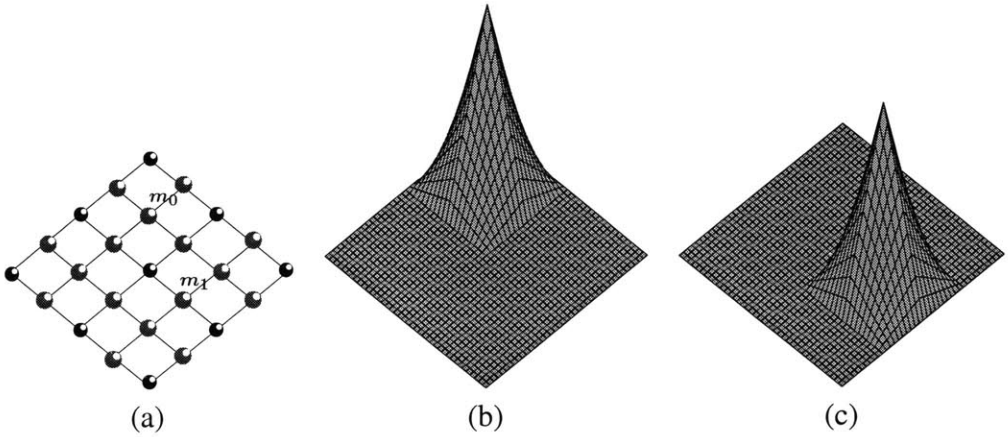

Figure 5-3: Two dimensional piecewise-bilinear hierarchical basis functions: (a) Two-level mesh; (b) φ_{j+1,m_0} centered around a face vertex and (c) φ_{j+1,m_1}centered around an edge vertex

For certain bilinear forms these rudimentary wavelets are naturally scale-orthogonal to

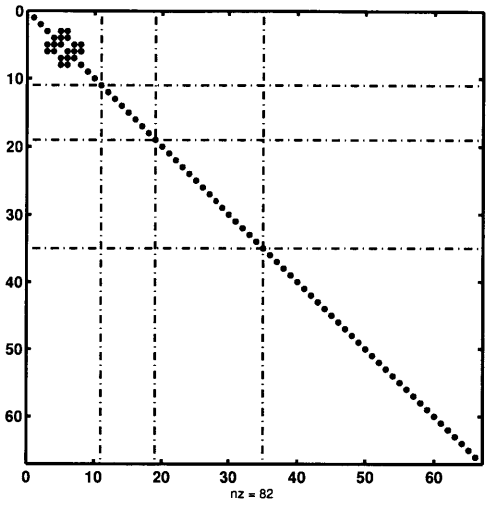

Figure 5-4: Multilevel stiffness matrix arising out the discretization of the weak-form for an Eulerian beam using piecewise cubic Hermite interpolating hierarchical basis functions

the scaling functions. For example, considering the bilinear form for the Poisson's equation,

$$a(u,v) = \int_{\Omega} \frac{\mathrm{d}u}{\mathrm{d}x} \frac{\mathrm{d}v}{\mathrm{d}x} \, \mathrm{d}x \tag{5.12}$$

and choosing the scaling functions to be piecewise linear Lagrange interpolating polynomials gives rise to a diagonal multilevel stiffness matrix [52, 53]. Similarly, considering the bilinear form for an Eulerian beam,

$$a(u,v) = \mathsf{E} \int_{\Omega} \frac{\mathrm{d}^2u}{\mathrm{d}x^2} \frac{\mathrm{d}^2v}{\mathrm{d}x^2} \, \mathrm{d}x \tag{5.13}$$

and choosing the scaling functions to be cubic Hermite polynomials results in a block-diagonal multiscale system of equations as can be seen from Figure 5-4. This property however breaks down for more general operators, higher order scaling functions and in higher dimensions and consquently hierarchical basis functions need to be customized in order to make them scale-orthogonal.

5.5 Scale-orthogonal wavelets using stable completion

The *stable completion* method proposed by Carnicer et al. [16] starts with an existing multiresolution analysis consisting of scaling functions $\varphi_{j,k}$ and wavelets $w_{j,m}^{\text{old}}$. The new wavelets $w_{j,m}$ are constructed as:

$$w_{j,m} = \sum_{m' \in B(j,m)} g_{j,m',m}^{\mathsf{T}} w_{j,m'}^{\text{old}} - \sum_{k \in A(j,m)} s_{j,k,m}^{\mathsf{T}} \varphi_{j,k}, \tag{5.14a}$$

which can be written out in matrix notation as:

$$w_j = \mathbf{G}_j^{\mathsf{T}} w_j^{\text{old}} - \mathbf{S}_j \varphi_j \tag{5.14b}$$

which generates a MRA under certain conditions on the matrix $\mathbf{G}_j$ (discussed in Section 5.5.1). One can then impose the required constraints on the wavelets and solve for the coefficients $\mathbf{G}_j$ and $\mathbf{S}_j$. As we shall see in Section 5.5.1, Eq (5.14a) is equivalent to Eq (5.8), except that it leads to a simpler condition to be verified to ensure that the scaling functions and wavelets are linearly independent.

When starting with the hierarchical basis framework, the equation for the customized wavelet, $w_{j,m}$ becomes:

$$w_{j,m} = \sum_{m' \in B(j,m)} g_{j,m',m}^{\mathsf{T}} \varphi_{j+1,m'} - \sum_{k \in A(j,m)} s_{j,k,m}^{\mathsf{T}} \varphi_{j,k}. \tag{5.15}$$

5.5.1 Linear independence of scaling functions and wavelets

Before proposing an algorithm for the construction of scale-orthogonal wavelets using stable completion, we first derive the conditions on the matrix $\mathbf{G}_j$ to ensure the linear independence of scaling functions and wavelets. First, observe that for hierarchical basis functions, the refinement and wavelet relations can be written in polyphase notation as:

$$\begin{bmatrix} \varphi_j \\ w_j^{\text{HB}} \end{bmatrix} = \begin{bmatrix} \mathbf{I} & \mathbf{H}_j \\ \mathbf{0} & \mathbf{I} \end{bmatrix} \begin{bmatrix} \mathbf{P}_{\text{E},j} \\ \mathbf{P}_{\text{O},j} \end{bmatrix} \varphi_{j+1} \tag{5.16}$$

Therefore, the refinement and wavelet relations for wavelets constructed out of stable completion can be written as:

$$\begin{bmatrix} \varphi_j \\ w_j \end{bmatrix} = \begin{bmatrix} \mathbf{I} & \mathbf{0} \\ -\mathbf{S}_j^\mathsf{T} & \mathbf{G}_j^\mathsf{T} \end{bmatrix} \begin{bmatrix} \varphi_{j+1} \\ w_j^{\mathrm{HB}} \end{bmatrix} = \begin{bmatrix} \mathbf{I} & \mathbf{0} \\ -\mathbf{S}_j^\mathsf{T} & \mathbf{G}_j^\mathsf{T} \end{bmatrix} \begin{bmatrix} \mathbf{I} & \mathbf{H}_j \\ \mathbf{0} & \mathbf{I} \end{bmatrix} \begin{bmatrix} \mathbf{P}_{\mathrm{E},j} \\ \mathbf{P}_{\mathrm{O},j} \end{bmatrix} \varphi_{j+1}, \tag{5.17}$$

whence on comparison with Eq (5.5) we obtain $\mathbf{S}_j \equiv -\mathbf{P}_{\mathrm{E},j} \left(\mathbf{H}_j^1\right)^\mathsf{T}$ and $\mathbf{G}_j \equiv \mathbf{P}_{\mathrm{O},j} \left(\mathbf{H}_j^1\right)^\mathsf{T} - \mathbf{H}_j^\mathsf{T} \mathbf{P}_{\mathrm{E},j} \left(\mathbf{H}_j^1\right)^\mathsf{T}$. *Hence the scaling functions and wavelets are linearly independent if and only if the matrix* $\mathbf{G}_j$ *is non-singular.* During filter design, checking for the rank of $\mathbf{G}_j$ is usually more convenient than first constructing the $\mathbf{H}_j^1$ filters and then verifying Eq (5.7b).

5.5.2 Inverse wavelet transform for wavelets constructed using stable completion

To derive the expressions for the inverse wavelet transform for wavelets constructed using the stable completion procedure, consider a function f_{j+1} written as

$$f_{j+1} = u_{j+1}^\mathsf{T} \varphi_{j+1} = \begin{bmatrix} u_j^\mathsf{T} & r_j^\mathsf{T} \end{bmatrix} \begin{bmatrix} \varphi_j \\ w_j \end{bmatrix} \tag{5.18}$$

On substituting the refinement and wavelet equations in the vector form, Eq (5.17) we have:

$$\left(u_{j+1}^\mathsf{T} - \begin{bmatrix} u_j^\mathsf{T} & r_j^\mathsf{T} \end{bmatrix} \begin{bmatrix} \mathbf{I} & \mathbf{0} \\ -\mathbf{S}_j^\mathsf{T} & \mathbf{G}_j^\mathsf{T} \end{bmatrix} \begin{bmatrix} \mathbf{I} & \mathbf{H}_j \\ \mathbf{0} & \mathbf{I} \end{bmatrix} \begin{bmatrix} \mathbf{P}_{\mathrm{E},j} \\ \mathbf{P}_{\mathrm{O},j} \end{bmatrix} \right) \varphi_{j+1} = 0 \tag{5.19}$$

Since the scaling functions at level $j+1$ are linearly independent (they form a basis for V_{j+1}) we have the expression for the coefficients u_j and r_j in matrix form as:

$$\begin{bmatrix} \mathbf{P}_{\mathrm{E},j} \\ \mathbf{P}_{\mathrm{O},j} \end{bmatrix} u_{j+1} = \begin{bmatrix} \mathbf{I} & \mathbf{0} \\ \mathbf{H}_j^\mathsf{T} & \mathbf{I} \end{bmatrix} \begin{bmatrix} \mathbf{I} & -\mathbf{S}_j \\ \mathbf{0} & \mathbf{G}_j \end{bmatrix} \begin{bmatrix} u_j \\ r_j \end{bmatrix} \tag{5.20a}$$

or in coefficient form as:

$$\begin{aligned} u_{j+1,k} &= u_{j,k} - \sum_{m' \in a(j,k)} s_{j,k,m'} r_{j,m'} && (k \in \mathcal{K}(j)) \\ u_{j+1,m} &= \sum_{m' \in b(j,m)} g_{j,m,m'} r_{j,m'} + \sum_{k \in N(j,m)} h^{\mathsf{T}}_{j,k,m} u_{j+1,k} && (m \in \mathcal{M}(j)) \end{aligned} \tag{5.20b}$$

where, $b(j,m) \stackrel{\text{def}}{=} \{m' \in \mathcal{M}(j) \text{ s.t. } m \in B(j,m')\}$ and $a(j,k) \stackrel{\text{def}}{=} \{m' \in \mathcal{M}(j) \text{ s.t. } k \in A(j,m')\}$.

Eq (5.20b) can be implemented as follows:

1. *Initialization*

$$\begin{aligned} \forall k \in \mathcal{K}(j) \quad u_{j+1,k} &= u_{j,k} \\ \forall m \in \mathcal{M}(j) \quad u_{j+1,m} &= 0 \end{aligned}$$

2. *Undo stable completion*

$$\forall m \in \mathcal{M}(j), \quad \begin{cases} u_{j+1,k} \; -= \; s_{j,k,m} r_{j,m} & \forall k \in A(j,m) \\ u_{j+1,m'} \; += \; g_{j,m',m} r_{j,m} & \forall m' \in B(j,m) \end{cases}$$

3. *Subdivision*

$$\forall m \in \mathcal{M}(j), \quad u_{j+1,m} += \sum_{k \in N(j,m)} h^{\mathsf{T}}_{j,k,m} u_{j+1,k}$$

5.5.3 Construction procedure for scale-orthogonal wavelets

The procedure for constructing wavelets that are scale orthogonal to the scaling functions with respect to a given bilinear form can then be summarized as follows:

1. For each customized wavelet, $w_{j,m}$ to be constructed at a given level j, start with the corresponding hierarchical basis and assume the neighborhood sets $A(j,m) \subset \mathcal{K}(j)$ and $B(j,m) \subset \mathcal{M}(j)$. This fixes the support of the wavelet. In practice, the sets $A(j,m)$ and $B(j,m)$ are initially chosen such that they contain the set of vertices lying in a one-ring neighborhood around each vertex $m \in \mathcal{M}(j)$.

2. Determine all the scaling functions at level j whose support overlaps that of the wavelet. Let $Q(j,m) = \{k \in \mathcal{K}(j) \text{ s.t. supp } \varphi_{j,k} \bigcap \text{supp } w_{j,m} \neq \emptyset\}$.

3. Compute the local interaction matrix around the wavelet, $\mathbf{K}_G^{\text{loc}} = \left[\mathbf{K}_{B,j}^{\text{loc}} \mid \mathbf{K}_{A,j}^{\text{loc}}\right]$, where:

$$\begin{aligned} \mathbf{K}_{B,j,k,m'}^{\text{loc}} &= a\left(\varphi_{j,k},\ \varphi_{j+1,m'}^{\mathsf{T}}\right) \qquad (k \in Q(j,m) \text{ and } m' \in B(j,m)) \\ \mathbf{K}_{A,j,k,m}^{\text{loc}} &= a\left(\varphi_{j,k},\ \varphi_{j,k'}^{\mathsf{T}}\right) \qquad (k \in Q(j,m) \text{ and } k' \in A(j,m)) \end{aligned}$$

4. The condition on $\{g_{j,m',m}\}_{m' \in B(j,m)}$ and $\{s_{j,k,m}\}_{k \in A(j,m)}$ for scale-orthogonality is:

$$\mathbf{K}_{G,j}^{\text{loc}}\, \mathbf{G}_j^{\text{loc}} = \mathbf{0} \tag{5.21a}$$

where

$$\mathbf{G}_j^{\text{loc}} = \left[\begin{array}{c} g_{j,0,m} \\ g_{j,1,m} \\ \vdots \\ \hline s_{j,0,m} \\ s_{j,1,m} \\ \vdots \end{array}\right] \tag{5.21b}$$

The filters can therefore be computed easily using techniques for computing a basis for the null space of the local interaction matrix, $\mathbf{K}_{G,j}^{\text{loc}}$ such as row-reduced echelon form reduction or singular-value decomposition.

5. If the matrix $\mathbf{K}_{G,j}^{\text{loc}}$ is non-singular, then there do not exist any scale-orthogonal wavelets with the assumed support. The support is therefore extended by considering a larger neighborhood around each vertex (in practice, a two-ring of vertices around each vertex in the set $\mathcal{M}(j)$)

The following lemma ensures that wavelets computed using the above procedure are linearly independent from the scaling functions (i.e., the resulting columns in the $\mathbf{G}_j$ matrix are linearly independent):

Lemma 5.1. *If $w_{j,m}$ is the set of wavelets constructed using the null-space procedure, Eq (5.21a) then the scale-orthogonal wavelets are linearly independent from the scaling functions $\varphi_{j,k}$, $(k \in \mathcal{K}(j))$.*

Proof. Assume the contrary, i.e., assume that there exists a set of solutions where the columns of the matrix $\mathbf{G}_j^{\text{loc}}$ are linearly independent, but the submatrix corresponding to the coefficients g_j does not have linearly independent columns. By taking suitable linear combinations of the g_j filters, we can therefore construct a set of wavelets $w_{j,m}$ of the form:

$$w_{j,m} = \sum_{k \in B(j,m)} s_{j,k,m}^{\mathsf{T}} \varphi_{j,k} \tag{5.22}$$

satisfying

$$a\left(\varphi_{j,k'},\ w_{j,m}^{\mathsf{T}}\right) = 0 \quad (k' \in Q(j,m)) \quad \text{or} \tag{5.23a}$$

$$\sum_{y \in B(j,k)} a\left(\varphi_{j,k'}, \varphi_{j,k}^{\mathsf{T}}\right) s_j = 0 \quad (k' \in Q(j,m)) \tag{5.23b}$$

Clearly this is not possible since (a) $B(j,k) \subsetneq Q(j,k)$, (b) the inner-product $a(\cdot,\cdot)$ is symmetric, positive definite and (c) the "interior" scaling functions $\varphi_{j,k}$, $k \in B(j,m)$ vanish along the boundary of supp $w_{j,m}$. □

As an example of constructing scale-orthogonal wavelets by computing the null-space of the local interaction matrix, let the bilinear form correspond to that of the Poisson's Equation in two dimensions:

$$a\left(u,v\right) = \int_{\Omega} \nabla u \cdot \nabla v \, \mathrm{d}\Omega \tag{5.24}$$

and select the scaling functions to be the piecewise bilinear finite element interpolation functions. It is easily shown that on tensor-product discretizations, the hierarchical basis functions centered on the newly introduced vertices on the element faces are scale-orthogonal to the scaling functions with respect to the $a\left(\cdot,\cdot\right)$ inner-product. However, the hierarchical basis functions centered on the edges are not scale-orthogonal and the null-space computation procedure described above can be used to customize scale-orthogonal wavelets centered around the edge vertices. Figures 5-5 (b) and (c) illustrate two such wavelets centered respectively on edge vertices in the interior and next to a Dirichlet boundary.

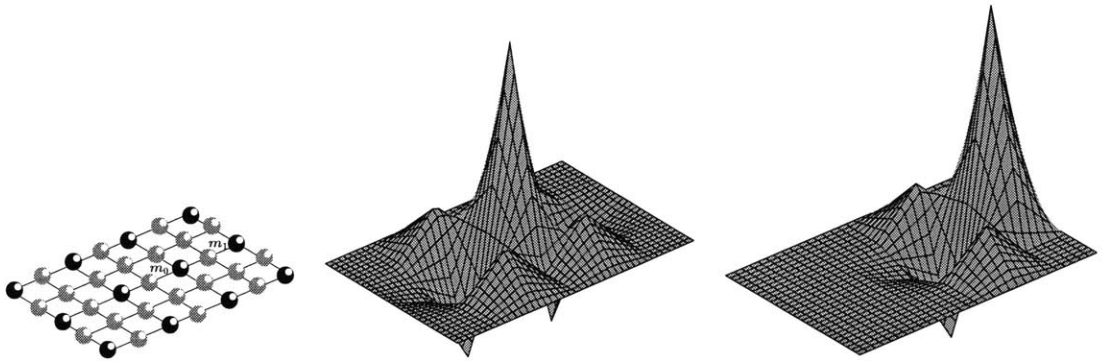

(a) (b) (c)

Figure 5-5: (a) Support of scale-orthogonal wavelets centered on edge vertices; (b) Scale-orthogonal wavelets associated with the interior vertex m_0 and (c) Scale-orthogonal wavelets associated with the boundary vertex m_1

We consider more complex examples (for instance, the biharmonic operator) in Chapter 7.

5.6 Scale-orthogonal wavelets using Gram-Schmidt orthogonalization

In constructing scale-orthogonal wavelets using the stable completion approach, the choice of filters, g_j and s_j for each wavelet is clearly non-unique since they are obtained by solving a homogeneous system of equations. To avoid solving a homogeneous system of equations it suffices to choose the filters g_j such that they satisfy the invertibility conditions described in Section 5.5.1; the filters s_j can then be determined by imposing the scale-orthogonality conditions and solving a linear system of equations. A particularly convenient and valid choice of the filters g_j is $g_{j,m',m} = \delta_{m',m}$ which results in the following equation for the customized wavelets:

$$w_{j,m} = \varphi_{j+1,m} - \sum_{k \in A(j,m)} s^{\mathsf{T}}_{j+1,k,m} \varphi_{j,k}, \tag{5.25a}$$

which can be written in vector form as:

$$w_j = w_j^{\mathrm{HB}} - \mathbf{S}_{j+1}^{\mathsf{T}} \varphi_j \tag{5.25b}$$

Note that Eqs (5.25a) and (5.25b) amount to performing a Gram-Schmidt orthogonalization of the hierarchical basis functions and scaling functions with respect to tha $a(\cdot,\cdot)$ inner-product. The filter matrix $\mathbf{S}_{j+1}$ is then obtained by solving:

$$\sum_{k \in A(j,m)} a\left(\varphi_{j,k'}, \varphi_{j,k}^{\mathsf{T}}\right) s_{j,k,m} = a\left(\varphi_{j,k'}, \varphi_{j+1,m}^{\mathsf{T}}\right) \quad (k' \in \mathcal{K}(j)) \quad \text{or} \tag{5.26a}$$

$$\mathbf{K}_j \quad \mathbf{S}_{j+1} = \mathbf{B}_{j+1}^{\mathrm{HB}}, \tag{5.26b}$$

where $\mathbf{B}_{j+1}^{\mathrm{HB}}$ represents the hierarchical basis interaction matrix.

For wavelets constructed using Gram-Schmidt orthogonalization, it is possible to assign the following interpretation of the detail matrix, $\mathbf{C}_{j+1}$ and right-hand side, g_j:

Lemma 5.2. *If the scale-orthogonal wavelets are constructed using Gram-Schmidt orthogonalization then the detail matrix corresponding to the orthogonalized wavelets is the Schur's complement of the hierarchical basis detail matrix and the right-hand side corresponds to the residual of the finite element solution, u_j at level $j+1$, i.e.,*

$$\mathbf{C}_{j+1} = \mathbf{C}_{j+1}^{HB} - \left(\mathbf{B}_{j+1}^{HB}\right)^{\mathsf{T}} \mathbf{K}_j \mathbf{B}_{j+1}^{HB} \quad \textit{and,} \tag{5.27a}$$

$$g_j = g_j^{HB} - \left(\mathbf{B}_{j+1}^{HB}\right)^{\mathsf{T}} u_j \tag{5.27b}$$

Proof. We have,

$$\begin{aligned}
\mathbf{C}_{j+1} &= a\left(w_j, w_j^{\mathsf{T}}\right) \\
&= a\left(w_j^{\mathrm{HB}}, \left(w_j^{\mathrm{HB}}\right)^{\mathsf{T}}\right) - a\left(w_j^{\mathrm{HB}}, \varphi_j^{\mathsf{T}}\right) \mathbf{S}_{j+1} - \mathbf{S}_{j+1}^{\mathsf{T}} a\left(\varphi_j, \left(w_j^{\mathrm{HB}}\right)^{\mathsf{T}}\right) + \mathbf{S}_{j+1}^{\mathsf{T}} a\left(\varphi_j, \varphi_j^{\mathsf{T}}\right) \mathbf{S}_{j+1} \\
&= \mathbf{C}_{j+1}^{\mathrm{HB}} - \left(\mathbf{B}_{j+1}^{\mathrm{HB}}\right)^{\mathsf{T}} \mathbf{S}_{j+1} - \mathbf{S}_{j+1}^{\mathsf{T}} \mathbf{B}_{j+1}^{\mathrm{HB}} + \mathbf{S}_{j+1}^{\mathsf{T}} \mathbf{K}_j \mathbf{S}_{j+1} \\
&= \mathbf{C}_{j+1}^{\mathrm{HB}} - \left(\mathbf{B}_{j+1}^{\mathrm{HB}}\right)^{\mathsf{T}} \mathbf{K}_j^{-1} \mathbf{B}_{j+1}^{\mathrm{HB}} - \left(\mathbf{B}_{j+1}^{\mathrm{HB}}\right)^{\mathsf{T}} \mathbf{K}_j^{-1} \mathbf{B}_{j+1}^{\mathrm{HB}} + \left(\mathbf{B}_{j+1}^{\mathrm{HB}}\right)^{\mathsf{T}} \mathbf{K}_j^{-1} \mathbf{K}_j \mathbf{K}_j^{-1} \mathbf{B}_{j+1}^{\mathrm{HB}} \\
&= \mathbf{C}_{j+1}^{\mathrm{HB}} - \left(\mathbf{B}_{j+1}^{\mathrm{HB}}\right)^{\mathsf{T}} \mathbf{K}_j \mathbf{B}_{j+1}^{\mathrm{HB}}
\end{aligned} \tag{5.28}$$

Similarly,

$$\begin{aligned} g_j &= l\left(w_j\right) \\ &= l\left(w_j^{\mathrm{HB}}\right) - \mathbf{S}_{j+1}^{\mathsf{T}} l\left(\varphi_j\right) \\ &= g_j^{\mathrm{HB}} - \mathbf{B}_{j+1}^{\mathrm{HB}} \mathbf{K}_j^{-1} f_j \\ &= g_j^{\mathrm{HB}} - \mathbf{B}_{j+1}^{\mathrm{HB}} u_j \end{aligned} \tag{5.29}$$

exactly as desired. □

5.7 Adaptive refinement and approximate Gram-Schmidt orthogonalization

The main disadvantage of constructing scale-orthogonal wavelets using a Gram-Schmidt procedure is that solving for the orthogonalization coefficients exactly involves the solution of a global system of equations at each level and the resulting wavelets often have global support (this is especially true in higher dimensions). In the case of the L^2 inner-product considered for instance by Vassilevski and Wang [48], Aksoylu and Holst [2] or Lounsbery, et al. [35], the coefficient matrix to be inverted in Eq (5.26b) corresponds to the nodal finite-element mass matrix, which is very well-conditioned, see Eq (4.14). The filters may therefore be computed efficiently by approximately solving the system of equations using only a few iterations of an inexpensive iterative solver like Gauss-Seidel or Jacobi. For more general bilinear forms such as the weak-forms corresponding to partial differential operators, such simplifications may not apply and computation of the coefficients, $\mathbf{S}_{j+1}$ at each level can be prohibitively expensive, particularly in the case of uniform refinement where the degrees of freedom at each level grow geometrically [52].

However, in the case of adaptive refinement where only a few wavelets are typically added at each level of discretization, the scale-orthogonal wavelets may be efficiently constructed using the following *approximate* Gram-Schmidt orthogonalization procedure:

$$w_j = w_j^{\mathrm{HB}} - \mathbf{S}_{0,j+1}^{\mathsf{T}} \varphi_0 - \sum_{i=0}^{j-1} \mathbf{S}_{i+1,j+1}^{\mathsf{T}} w_i \tag{5.30}$$

since the orthogonalization coefficients at each level $i < j$ can be computed in an entirely scale-decoupled manner by solving a small system of equations of the form:

$$\mathbf{C}_{i+1}\, \mathbf{S}_{i+1,j+1} = \mathbf{B}_{i+1,j+1} \quad i = -1, \ldots, j-1 \tag{5.31}$$

where $\mathbf{C}_0 = \mathbf{K}_0$, $\mathbf{B}_{0,j+1} = a\left(\varphi_0, \left(w_j^{\mathrm{HB}}\right)^{\mathsf{T}}\right)$ and $\mathbf{B}_{i+1,j+1} = a\left(w_i, \left(w_j^{\mathrm{HB}}\right)^{\mathsf{T}}\right)$.

In the uniform refinement setting, Eq (5.25b) and Eq (5.30) are of course entirely equivalent. However, this is not the case in an adaptive refinement setting, since Eq (5.25b) ensures that the wavelets at level j are orthogonal to *all* wavelets at the coarser level (irrespective of whether they are used for computing the solution or not), whereas Eq (5.30) ensures that the wavelets at level j are orthogonal *only* to those wavelets at the coarser level which are actually used for computing the solution. This subtle difference becomes important in the *a priori* analysis of the error estimation techniques proposed in Chapter 6.

5.7.1 On the efficient implementation of approximate Gram-Schmidt orthogonalization

Directly computing the inner-products of the hierarchical basis functions with the orthogonalized wavelets, $\mathbf{B}_{i+1,j+1}$ in Eq (5.31) can be very inconvenient in practice since the bilinear form $a(\cdot,\cdot)$ might involve integrals of a large number of terms as in the analysis of plates and shells. In this section, we therefore propose an algorithm for computing the orthogonalization coefficients $\mathbf{S}_{i+1,j+1}$ and the detail matrices $\mathbf{C}_{j+1}$ at level j, cf. Eq (5.31), starting with the hierarchical basis interaction and detail matrices

$$\mathbf{B}_{i+1,j+1}^{\mathrm{HB}} = a\left(w_i^{\mathrm{HB}}, \left(w_j^{\mathrm{HB}}\right)^{\mathsf{T}}\right), \quad i < j \tag{5.32a}$$

$$\mathbf{C}_{j+1}^{\mathrm{HB}} = a\left(w_j^{\mathrm{HB}}, \left(w_j^{\mathrm{HB}}\right)^{\mathsf{T}}\right) \tag{5.32b}$$

which, in contrast are extremely easy to assemble in an element-wise fashion (see for example, the implementation techinque described in [44]). Our construction procedure relies on the following close connection between Gram-Schmidt orthogonalization and $\mathbf{LDL}^{\mathsf{T}}$ factorization of the Grammian matrix for general inner-product spaces:

Lemma 5.3. *Let $\{\phi_i\}_{i=1}^N$ be a collection of N sets of linearly independent functions in an inner-product space V equipped with an inner-product $b(\cdot,\cdot)$. Let the block matrices $\mathbf{A}_{i,j} = b\left(\phi_i, \phi_j^{\mathsf{T}}\right)$ denote the interactions of these basis function sets and let*

$$\mathbf{A} = \begin{bmatrix} \mathbf{A}_{1,1} & \mathbf{A}_{1,2} & \cdots & \mathbf{A}_{1,N} \\ \mathbf{A}_{1,2}^{\mathsf{T}} & \mathbf{A}_{2,2} & \cdots & \mathbf{A}_{2,N} \\ \vdots & \vdots & \ddots & \vdots \\ \mathbf{A}_{1,N}^{\mathsf{T}} & \mathbf{A}_{2,N}^{\mathsf{T}} & \cdots & \mathbf{A}_{N,N} \end{bmatrix} \tag{5.33}$$

denote the overall Grammian matrix. Let $\{\psi_i\}_{i=1}^N$ denote the set of orthogonal basis functions constructed via a Gram-Schmidt orthogonalization procedure, i.e.,

$$\psi_1 = \phi_1 \quad \textit{and} \tag{5.34a}$$

$$\psi_j = \phi_j - \sum_{i=1}^{j-1} \mathbf{S}_{i,j}^{\mathsf{T}} \psi_i \quad j > 1 \tag{5.34b}$$

such that $b\left(\psi_i, \psi_j^{\mathsf{T}}\right) = 0,\ i \neq j$. Then, the matrix $\mathbf{A}$ may be decomposed as

$$\mathbf{A} = \mathbf{LDL}^{\mathsf{T}} \tag{5.35a}$$

where $\mathbf{L}$ is a lower triangular matrix of the form

$$\mathbf{L} = \begin{bmatrix} \mathbf{I} & & & \\ \mathbf{S}_{1,2}^{\mathsf{T}} & \mathbf{I} & & \\ \vdots & \vdots & \ddots & \\ \mathbf{S}_{1,N}^{\mathsf{T}} & \mathbf{S}_{2,N}^{\mathsf{T}} & \cdots & \mathbf{I} \end{bmatrix} \tag{5.35b}$$

containing the orthogonalization coefficients and $\mathbf{D}$ *is a block-diagonal matrix of the form*

$$\mathbf{D} = \begin{bmatrix} \mathbf{C}_1 & & & \\ & \mathbf{C}_2 & & \\ & & \ddots & \\ & & & \mathbf{C}_N \end{bmatrix} \tag{5.35c}$$

with $\mathbf{C}_i = b\left(\psi_i, \psi_i^{\mathsf{T}}\right)$ *. Gaussian elimination on the Grammian matrix is therefore equivalent to performing Gram-Schmidt orthgonalization on the existing set of basis functions.*

Proof. We use the convention that matrix entries not explicitly shown are assumed to be 0. First, we create functions that are orthogonal only with respect to ϕ_1:

$$\psi_j = \phi_j - \mathbf{S}_{1,j}^{\mathsf{T}} \psi_1 \quad j \geq 2 \tag{5.36}$$

where $\mathbf{A}_{1,j} = \mathbf{S}_{1,j}\mathbf{C}_1 = \mathbf{S}_{1,j}\mathbf{A}_{1,1}$. Using an approach similar to Lemma 5.2 the inner products of the orthogonalized basis functions are then given as

$$\mathbf{A}_{i,j} = b\left(\psi_i, \psi_j^{\mathsf{T}}\right) = \mathbf{A}_{i,j} - \mathbf{S}_{1,i}^{\mathsf{T}} \mathbf{A}_{1,j}, \; i \geq 2, \; j \geq i \tag{5.37}$$

with $\mathbf{C}_2 = \mathbf{A}_{2,2}$ and therefore

$$\underbrace{\begin{bmatrix} \mathbf{C}_1 & & & \\ & \mathbf{C}_2 & \cdots & \mathbf{A}_{2,N} \\ & \vdots & \ddots & \vdots \\ & \mathbf{A}_{2,N}^{\mathsf{T}} & \cdots & \mathbf{A}_{N,N} \end{bmatrix}}_{\mathbf{D}_1} = \underbrace{\begin{bmatrix} \mathbf{I} & & & \\ -\mathbf{S}_{1,2}^{\mathsf{T}} & \mathbf{I} & & \\ \vdots & & \ddots & \\ -\mathbf{S}_{1,N}^{\mathsf{T}} & & & \mathbf{I} \end{bmatrix}}_{\mathbf{S}_1^{-\mathsf{T}}} \underbrace{\begin{bmatrix} \mathbf{A}_{1,1} & \mathbf{A}_{1,2} & \cdots & \mathbf{A}_{1,N} \\ \mathbf{A}_{1,2}^{\mathsf{T}} & \mathbf{A}_{2,2} & \cdots & \mathbf{A}_{2,N} \\ \vdots & \vdots & \ddots & \vdots \\ \mathbf{A}_{1,N}^{\mathsf{T}} & \mathbf{A}_{2,N}^{\mathsf{T}} & \cdots & \mathbf{A}_{N,N} \end{bmatrix}}_{\mathbf{A}} \underbrace{\begin{bmatrix} \mathbf{I} & -\mathbf{S}_{1,2} & \cdots & -\mathbf{S}_{1,N} \\ & \mathbf{I} & & \\ & & \ddots & \\ & & & \mathbf{I} \end{bmatrix}}_{\mathbf{S}_1^{-1}} \tag{5.38}$$

or since $\mathbf{S}_1$ is a unit upper-triangular matrix,

$$\mathbf{A} = \mathbf{S}_1^{\mathsf{T}} \, \mathbf{D}_1 \, \mathbf{S}_1 \tag{5.39}$$

Now, given $1 < i \leq N$ assume that the functions $\psi_j, j = i, \ldots, N$ are orthogonalized with respect to the functions $\psi_k, k = 1, \ldots, i-1$. On orthogonalization of $\psi_j, j = i+1, \ldots, N$

with respect to ψ_i we have:

$$\begin{bmatrix} \mathbf{C}_i & \mathbf{A}_{i,i+1} & \cdots & \mathbf{A}_{i,N} \\ \mathbf{A}_{i,i+1}^{\mathsf{T}} & \mathbf{A}_{i+1,i+1} & \cdots & \mathbf{A}_{i+1,N} \\ \vdots & \vdots & \ddots & \vdots \\ \mathbf{A}_{i,N}^{\mathsf{T}} & \mathbf{A}_{i+1,N}^{\mathsf{T}} & \cdots & \mathbf{A}_{N,N} \end{bmatrix} = \begin{bmatrix} \mathbf{I} & & & \\ \mathbf{S}_{i,i+1}^{\mathsf{T}} & \mathbf{I} & & \\ \vdots & & \ddots & \\ \mathbf{S}_{i,N}^{\mathsf{T}} & & & \mathbf{I} \end{bmatrix} \begin{bmatrix} \mathbf{C}_i & & & \\ & \mathbf{C}_{i+1} & \cdots & \mathbf{A}_{i+1,N} \\ & \vdots & \ddots & \vdots \\ & \mathbf{A}_{i+1,N}^{\mathsf{T}} & \cdots & \mathbf{A}_{N,N} \end{bmatrix} \begin{bmatrix} \mathbf{I} & \mathbf{S}_{i,i+1} & \cdots & \mathbf{S}_{i,N} \\ & \mathbf{I} & & \\ & & \ddots & \\ & & & \mathbf{I} \end{bmatrix}, \tag{5.40}$$

where $\mathbf{S}_{i,j} = \mathbf{C}_i^{-1}\mathbf{A}_{i,j}, j = i+1, \ldots, N$. Now observe that

$$\underbrace{\begin{bmatrix} \mathbf{C}_1 & & & & \\ & \ddots & & & \\ & & \mathbf{C}_i & \mathbf{A}_{i,i+1} & \cdots & \mathbf{A}_{i,N} \\ & & \mathbf{A}_{i,i+1}^{\mathsf{T}} & \mathbf{A}_{i+1,i+1} & \cdots & \mathbf{A}_{i+1,N} \\ & & \vdots & \vdots & \ddots & \vdots \\ & & \mathbf{A}_{i,N}^{\mathsf{T}} & \mathbf{A}_{i+1,N}^{\mathsf{T}} & \cdots & \mathbf{A}_{N,N} \end{bmatrix}}_{\mathbf{D}_{i-1}} = \underbrace{\begin{bmatrix} \mathbf{I} & & & & \\ & \ddots & & & \\ & & \mathbf{I} & & & \\ & & \mathbf{S}_{i,i+1}^{\mathsf{T}} & \mathbf{I} & & \\ & & \vdots & & \ddots & \\ & & \mathbf{S}_{i,N}^{\mathsf{T}} & & & \mathbf{I} \end{bmatrix}}_{\mathbf{S}_i^{\mathsf{T}}} \times \underbrace{\begin{bmatrix} \mathbf{C}_1 & & & & \\ & \ddots & & & \\ & & \mathbf{C}_i & & & \\ & & & \mathbf{C}_{i+1} & \cdots & \mathbf{A}_{i+1,N} \\ & & & \vdots & \ddots & \vdots \\ & & & \mathbf{A}_{i+1,N}^{\mathsf{T}} & \cdots & \mathbf{A}_{N,N} \end{bmatrix}}_{\mathbf{D}_i} \times$$

$$\underbrace{\begin{bmatrix} \mathbf{I} & & & & \\ & \ddots & & & \\ & & \mathbf{I} & \mathbf{S}_{i,i+1} & \cdots & \mathbf{S}_{i,N} \\ & & & \mathbf{I} & & \\ & & & & \ddots & \\ & & & & & \mathbf{I} \end{bmatrix}}_{\mathbf{S}_i} \tag{5.41}$$

and therefore,

$$\mathbf{A} = \mathbf{S}_1^{\mathsf{T}}\,\mathbf{D}_1\,\mathbf{S}_1 = \mathbf{S}_1^{\mathsf{T}}\mathbf{S}_2^{\mathsf{T}}\,\mathbf{D}_2\,\mathbf{S}_2\mathbf{S}_1 \cdots = \mathbf{S}_1^{\mathsf{T}}\mathbf{S}_2^{\mathsf{T}} \cdots \mathbf{S}_{N-1}^{\mathsf{T}}\,\mathbf{D}_{N-1}\,\mathbf{S}_{N-1} \cdots \mathbf{S}_2\mathbf{S}_1 \tag{5.42}$$

Finally, notice that $\mathbf{L} = \mathbf{S}_1^{\mathsf{T}}\mathbf{S}_2^{\mathsf{T}} \cdots \mathbf{S}_{N-1}^{\mathsf{T}}$, $\mathbf{D} = \mathbf{D}_{N-1}$ and therefore $\mathbf{A} = \mathbf{L}\mathbf{D}\mathbf{L}^{\mathsf{T}}$ as desired.

□

Remark. In the above proof, we did not explicitly prove that the block matrices $\mathbf{C}_i$ are strictly positive definite (and therefore the coefficients $\mathbf{S}_i$ are bounded). However, observe that the assumption that the function sets are linearly independent implies that the spaces spanned by them have the direct sum property. Therefore, we can derive explicit bounds on the eigenvalues of these matrices based on the strengthened Cauchy-Schwarz inequality. From the analysis of Riesz stability, Section 5.9, this therefore means that the minimum eigenvalue of each of the $\mathbf{C}_i$ matrices is bounded away from 0.

Lemma 5.3 is particularly useful in cases where computing the original Grammian is straightforward, but computing the intermediate inner products, $b\left(\phi_j, \psi_i^{\mathsf{T}}\right)$, $i < j$ is highly

inconvenient since one can then simply start with the original Grammian matrix and compute the orthogonalization coefficients using Gauss elimination. This is exactly the case with the construction of scale-orthogonal wavelets by Gram-Schmidt orthogonalization of the hierarchical basis. The next theorem is a straightforward extension of Lemma 5.3 to the space of hierarchical basis functions.

Theorem 5.4. *The construction of scale-orthogonal wavelets using Gram-Schmidt orthogonalization amounts to performing a block* $\mathbf{LDL}^{\mathsf{T}}$ *-type factorization of the hierarchical basis stiffness matrix,* $\hat{\mathbf{K}}_{j+1}^{HB}$ *where the blocks correspond to the degrees of freedom added at each level. The orthogonalization coefficients* $\mathbf{S}_{i,k}$ *are the entries in the triangular matrix,* $\mathbf{L}_{j+1}$*, and the detail matrices at each level are the entries in the block-diagonal multilevel stiffness matrix matrix,* $\hat{\mathbf{K}}_{j+1}$ *corresponding to the scale-orthogonal wavelets. Further, if* $\mathbf{W}_{j+1}^{HB}$ *denotes the wavelet transform matrix corresponding to hierarchical basis functions, then* $\hat{\mathbf{K}}_{j+1}$ *can be computed from the nodal finite element stiffness matrix stiffness matrix,* $\mathbf{K}_{j+1}$ *as*

$$\hat{\mathbf{K}}_{j+1} = \left(\mathbf{L}_{j+1}^{\mathsf{T}}\mathbf{W}_{j+1}^{HB}\right)^{-\mathsf{T}} \mathbf{K}_{j+1} \left(\mathbf{L}_{j+1}^{\mathsf{T}}\mathbf{W}_{j+1}^{HB}\right)^{-1} \tag{5.43}$$

Proof. The first part of the theorem follows from Lemma 5.3 simply by setting the inner-product, $b(\cdot,\cdot) = a(\cdot,\cdot)$ corresponding to the operator bilinear form, $N = j+1$, $\phi_1 = \varphi_0$ and $\phi_i = w_{i-1}^{\mathrm{HB}}$, $i = 1,\ldots,j+1$ and observing that the Grammian now corresponds to the hierarchical basis stiffness matrix at level $j+1$, $\hat{\mathbf{K}}_{j+1}^{\mathrm{HB}}$. Now, $\hat{\mathbf{K}}_{j+1}^{\mathrm{HB}}$ may be obtained from the single-level finite element stiffness matrix at level $j+1$ as

$$\hat{\mathbf{K}}_{j+1}^{\mathrm{HB}} = \left(\mathbf{W}_{j+1}^{\mathrm{HB}}\right)^{-\mathsf{T}} \mathbf{K}_{j+1} \left(\mathbf{W}_{j+1}^{\mathrm{HB}}\right)^{-1} \tag{5.44}$$

Further, by Lemma 5.3, $\hat{\mathbf{K}}_{j+1}^{\mathrm{HB}}$ can be decomposed as

$$\hat{\mathbf{K}}_{j+1}^{\mathrm{HB}} = \mathbf{L}_{j+1}\hat{\mathbf{K}}_{j+1}\mathbf{L}_{j+1}^{\mathsf{T}} \tag{5.45a}$$

where

$$\mathbf{L}_{j+1}^{\mathsf{T}} = \begin{bmatrix} \mathbf{I} & \mathbf{S}_{0,1} & \cdots & \mathbf{S}_{0,j+1} \\ & \mathbf{I} & \cdots & \mathbf{S}_{1,j+1} \\ & & \ddots & \mathbf{S}_{j,j+1} \\ & & & \mathbf{I} \end{bmatrix} \tag{5.45b}$$

is the (unit upper-triangular) matrix of orthogonalization coefficients and

$$\hat{\mathbf{K}}_{j+1} = \begin{bmatrix} \mathbf{K}_0 & & & \\ & \mathbf{C}_1 & & \\ & & \ddots & \\ & & & \mathbf{C}_{j+1} \end{bmatrix} \tag{5.45c}$$

is the block-diagonal stiffness matrix corresponding to the scale-orthogonal wavelets. Therefore

$$\hat{\mathbf{K}}_{j+1} = (\mathbf{L}_{j+1})^{-1} \hat{\mathbf{K}}_{j+1}^{\text{HB}} \mathbf{L}_{j+1}^{-\mathsf{T}} = \left(\mathbf{L}_{j+1}^{\mathsf{T}} \mathbf{W}_{j+1}^{\text{HB}}\right)^{-\mathsf{T}} \mathbf{K}_{j+1} \left(\mathbf{L}_{j+1}^{\mathsf{T}} \mathbf{W}_{j+1}^{\text{HB}}\right)^{-1}$$

exactly as required. □

We now present two versions of the algorithm for computing the orthogonalization coefficients $\mathbf{S}_{i+1,j+1} (i < j)$ and detail matrix $\mathbf{C}_{j+1}$ corresponding to the scale-orthogonal wavelets at level j using Lemma 5.3. Observe how each approach updates the coefficients and the detail matrices corresponding only to the newly introduced degrees of freedom at level $j + 1$. Also note that in the algorithms described Gram-Schmidt orthogonalization is carried out at all levels upto level 0. In practice, we can choose to perform orthogonalization only upto a certain fixed number of levels.

5.7.1.1 Version 1 (Requiring auxilliary storage)

In this first version, Algorithm 1, the orthogonalization coefficients and the detail matrix are computed out of place, i.e., the interaction matrices, $\mathbf{B}_{i+1,j+1}^{\text{HB}}$, $i < j$ and the detail matrix $\mathbf{C}_{j+1}^{\text{HB}}$ are not overwritten respectively with the coefficients $\mathbf{S}_{i+1,j+1}$, $i < j$ and the detail matrix $\mathbf{C}_{j+1}$. The function `BackSolve` is simply a function to solve a system of equation given the Cholesky factor of the coefficient matrix, whereas the function `Cholesky`

returns the Cholesky factorization of a symmetric, positive definite matrix.

Input: Interaction matrices $\mathbf{B}^{\text{HB}}_{i+1,j+1}, i = -1, \ldots, j-1$ and detail matrix $\mathbf{C}^{\text{HB}}_{j+1}$ corresponding to hierarchical basis functions introduced at level j.
Output: The orthogonalization coefficients, $\mathbf{S}_{i+1,j+1}$ and the Cholesky factor of the detail matrix, $\mathbf{C}_{j+1}$ corresponding to the orthogonalized wavelets.

```
// Initialize B_{i+1,j+1}, i = -1,...,j-1
for i ← -1 to j - 1 do
    B_{i+1,j+1} ⟵ B^{HB}_{i+1,j+1} ;
end
// Initialize C_{j+1}
C_{j+1} ⟵ C^{HB}_{j+1} ;
for i ← -1 to j - 1 do
    // Compute orthogonalization coefficients
    S_{i+1,j+1} ⟵ BackSolve(C_{i+1}, B_{i+1,j+1});
    for k ← i + 1 to j - 1 do
        // Update interaction matrices at the finer levels
        B_{k+1,j+1} ⟵ B_{k+1,j+1} - S^T_{i+1,k+1} B_{i+1,j+1};
    end
    // Update decoupled stiffness matrix at level j
    C_{j+1} ⟵ C_{j+1} - S^T_{i+1,j+1} B_{i+1,j+1};
end
// Replace updated stiffness matrix with its Cholesky
   factor
C_{j+1} ⟵ Cholesky(C_{j+1});
```

Algorithm 1: Algorithm for efficiently computing the orthogonalization coefficients and factorizing the detail matrices when the wavelets are constructed using Gram-Schmidt orthogonalization. This version requires storage for the orthogonalization coefficients as well as the final decoupled stiffness matrix.

5.7.1.2 Version 2 (Not requiring auxilliary storage)

In the second version, Algorithm 2, we overwrite the hierarchical basis interaction matrices $\mathbf{B}^{\text{HB}}_{i+1,j+1}$, $i < j$ with the orthogonalization coefficients $\mathbf{S}_{i+1,j+1}$, $i < j$ and the hierarchical basis detail matrix $\mathbf{C}^{\text{HB}}_{j+1}$ with the Cholesky factor of the detail matrix $\mathbf{C}_{j+1}$ corresponding to the orthogonalized wavelets. Observe the similarity between this version and the active-column solver described in Bathe [10].

Input: Interaction matrices $\mathbf{B}^{\mathrm{HB}}_{i+1,j+1}, i = -1, \ldots, j-1$ and detail matrix $\mathbf{C}^{\mathrm{HB}}_{j+1}$ corresponding to hierarchical basis functions introduced at level j

Output: The orthogonalization coefficients and the Cholesky factor of the detail matrix corresponding to the orthogonalized wavelets. The interaction matrices, $\mathbf{B}_{i+1,j+1}$ are replaced by the corresponding matrix of orthogonalization coefficients, $\mathbf{S}_{i+1,j+1}$ and the hierarchical basis detail matrix, $\mathbf{C}^{\mathrm{HB}}_{j+1}$ is replaced by the Cholesky factor of the detail matrix, $\mathbf{C}_{j+1}$ corresponding to the scale-orthogonal wavelets.

for $i \leftarrow -1$ **to** $j-1$ **do**
  // Compute orthogonalization coefficients
  $\mathbf{S}_{i+1,j+1} \longleftarrow$ BackSolve $(\mathbf{C}_{i+1}, \mathbf{B}_{i+1,j+1})$;
  for $k \leftarrow i+1$ **to** $j-1$ **do**
    // Update interaction matrices
    $\mathbf{B}_{k+1,j+1} \longleftarrow \mathbf{B}_{k+1,j+1} - \mathbf{B}^{\mathsf{T}}_{i+1,k+1}\mathbf{B}_{i+1,j+1}$;
  end
  // Update stiffness matrix at level $j+1$
  $\mathbf{C}_{j+1} \longleftarrow \mathbf{C}_{j+1} - \mathbf{S}^{\mathsf{T}}_{i+1,j+1}\mathbf{B}_{i+1,j+1}$;
  // Replace interaction matrix with matrix of orthogonalization coefficients
  $\mathbf{B}_{i+1,j+1} \longleftarrow \mathbf{S}_{i+1,j+1}$;
end
// Replace updated stiffness matrix with its Cholesky factor
$\mathbf{C}_{j+1} \longleftarrow$ Cholesky$(\mathbf{C}_{j+1})$;

Algorithm 2: Algorithm for efficiently computing the orthogonalization coefficients and factorizing the decoupled stiffness matrix when the wavelets are constructed using Gram-Schmidt orthogonalization. This version of the algorithm requires no auxilliary storage for the orthogonalization coefficients.

5.7.2 Complexity Analysis

We now provide an analysis of Algorithm 1 for the case of adaptive refinement over several levels. There are two cases to be considered: In the first case, the cost of the algorithm is dominated by the cost of computing the filters at the coarsest resolution whereas in the second case, the cost is dominated by computing the filters at the finer resolutions.

Assume that the coarsest level has N degrees of freedom and the stiffness matrix is banded with bandwidth b. Assume that each subsequent level contributes $n \ll N$ degrees of freedom. The cost incurred in assembling and factoring the detail matrix at level j, $\mathbf{C}_{j+1}$ can be split into three parts:

1. Computing the coefficients $\mathbf{S}_{i+1,j+1}$ for $i = -1, 1, \ldots, j-1$

2. Computing the updated interaction matrices and detail matrix at level j, and

3. Factoring $\mathbf{C}_{j+1}$.

Further, since the stiffness matrix at the coarsest level is sparse, for steps (1) and (2), we need to consider the case $i = 0$ separately from the cases $i = 1, \ldots, j-1$. Considering level 0, we have:

1. Computing $\mathbf{S}_{0,j+1} = \mathbf{C}_0^{-1}\mathbf{B}_{0,j+1}^{\mathrm{HB}}$ is $\mathcal{O}(bNn)$ since the matrix $\mathbf{C}_0$ is already factored and hence computing the matrix $\mathbf{S}_{0,j+1}$ only involves elimination and backsubstitution for the n columns of $\mathbf{B}_{0,j+1}^{\mathrm{HB}}$.

2. Consider $\mathbf{B}_{i+1,j+1} = \mathbf{B}_{i+1,j+1} - \mathbf{S}_{0,j+1}^{\mathsf{T}}\mathbf{B}_{0,j+1}^{\mathrm{HB}}$ for each $i = 0, \ldots, j-1$. Since $\mathbf{B}_{0,j+1}^{\mathrm{HB}}$ has very few non-zero entries, computing each entry in $\mathbf{S}_{0,j+1}^{\mathsf{T}}\mathbf{B}_{0,j+1}^{\mathrm{HB}}$ requires only a constant number of operations. Since the matrix $\mathbf{B}_{i+1,j+1}$ is $n \times n$ and j such matrices have to be updated, the overall cost is $\mathcal{O}(jn^2)$.

Now consider all levels $i = 1, \ldots, j-1$:

1. Computing $\mathbf{S}_{i+1,j+1} = \mathbf{C}_{i+1}^{-1}\mathbf{B}_{i+1,j+1}$ for each level i is $\mathcal{O}(n^3)$ since it involves n elimination and back-substitution steps corresponding to n columns of the matrix $\mathbf{B}_{i+1,j+1}$. Hence for all levels from $1, \ldots, j-1$, the cost is $\mathcal{O}(jn^3)$.

2. Computing $\mathbf{B}_{k+1,j+1} = \mathbf{B}_{k+1,j+1} - \mathbf{S}_{i+1,k+1}^{\mathsf{T}}\mathbf{B}_{i+1,j+1}$ for each level is $\mathcal{O}(n^3)$ since the matrices $\mathbf{S}_{i+1,k+1}$ and $\mathbf{B}_{i+1,j+1}$ are both dense in general. Hence over all levels, the complexity is $\mathcal{O}(jn^3)$.

Finally, factoring the matrix $\mathbf{C}_{j+1}$ is $\mathcal{O}(n^3)$.

For the coarsest level to dominate the cost of the algorithm, we require that $bN \gg jn^2$. In this case the cost of adding details at level j is $\mathcal{O}(bNn)$. On the contrary, suppose that a sufficiently high number of refinements have been performed, such that $jn^2 \gg bN$ then the asymptotic complexity at adding details at a level $j \gg 0$ is $\mathcal{O}(jn^3)$.

In contrast to incremental solution using orthogonal wavelets, assume that the hierarchical basis stiffness matrix has to be refactorized after addition of details at each level. The computational cost of factoring the entire stiffness matrix can then be estimated as $\mathcal{O}\left((b+jn)^2\,(N+jn)\right) = \mathcal{O}\left(j^3n^3\right)$ provided j^3n^3 dominates b^2N. Therefore, in factoring the stiffness matrix incrementally, the asymptotic cost is $\mathcal{O}\left(jn^3\right)$ as compared to $\mathcal{O}\left(j^3n^3\right)$ for factoring the entire matrix at each level.

5.8 Decay properties of scale-orthogonal wavelets

It has been observed before (see for example [2, 35, 48]) that scale-orthogonal wavelets in two and three dimensions constructed by Gram-Schmidt orthogonalization of hierarchical basis functions with respect to the L^2 inner product have a global support, but tend to decay rapidly. One might therefore wonder if similar decay properties are also observed in wavelets that are scale-orthogonal with respect to the inner-product induced by the weak form, $a(\cdot,\cdot)$. If so, one would further be interested in deriving bounds for the point-wise value of these wavelets at locations that are far removed from the support of the original hierarchical basis function. In this section, we show that wavelets constructed using the Gram-Schmidt orthogonalization procedure, Eq (5.25b) do in fact decay rapidly and further derive upper bounds for their point-wise values away from the support of the hierarchical basis function.

For a point $x_0 \in \Omega$, let $\mathcal{G}_0$ be the Green's function corresponding to the bilinear form $a(\cdot,\cdot)$, i.e., $\mathcal{G}_0$ satisfies

$$a(\mathcal{G}_0, v) = v(x_0) \quad (v \in V) \tag{5.46}$$

Similarly, for $k \in \mathcal{K}(j)$, let $\mathcal{G}_{j,k}$ be the projection of $\mathcal{G}_k$ onto V_j, i.e., $\mathcal{G}_{j,k}$ satisfies

$$a(\mathcal{G}_{j,k}, v_j) = v_j(x_k) \quad (v_j \in V_j) \tag{5.47}$$

and let $\mathcal{G}_{j,k,k'} \stackrel{\text{def}}{=} \mathcal{G}_{j,k}(x_{k'}),\ k' \in \mathcal{K}(j)$.

Then, if the set of scale-orthogonal wavelets are constructed using Gram-Schmidt orthogonalization, Eq (5.25b) the coefficients $s_{j,k,m}$ in Eq (5.26a) can be expressed using the

coefficients of the projection of the Green's function as

$$s_{j,k,m} = \sum_{k' \in \mathcal{K}(j)} \mathcal{G}_{j,k',k} \mathbf{B}^{\mathrm{HB}}_{j+1,k',m} \tag{5.48}$$

Now, let $N(j,m) \stackrel{\text{def}}{=} \{k \in \mathcal{K}(j) \text{ s.t. } m \in n(j,k)\}$ where the refinement neighborhood $n(j,k)$ is as defined in Eq (3.8). Then due to the compact support of the hierarchical basis, $\mathbf{B}^{\mathrm{HB}}_{j+1,k',m} = 0,\ k' \notin N(j,m)$ and therefore

$$s_{j,k,m} = \sum_{k' \in N(j,m)} \mathcal{G}_{j,k',k} \mathbf{B}^{\mathrm{HB}}_{j+1,k',m} \tag{5.49}$$

For simplicity, we now consider the point-wise value of the scale-orthogonal wavelet $w_{j,m}$ at a point $\tilde{k} \in \mathcal{K}(j) \setminus N(j,m)$. A similar, albeit more involved analysis may be performed for an arbitrary point on the domain outside supp $\varphi_{j+1,m}$. We first have

$$w_{j,m}(x_{\tilde{k}}) = \varphi_{j+1,m}(x_{\tilde{k}}) - \sum_{k \in \mathcal{K}(j)} s_{j,k,m} \varphi_{j,k}(x_{\tilde{k}}) \tag{5.50}$$

From the interpolating property of the scaling functions we have $\varphi_{j+1,m}(x_{\tilde{k}}) = 0$ and $\varphi_{j,k}(x_{\tilde{k}}) = \delta_{k,\tilde{k}}$ and hence from Eq (5.49)

$$\begin{aligned} |w_{j,m}(x_{\tilde{k}})| &= \left| \sum_{k' \in N(j,m)} \mathcal{G}_{j,k',\tilde{k}} \mathbf{B}^{\mathrm{HB}}_{j+1,k',m} \right| \\ &\leq c(m) \max_{k' \in N(j,m)} \left| \mathcal{G}_{j,k',\tilde{k}} \right| \end{aligned} \tag{5.51}$$

where $c(m) = \max_{k' \in N(j,m)} |\mathbf{B}^{\mathrm{HB}}_{j+1,k',m}|$ is a constant that depends only on m. Hence, the point-wise value of the wavelet depends directly upon the projection of the Green's function of the operator. For many operators it is possible to determine the decay of this projection in an *a priori* manner and hence we can further conclude that in such cases one can construct approximately scale-orthogonal wavelets with local support by considering only a small, fixed neighborhood around each new vertex in the subdivided mesh. The construction of such wavelets (and more importantly, analysis of their accuracy and stability properties)

appears to be a promising avenue for further investigation (see also Chapter 8). In the rest of this thesis however, we restrict our attention to the approximately scale-orthogonal wavelets constructed using the procedure outlined in Section 5.7 as they are also very efficient in an adaptive refinement setting and in addition have easily quantifiable accuracy and stability properties.

5.9 Stability properties of scale-orthogonal wavelets

In this section, we derive the stability properties of scale-orthogonal wavelets constructed via Gram-Schmidt orthogonalization and in particular show that the wavelets are Riesz stable in the energy norm. We first define the concept of a E-Riesz stable basis and explain the importance of such a basis in our multilevel approach. Then, we go on to prove a number of norm-equivalence lemmas that will eventually lead to the desired result, Lemma 5.14. Finally, we demonstrate the validity of our results on a model problem.

Definition 5.5 (E-Riesz Stable Basis)**.** A family of basis functions $\left\{\{\phi_{j,m}\}_{m\in\mathcal{M}(j)}\right\}_{j=0}^{\infty}$ is defined to be *E-Riesz stable* if there exist two constants $0 < c_1 \leq c_2 < \infty$ independent of j such that

$$c_1 \sum_{m\in\mathcal{M}(j)} \left\|\rho_{j,m}^{\mathsf{T}}\phi_{j,m}\right\|_{\mathrm{E}}^2 \leq \left\| \sum_{m\in\mathcal{M}(j)} \rho_{j,m}^{\mathsf{T}}\phi_{j,m} \right\|_{\mathrm{E}}^2 \leq c_2 \sum_{m\in\mathcal{M}(j)} \left\|\rho_{j,m}^{\mathsf{T}}\phi_{j,m}\right\|_{\mathrm{E}}^2 \tag{5.52}$$

for any choice of bounded coefficients $\{\rho_{j,m}\}_{m\in\mathcal{M}(j)}$. In the following discussion, we use the terms E-Riesz stable basis and Riesz stable basis interchangeably.

Remark. Our definition of Riesz stability differs slightly from that given in Aksoylu and Holst [2] in that our definition does not depend upon the choice of normalization of the basis functions and applies without any modifications even when the basis functions have different dimensions (e.g. displacements and rotations).

Observe that when the basis functions at the same level j form an a-orthogonal basis for the wavelet spaces, we have $c_1 = c_2 = 1$ and Eq (5.52) reduces to the Pythagorean

theorem:

$$\sum_{m\in\mathcal{M}(j)} \left\|\rho_{j,m}^{\mathsf{T}}\phi_{j,m}\right\|_{\mathrm{E}}^2 = \left\|\sum_{m\in\mathcal{M}(j)} \rho_{j,m}^{\mathsf{T}}\phi_{j,m}\right\|_{\mathrm{E}}^2 \tag{5.53}$$

The ratio of the Riesz constants c_1/c_2 therefore gives an indication of how close a basis is to an a-orthogonal basis for W_j.

In the construction of adaptive multiresolution solvers, we desire that the scale-orthogonal wavelets $w_{j,m},\ m \in \mathcal{M}(j)$ form a Riesz stable basis for the spaces W_j in the energy norm. This is because, for a function $\rho_j = \sum_{m\in\mathcal{M}(j)} \rho_{j,m}^{\mathsf{T}} w_{j,m}$ lying in the space of scale-orthogonal wavelets, the adaptation error incurred by representing ρ_j using wavelets belonging to a set $\mathcal{M}'(j) \subset \mathcal{M}(j)$ can be given as

$$\rho_j - \sum_{m'\in\mathcal{M}'(j)} \rho_{j,m}^{\mathsf{T}} w_{j,m} = \sum_{m''\in\mathcal{M}(j)\setminus\mathcal{M}'(j)} \rho_{j,m}^{\mathsf{T}} w_{j,m} \tag{5.54}$$

If the wavelets are Riesz stable in the energy norm, then the adaptation error in the energy norm can be bounded as

$$c_1 \sum_{m''\in\mathcal{M}(j)\setminus\mathcal{M}'(j)} \left\|\rho_{j,m}^{\mathsf{T}} w_{j,m}\right\|_{\mathrm{E}}^2 \le \left\|\rho_j - \sum_{m'\in\mathcal{M}'(j)} \rho_{j,m}^{\mathsf{T}} w_{j,m}\right\|_{\mathrm{E}}^2 \le c_2 \sum_{m''\in\mathcal{M}(j)\setminus\mathcal{M}'(j)} \left\|\rho_{j,m}^{\mathsf{T}} w_{j,m}\right\|_{\mathrm{E}}^2 \tag{5.55}$$

and hence an adapted solution that is accurate in the energy norm can be obtained simply by retaining only those wavelets that have coefficients with large energy norms.

The ideal situation in an adaptive refinement setting is to have (a) scale-orthogonality (that leads to block-diagonal stiffness matrices) (b) local support of the basis functions (that ensures that the individual blocks are sparse) and (c) Riesz stability in the energy norm (that ensures that the blocks are well-conditioned). The construction procedure described in Section 5.5 enables the construction of wavelets satisfying conditions (a) and (b), but not necessarily (c). Likewise, as shown later in this section wavelets constructed using Gram-Schmidt orthogonalization satisfy conditions (a) and (c), but not necessarily (b). It is not known if there is a practical technique for ensuring all the three properties simultaneously in general. However, since there is no unique way of choosing the filters g_j, it does appear

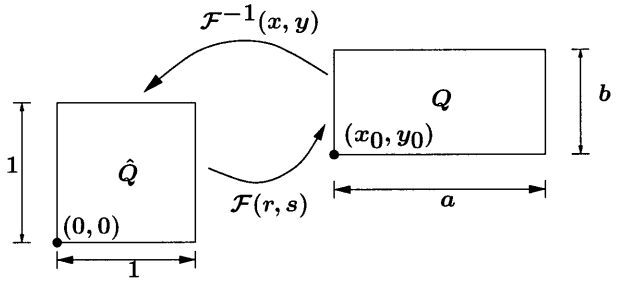

that the *a priori* Riesz stability constraint could be built into the procedure described in Section 5.5.

The derivation of estimates for the Riesz bounds for scale-orthogonal wavelets are based on the use of *inverse* and *oscillatory* estimates (see for instance Yserentant [51]) that are well-established for piecewise linear basis functions. In this section, we first extend those results to higher-order scaling functions (in particular the Bogner-Fox-Schmidt interpolation functions) and then proceed to prove the Riesz stability of the scale-orthogonal wavelets constructed from these interpolating functions.

5.9.1 Derivation of inverse and oscillatory estimates for Bogner-Fox-Schmidt interpolating functions

5.9.1.1 Derivation of inverse estimates

Lemma 5.6. *There exists a constant c, independent of the level of discretization, j such that for any element $v_j \in V_j$,*

$$\|v_j\|_2 \leq c\, 2^{2j}\ \|v_j\|_0 \tag{5.56}$$

Proof. Consider a typical element $Q \in S_{j,v}$ with sides a and b whose coordinate system can be mapped to that of a unit square, $\hat{Q}$, as:

$$x = x_0 + a\, r \tag{5.57a}$$

$$y = y_0 + b\, s \tag{5.57b}$$

For a function $v_j \in V_j$, the $W^{s,2}$ seminorm can be decomposed as

$$|v_j|_s^2 = \sum_{Q \in S_{j,v}} |v_j|_{s;Q}^2 \qquad s = 0, 1, 2. \tag{5.58}$$

First consider

$$|v_j|_{2;Q}^2 = ab \int_{r=0}^{1} \int_{s=0}^{1} \left(\frac{1}{a^2} \hat{v}_{rr} + \frac{2}{ab} \hat{v}_{rs} + \frac{1}{b^2} \hat{v}_{ss} \right)^2 \mathrm{d}r\mathrm{d}s \tag{5.59a}$$

$$= \frac{1}{ab} \int \int \left(\frac{b}{a} \hat{v}_{rr} + 2\, \hat{v}_{rs} + \frac{a}{b} \hat{v}_{ss} \right)^2 \mathrm{d}r\mathrm{d}s \tag{5.59b}$$

$$\leq h^{-2} \mu^2 \, |\hat{v}|_2^2 \tag{5.59c}$$

where h is the minimum edge length and μ is the aspect ratio of the mesh. Now, all norms on the unit square are equivalent. Hence there is a constant c such that $|\hat{v}|_2^2 \leq \|\hat{v}\|_2^2 \leq c \, \|\hat{v}\|_0^2$. But $\|\hat{v}\|_0^2 = \frac{1}{ab} \|v_j\|_{0;Q}^2 \leq h^{-2} \|v_j\|_{0;Q}^2$ and therefore

$$|v_j|_{2;Q}^2 \leq c \, \mu^2 \, h^{-4} \, \|v_j\|_{0;Q}^2 \tag{5.60}$$

Similar analysis for the $W^{1,2}$ semi-norm gives

$$|v_j|_{1;Q}^2 \leq c \, \mu^2 \, h^{-2} \, \|v_j\|_{0;Q}^2 \leq c \, \mu^2 \, h^{-4} \, \|v_j\|_{0;Q}^2 \tag{5.61}$$

and hence $\|v_j\|_2^2 \leq c \, \mu^2 \, h^{-4} \, \|v_j\|_0^2$ for a given mesh. Now assuming that regular subdivision is performed (splitting each edge along the middle so that the aspect ratio μ does not vary across levels), we have $\|v_j\|_2^2 \leq c \, 2^{4j} \, \|v_j\|_0^2$ exactly as desired. □

5.9.1.2 Derivation of oscillatory estimates

The oscillatory estimates (see also Yserentant [51, 52]) relate the Sobolev and L^2 norms of an element in W_j^{HB}. By definition of the Sobolev norms, Eq (2.3b), we have for any element $v \in V$,

$$\|v\|_0^2 \leq \|v\|_s^2, \quad s > 0 \tag{5.62}$$

However, for elements lying in the space W_j^{HB} composed of oscillatory functions that vanish at all the nodes in $\mathcal{K}(j)$, see Figure 5-6, we can actually derive tighter upper-bounds on

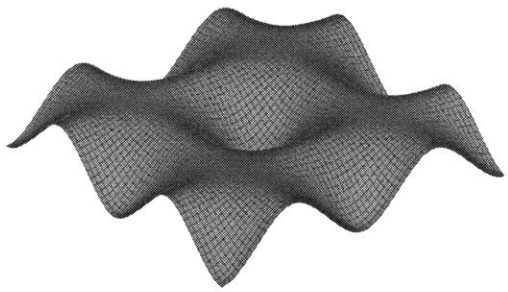

Figure 5-6: An oscillating function

the L^2 norms as given in the following lemma:

Lemma 5.7. *There exists a constant c independent of the level j such that for any element $\rho_j \in W_j^{HB}$,*

$$\|\rho_j\|_0 \leq c\, 2^{-2j}\ \|\rho_j\|_2 \tag{5.63}$$

Remark. Assuming that regular subdivision is performed, the L^2 norm of finite element shape functions varies as 2^{-j} and the $W^{2,2}$ seminorm varies as 2^j.

Proof. As in Section 5.9.1.1 we decompose the seminorm of a function ρ_j in W_j^{HB} as

$$|\rho_j|_s^2 = \sum_{Q \in S_{j-1,v}} |\rho_j|_{s;Q}^2 \qquad s = 0, 1, 2 \tag{5.64}$$

Note that the summation is taken over elements at the coarser level - this will be crucial in proving the desired estimates (see Yserentant[51]). From Figure 5-7, for any such an element Q, there exist five nodes in $\mathcal{M}(j)$ such that

$$|\rho_j|_{s;Q}^2 = \left| \sum_{i=1}^{5} \rho_{j,m_i} \varphi_{j+1,m_i} \right|_{s;Q}^2 \qquad s = 0, 1, 2 \tag{5.65}$$

For the case $s = 0$, there is a constant c independent of the mesh width such that

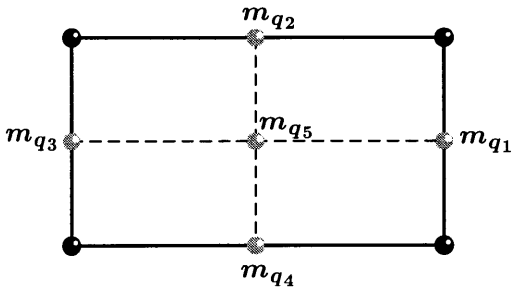

Figure 5-7: Illustration of a subdivided element

$$\|\rho_j\|^2_{0;Q} = \left\| \sum_{i=1}^{5} \rho_{j,m_i} \varphi_{j+1,m_1} \right\|^2_{0;Q} \leq c \sum_{i=1}^{5} \|\rho_{j,m_i} \varphi_{j+1,m_i}\|^2_{0;Q} \leq c\, 2^{-4j} \sum_{i=1}^{5} |\rho_{j,m_i} \varphi_{j+1,m_i}|^2_{2;Q} \tag{5.66}$$

Now, due to the interpolating nature of the Bogner-Fox-Schmidt basis functions, ρ_j, $\frac{\partial \rho_j}{\partial x}$, $\frac{\partial \rho_j}{\partial y}$, $\frac{\partial^2 \rho_j}{\partial x \partial y}$ all vanish at the nodes in $\mathcal{K}(j)$. Hence the $W^{1,2}$ and $W^{2,2}$ seminorms in Q are in fact bona-fide norms since $|\rho_j|_{s;Q} = 0 \iff \rho_j|_Q = 0$ for $s = 1, 2$ (Note that the higher order seminorms can vanish in general for constant and linear functions respectively. But the only constant (resp. linear) function that vanishes at the nodes in $\mathcal{K}(j)$ along with it's first derivatives and the cross derivative is the 0 function). We can therefore apply equivalence between the two norms

$$\sum_{i=1}^{5} |\rho_{j,m_i} \varphi_{j+1,m_i}|^2_{2;Q} \quad \text{and} \quad \left| \sum_{i=1}^{5} \rho_{j,m_i} \varphi_{j+1,m_i} \right|^2_{2;Q} = |\rho_j|^2_{2;Q}$$

to give

$$\|\rho_j\|^2_{0;Q} \leq c\, 2^{-4j}\ |\rho_j|^2_{2;Q} \leq c\, 2^{-4j}\ \|\rho_j\|^2_{2;Q} \tag{5.67}$$

□

Summing over all the rectangles immediately provides the desired estimate.

5.9.2 Riesz stability of scale-orthogonal wavelets

Having derived the inverse and oscillatory estimates for higher-order interpolation functions, we can give a proof of Riesz stability of the scale-orthogonal wavelets. This will be

accomplished as follows: We first prove Lemma 5.8 that establishes norm equivalence between the hierarchical basis functions and the orthogonalized wavelets. We then only need to show that the lazy wavelets are Riesz stable with respect to the energy norm. This second result is well established for second-order problems (see for instance Yserentant[51], Vassilevski and Wang [48] or Aksoylu and Holst [2]). Our extension to fourth-order problems discretized using Bogner-Fox-Schmidt basis functions is an extension of the same principles involving inverse and oscillatory estimates.

Recalling our convention in Section 2.2 of not distinguishing between a *function* and the *vector of its coefficients* in a given basis, an element $\rho_j \in W_j^{\text{HB}}$ will have a representation of the form:

$$\rho_j = \sum_{m \in \mathcal{M}(j)} \rho_{j,m}^{\mathsf{T}} \varphi_{j+1,m} = \rho_j^{\mathsf{T}} w_j^{\text{HB}} \tag{5.68}$$

and let $\Pi_j \rho_j$ denote its a- projection onto V_j, i.e.

$$a(v_j, \Pi_j \rho_j) = a(v_j, \rho_j) \quad (v_j \in V_j) \tag{5.69}$$

Then, each wavelet $w_{j,m},\ m \in \mathcal{M}(j)$ constructed by Gram-Schmidt orthogonalization of a hierarchical basis function, $w_{j,m}^{\text{HB}}$ cf. Eq (5.25a) can be written as

$$w_{j,m} = w_{j,m}^{\text{HB}} - \Pi_j w_{j,m}^{\text{HB}} \tag{5.70}$$

Remark. The mapping $W_j^{\text{HB}} \mapsto W_j$ from the space of hierarchical basis functions to the space of scale-orthogonal wavelets constructed via the Gram-Schmidt procedure is evidently one-one and onto and is therefore invertible.

Lemma 5.8. *The following norm equivalence holds:*

$$c_1 \ \|\rho_j\|_E^2 \leq \|\rho_j - \Pi_j \rho_j\|_E^2 \leq c_2 \ \|\rho_j\|_E^2 \qquad (\rho_j \in W_j^{HB}) \tag{5.71}$$

where the constants $0 < c_1 \leq c_2$ are independent of the level j.

Proof. To prove the lower-bound estimate, we use the strengthened Cauchy-Schwarz in-

equality, Lemma 4.1. We therefore have from Lemma 4.2,

$$(1-\gamma^2)\,\|\rho_j\|_{\mathrm{E}}^2 \leq \|\rho_j - \Pi_j\rho_j\|_{\mathrm{E}}^2 \tag{5.72}$$

To prove the upper-bound, observe that from Galerkin orthogonality,

$$a\,(\rho_j - \Pi_j\rho_j, \rho_j) = 0 \tag{5.73}$$

Therefore

$$\begin{aligned}\underbrace{a\,(\rho_j,\rho_j)}_{\|\rho_j\|_{\mathrm{E}}^2} &= a\,(\rho_j - \Pi_j\rho_j + \Pi_j\rho_j, \rho_j - \Pi_j\rho_j + \Pi_j\rho_j) \\ &= \underbrace{a\,(\Pi_j\rho_j, \Pi_j\rho_j)}_{\|\Pi_j\rho_j\|_{\mathrm{E}}^2} + \underbrace{a\,(\rho_j - \Pi_j\rho_j, \rho_j - \Pi_j\rho_j)}_{\|\rho_j - \Pi_j\rho_j\|_{\mathrm{E}}^2} \quad \text{or} \end{aligned} \tag{5.74}$$

$$\|\rho_j - \Pi_j\rho_j\|_{\mathrm{E}} \leq \|\rho_j\|_{\mathrm{E}} \tag{5.75}$$

□

Remark. In the proofs by Vassilevski and Wang [48] and Aksoylu and Holst [2], Π_j corresponded to the L^2 projection and hence proving the upper-bound in Eq (5.71) was slightly more involved. By using the energy projection, we have obtained tight upper-bounds in a relatively straightforward manner.

In the subsequent discussion, we choose the bilinear form $a(\cdot,\cdot)$ to correspond to the bending energy of a Kirchhoff plate and choose the scaling functions as the Bogner-Fox-Schmidt interpolating functions.

Lemma 5.9. *The following norm equivalence between the energy norm and the L^2 norm holds in the space spanned by the hierarchical basis:*

$$c_1\,2^{4j}\;\|\rho_j\|_0^2 \leq \|\rho_j\|_E^2 \leq c_2\,2^{4j}\;\|\rho_j\|_0^2 \qquad (\rho_j \in W_j^{HB}) \tag{5.76}$$

where the constants $0 < c_1 \leq c_2$ are independent of the level j.

Proof. Since the bilinear form is continuous and coercive, the energy norm is equivalent to the $W^{2,2}$ norm. The upper-bound then follows from the standard inverse estimates, Lemma 5.6:

$$\|\rho_j\|_{\mathrm{E}}^2 \leq c \ \|\rho_j\|_2^2 \leq c\, c'\, 2^{4j}\, \|\rho_j\|_0^2 = c_2\, 2^{4j} \ \|\rho_j\|_0^2 \tag{5.77}$$

where the constant c' depends on the aspect ratio of the mesh, which remains constant across all levels provided the mesh is subdivided in a regular manner. Now, from the oscillatory estimates, Lemma 5.7 we have

$$\|\rho_j\|_0^2 \leq c\, 2^{-4j}\, \|\rho_j\|_2^2\,, \text{ or, } c_1\, 2^{4j} \ \|\rho_j\|_0^2 \leq \|\rho_j\|_{\mathrm{E}}^2 \tag{5.78}$$

□

Remark. In the case of nodal finite element shape functions, the inequality $\|\rho_j\|_0^2 \leq \|\rho_j\|_2^2$ follows trivially. However, the oscillatory estimates, Lemma 5.7 provide a stronger bound on the L^2 norm of a function lying in the space spanned by hierarchical basis functions.

Lemma 5.10. *The hierarchical basis is uniformly L^2-Riesz stable, i.e.,*

$$c_1 \ \|\rho_j\|_0^2 \leq \sum_{m \in \mathcal{M}(j)} \left\|\rho_{j,m}^{\mathsf{T}} w_{j,m}^{HB}\right\|_0^2 \leq c_2 \ \|\rho_j\|_0^2 \qquad (\rho_j \in W_j^{HB}) \tag{5.79}$$

Proof. The function ρ_j belongs to the finite-element space V_{j+1} and hence the L^2 norm equivalence for finite element spaces can be directly applied (see also Section 4.3.1). □

Corollary 5.11. *The eigenvalues of the unscaled mass matrix corresponding to the hierarchical basis functions alone satisfy*

$$c_1\, 2^{-2j} \leq \lambda_{j,min} \leq \lambda_{j,max} \leq c_2\, 2^{-2j} \tag{5.80}$$

Proof. Assume that all the degrees of freedom are scaled to have the same dimension (i.e, a derivative degree of freedom of order m is multipled by h^m. Then the L^2 norm of the basis functions satisfy

$$c_1\, 2^{-2j} \leq \left\|w_{j,m}^{\mathrm{HB}}\right\|_0^2 \leq c_2\, 2^{-2j} \tag{5.81}$$

and hence

$$c_1 \ \|\rho_j\|_0^2 \leq 2^{-2j} \ \rho_j^{\mathsf{T}} \rho_j \leq c_2 \ \|\rho_j\|_0^2 \tag{5.82}$$

from which the inequality follows trivially. □

Lemma 5.12. *The hierarchical basis is uniformly E - Riesz stable, i.e.,* $\exists\, 0 < c_1 \leq c_2 < \infty$ *independent of the level* j *such that*

$$c_1 \, \|\rho_j\|_E^2 \leq \sum_{m \in \mathcal{M}(j)} \left\|\rho_{j,m}^{\mathsf{T}} \varphi_{j+1,m}\right\|_E^2 \leq c_2 \, \|\rho\|_E^2 \qquad (\rho_j \in W_j^{HB}) \tag{5.83}$$

Proof. Note that Eq (5.78) and Eq (5.77) apply to *each* element of the space W_j^{HB} and in particular to each element of the form $\rho_{j,m}^{\mathsf{T}} \varphi_{j+1,m}$, $m \in \mathcal{M}(j)$. We therefore have

$$\sum_{m \in \mathcal{M}(j)} \left\|\rho_{j,m}^{\mathsf{T}} \varphi_{j+1,m}\right\|_{\mathrm{E}}^2 \leq c \, 2^{4j} \sum_{m \in \mathcal{M}(j)} \left\|\rho_{j,m}^{\mathsf{T}} \varphi_{j+1,m}\right\|_0^2 \leq c \, 2^{4j} \ \|\rho_j\|_0^2 \leq c_2 \, 2^{4j} \, 2^{-4j} \ \|\rho_j\|_{\mathrm{E}}^2 = c_2 \ \|\rho_j\|_{\mathrm{E}}^2 \tag{5.84a}$$

and

$$\sum_{m \in \mathcal{M}(j)} \left\|\rho_{j,m}^{\mathsf{T}} \varphi_{j+1,m}\right\|_{\mathrm{E}}^2 \geq c \, 2^{-4j} \sum_{m \in \mathcal{M}(j)} \left\|\rho_{j,m}^{\mathsf{T}} \varphi_{j+1,m}\right\|_0^2 \geq c \, 2^{-4j} \, \|\rho_j\|_0^2 \geq c_1 \, 2^{-4j} \, 2^{4j} \, \|\rho_j\|_{\mathrm{E}}^2 = c_1 \, \|\rho_j\|_{\mathrm{E}}^2 \tag{5.84b}$$

□

Corollary 5.13. *The eigenvalues of the unscaled stiffness matrix corresponding to the hierarchical basis functions alone satisfy*

$$c_1 \, 2^{2j} \leq \lambda_{j,min} \leq \lambda_{j,max} \leq c_2 \, 2^{2j}. \tag{5.85}$$

Proof. From the inverse inequality, Eq (5.77) we have for any $\rho_j \in W_j^{\mathrm{HB}}$

$$\|\rho_j\|_{\mathrm{E}}^2 \leq c \, 2^{4j} \, \|\rho_j\|_0^2 \leq c_1 \, 2^{4j} \, 2^{-2j} \, \rho_j^{\mathsf{T}} \rho_j = c_1 \, 2^{2j} \, \rho_j^{\mathsf{T}} \rho_j \tag{5.86a}$$

and

$$\|\rho_j\|_{\mathrm{E}}^2 \geq c \, 2^{4j} \, \|\rho_j\|_0^2 \geq c_2 \, 2^{4j} \, 2^{-2j} \, \rho_j^{\mathsf{T}} \rho_j = c_2 \, 2^{2j} \, \rho_j^{\mathsf{T}} \rho_j \tag{5.86b}$$

□

We are finally ready to prove the main result for wavelets constructed using Gram-Schmidt orthogonalization with respect to the $a(\cdot,\cdot)$-inner-product. Let, W_j as before, be the space spanned by such scale-orthogonal wavelets.

Lemma 5.14. *Scale-orthogonal wavelets constructed using Gram-Schmidt orthogonalization are uniformly E- Riesz stable, i.e.,* $\exists\ 0 < c_1 \leq c_2 < \infty$ *independent of the level* j *such that*

$$c_1 \|\xi_j\|_E^2 \leq \sum_{m\in\mathcal{M}(j)} \left\|\xi_{j,m}^{\mathsf{T}} w_{j,m}\right\|_E^2 \leq c_2 \|\xi_j\|_E^2 \qquad (\xi_j \in W_j) \tag{5.87}$$

Proof. This is a straightforward application of Lemma 5.8 and Lemma 5.12:

$$\begin{aligned}
\|\xi_j\|_{\mathrm{E}}^2 &= \left\| \sum_{m\in\mathcal{M}(j)} \xi_{j,m}^{\mathsf{T}} w_{j,m} \right\|_{\mathrm{E}}^2 \\
&\leq c \left\| \sum_{m\in\mathcal{M}(j)} \xi_{j,m}^{\mathsf{T}} w_{j,m}^{\mathrm{HB}} \right\|_{\mathrm{E}}^2 \quad \text{(Lemma 5.8)} \\
&\leq c \sum_{m\in\mathcal{M}(j)} \left\|\xi_{j,m}^{\mathsf{T}} w_{j,m}^{\mathrm{HB}}\right\|_{\mathrm{E}}^2 \quad \text{(Lemma 5.12)} \\
&\leq \frac{1}{c_1} \sum_{m\in\mathcal{M}(j)} \left\|\xi_{j,m}^{\mathsf{T}} w_{j,m}\right\|_{\mathrm{E}}^2 \quad \text{(Lemma 5.8)}
\end{aligned} \tag{5.88a}$$

Similarly

$$\begin{aligned}
\|\xi_j\|_{\mathrm{E}}^2 &= \left\| \sum_{m\in\mathcal{M}(j)} \xi_{j,m}^{\mathsf{T}} w_{j,m} \right\|_{\mathrm{E}}^2 \\
&\geq c \left\| \sum_{m\in\mathcal{M}(j)} \xi_{j,m}^{\mathsf{T}} w_{j,m}^{\mathrm{HB}} \right\|_{\mathrm{E}}^2 \quad \text{(Lemma 5.8)} \\
&\geq c \sum_{m\in\mathcal{M}(j)} \left\|\xi_{j,m}^{\mathsf{T}} w_{j,m}^{\mathrm{HB}}\right\|_{\mathrm{E}}^2 \quad \text{(Lemma 5.12)} \\
&\geq \frac{1}{c_2} \sum_{m\in\mathcal{M}(j)} \left\|r_{j,m}^{\mathsf{T}} w_{j,m}\right\|_{\mathrm{E}}^2 \quad \text{(Lemma 5.8)}
\end{aligned} \tag{5.88b}$$

□

Remark. The eigenvalues of the stiffness matrix corresponding to the un-normalized scale-orthogonal wavelets alone satisfy the same estimates as Corollary 5.13.

5.9.3 Numerical Verification of Riesz bounds

We now numerically verify the bounds derived in Lemmas 5.8 to 5.14 for an *ad hoc* test problem of a clamped square Kirchhoff plate discretized using Bogner-Fox-Schmidt finite elements.

5.9.3.1 Norm equivalence between hierarchical basis functions and scale-orthogonal wavelets

Let the stiffness matrices corresponding to hierarchical basis functions and modified wavelets be denoted as $\mathbf{C}_{j+1}^{\mathrm{HB}}$ and $\mathbf{C}_{j+1}$ respectively. We then require that the extremal eigenvalues of the mixed eigenproblem

$$\mathbf{C}_{j+1}\, v = \lambda\, \mathbf{C}_{j+1}^{\mathrm{HB}}\, v \tag{5.89}$$

remain bounded independent of the level j. Moreover, the maximum eigenvalue must always be less than or equal to 1. This is experimentally confirmed in Figure 5-8.

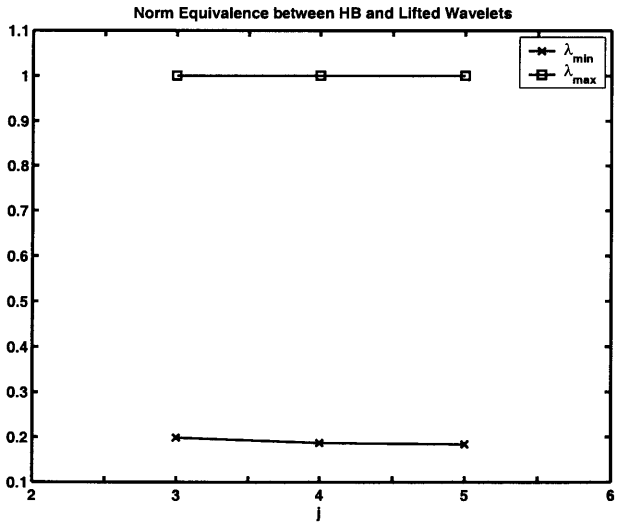

Figure 5-8: Numerical verification of Lemma 5.8

5.9.3.2 Riesz stability of hierarchical basis functions

Let $\mathbf{D}_{j+1}^{\mathrm{HB}}$ be the Jacobi preconditioner for $\mathbf{C}_{j+1}^{\mathrm{HB}}$, i.e., it is a block-diagonal matrix composed of the diagonal elements of $\mathbf{C}_{j+1}^{\mathrm{HB}}$. Then, from Lemma 5.12 we have that that the maximum and minimum eigenvalues of the mixed eigenproblem

$$\mathbf{C}_{j+1}^{\mathrm{HB}}\, v = \lambda\, \mathbf{D}_{j+1}^{\mathrm{HB}}\, v \tag{5.90}$$

remain independent of the level of discretization, j. This is also experimentally verified in Figure 5-9.

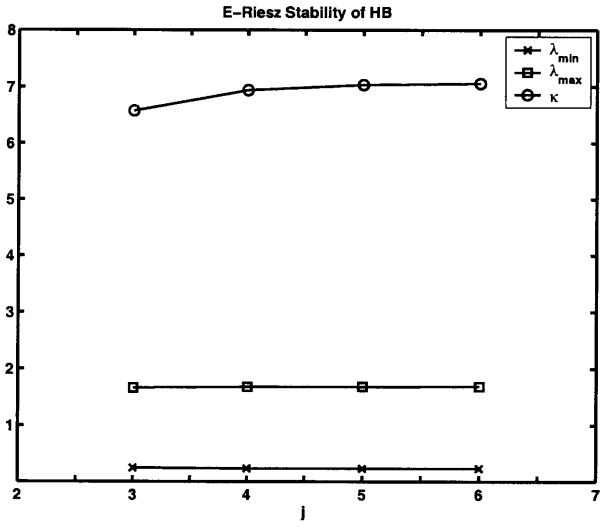

Figure 5-9: Numerical verification of Lemma 5.12

5.9.3.3 Growth of eigenvalues of the matrix $\mathbf{C}_{j+1}^{\mathrm{HB}}$

From Corollary 5.13, we have that the minimum and maximum eigenvalues of the hierarchical basis detail matrix, $\mathbf{C}_{j+1}^{\mathrm{HB}}$ increase as 4^j. This is experimentally verified in Figure 5-10 which shows the theoretical and observed growth rates of the minimum and maximum eigenvalues.

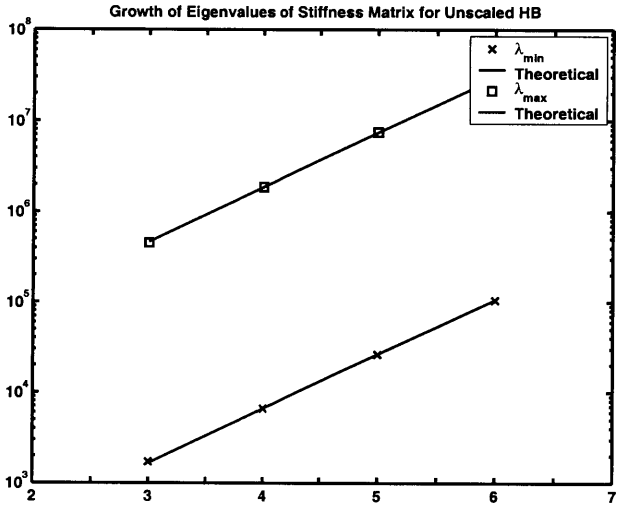

Figure 5-10: Numerical verification of Corollary 5.13.

5.9.3.4 Riesz stability of scale-orthogonal wavelets

The statement of the main result, Lemma 5.14 is experimentally verified in Figure 5-11 which claims that if $\mathbf{D}_{j+1}$ is the Jacobi preconditioner for $\mathbf{C}_{j+1}$ then the extremal eigenvalues (and hence the condition number) of the mixed eigenproblem,

$$\mathbf{C}_{j+1}\, v = \lambda\, \mathbf{D}_{j+1}\, v \tag{5.91}$$

remain bounded independent of the level of discretization, j.

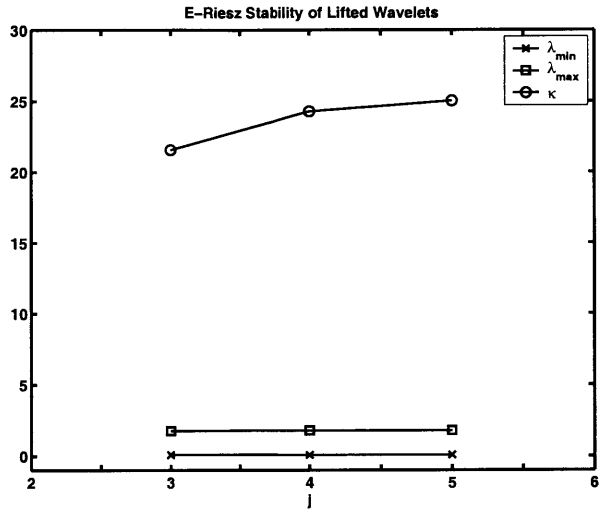

Figure 5-11: Numerical verification of Lemma 5.14.

5.9.3.5 Growth of eigenvalues for the matrix $\mathbf{C}_{j+1}$

Finally, in Figure 5-12 we experimentally verify the result that the extremal eigenvalues of the detail matrix $\mathbf{C}_{j+1}$ corresponding to scale-orthogonal wavelets constructed using Gram-Schmidt orthogonalization grow at the same rate as the extremal eigenvalues of the hierarchical basis detail matrix $\mathbf{C}_{j+1}^{\mathrm{HB}}$.

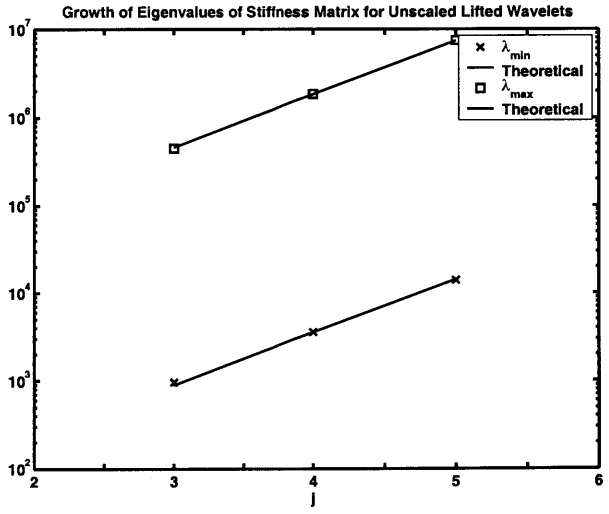

Figure 5-12: Growth of extremal eigenvalues of the matrix $\mathbf{C}_{j+1}$ with discretization levels.

5.10 Closure

In this chapter, we discussed two techniques for the construction of wavelets that were orthogonal to the scaling functions at each level with respect to the bilinear form, $a(\cdot,\cdot)$ by customization of hierarchical basis functions. The first technique based on the stable completion approach of Carnicer, et al. resulted in wavelets in the interior of the domain that had compact support. However, it required the construction of special wavelets at the boundaries and did not ensure *a priori* that the wavelets were Riesz stable in the energy norm. We therefore focused our attention for the rest of the chapter on the second method, Gram-Schmidt orthogonalization. While this procedure often led to globally supported wavelets (albeit with fast decay rates), we demonstrated how the corresponding detail matrices could be efficiently assembled and factored for the case of adaptive mesh refinement using Gauss elimination. We further characterized the stability properties of these wavelets, demonstrating their *a priori* Riesz stability in Lemma 5.14. We conclude this chapter by pointing out an important connection between scale-orthogonal wavelets constructed out of Gram-Schmidt orthogonalization and stable completion.

5.10.1 Gram-Schmidt orthogonalization and stable completion

Let w_j^{GS} denote the set of wavelets constructed using the Gram-Schmidt orthogonalization process. The refinement and wavelet relations may be written in matrix notation as:

$$\begin{bmatrix} \varphi_j \\ w_j^{\mathrm{GS}} \end{bmatrix} = \begin{bmatrix} \mathbf{I} & \mathbf{0} \\ -\left(\mathbf{S}_{j+1}^{\mathrm{GS}}\right)^{\mathsf{T}} & \mathbf{I} \end{bmatrix} \begin{bmatrix} \mathbf{I} & \mathbf{H}_j \\ \mathbf{0} & \mathbf{I} \end{bmatrix} \begin{bmatrix} \mathbf{P}_{\mathrm{E},j} \\ \mathbf{P}_{\mathrm{O},j} \end{bmatrix} \varphi_{j+1} \tag{5.92}$$

where the scaling functions and wavelets satisfy $a\left(\varphi_j, \left(w_j^{\mathrm{GS}}\right)^{\mathsf{T}}\right) = 0$. We therefore have,

$$\begin{bmatrix} \mathbf{I} & \mathbf{H}_j \\ \mathbf{0} & \mathbf{I} \end{bmatrix} \begin{bmatrix} \mathbf{P}_{\mathrm{E},j} \\ \mathbf{P}_{\mathrm{O},j} \end{bmatrix} \varphi_{j+1} = \begin{bmatrix} \mathbf{I} & \mathbf{0} \\ \left(\mathbf{S}_{j+1}^{\mathrm{GS}}\right)^{\mathsf{T}} & \mathbf{I} \end{bmatrix} \begin{bmatrix} \varphi_j \\ w_j^{\mathrm{GS}} \end{bmatrix} \tag{5.93}$$

If we let w_j^{SC} denote the set of scale-orthogonal wavelets constructed using stable completion, the refinement and wavelet equations can be written in the polyphase form as:

$$\begin{aligned}\begin{bmatrix} \varphi_j \\ w_j^{\mathrm{SC}} \end{bmatrix} &= \begin{bmatrix} \mathbf{I} & \mathbf{0} \\ -\left(\mathbf{S}_j^{\mathrm{SC}}\right)^{\mathsf{T}} & \mathbf{G}_j^{\mathsf{T}} \end{bmatrix} \begin{bmatrix} \mathbf{I} & \mathbf{H}_j \\ \mathbf{0} & \mathbf{I} \end{bmatrix} \begin{bmatrix} \mathbf{P}_{\mathrm{E},j} \\ \mathbf{P}_{\mathrm{O},j} \end{bmatrix} \varphi_{j+1} \\ &= \begin{bmatrix} \mathbf{I} & \mathbf{0} \\ -\left(\mathbf{S}_j^{\mathrm{SC}}\right)^{\mathsf{T}} & \mathbf{G}_j^{\mathsf{T}} \end{bmatrix} \begin{bmatrix} \mathbf{I} & \mathbf{0} \\ \left(\mathbf{S}_{j+1}^{\mathrm{GS}}\right)^{\mathsf{T}} & \mathbf{I} \end{bmatrix} \begin{bmatrix} \varphi_j \\ w_j^{\mathrm{GS}} \end{bmatrix} \end{aligned} \tag{5.94}$$

from which we have

$$\left(w_j^{\mathrm{SC}}\right)^{\mathsf{T}} = \varphi_j^{\mathsf{T}} \left(-\mathbf{S}_j^{\mathrm{SC}} + \mathbf{S}_{j+1}^{\mathrm{GS}} \mathbf{G}_j\right) + \left(w_j^{\mathrm{GS}}\right)^{\mathsf{T}} \mathbf{G}_j \tag{5.95}$$

Once again applying the constraint that $a\left(\varphi_j, \left(w_j^{\mathrm{SC}}\right)^{\mathsf{T}}\right) = 0$ we obtain the relation:

$$\mathbf{S}_j^{\mathrm{SC}} = \mathbf{S}_{j+1}^{\mathrm{GS}}\, \mathbf{G}_j \tag{5.96}$$

On substituting Eq (5.96) into Eq (5.95) we therefore obtain the following relation between wavelets constructed using stable completion and Gram-Schmidt orthogonalization:

$$w_j^{\mathrm{SC}} = \mathbf{G}_j^{\mathsf{T}} w_j^{\mathrm{GS}} \quad \text{or} \quad w_{j,m}^{\mathrm{SC}} = \sum_{m' \in B(j,m)} \left(g_j[m', m]\right)^{\mathsf{T}}\, w_{j,m'}^{\mathrm{GS}} \tag{5.97}$$

Similarly, we can relate the wavelet coefficients at level j corresponding to the two types of basis functions as:

$$\left(r_j^{\mathrm{SC}}\right)^{\mathsf{T}} w_j^{\mathrm{SC}} = \left(\mathbf{G}_j\, r_j^{\mathrm{SC}}\right)^{\mathsf{T}} w_j^{\mathrm{GS}} = \left(r_j^{\mathrm{GS}}\right)^{\mathsf{T}} w_j^{\mathrm{GS}} \tag{5.98}$$

or, $r_j^{\mathrm{GS}} = \mathbf{G}_j\, r_j^{\mathrm{SC}}$.

Finally, we can relate the detail matrices corresponding to the two types of basis functions as:

$$\mathbf{C}_{j+1}^{\mathrm{SC}} = a\left(w_j^{\mathrm{SC}}, \left(w_j^{\mathrm{SC}}\right)^{\mathsf{T}}\right) = \mathbf{G}_j^{\mathsf{T}}\, a\left(w_j^{\mathrm{GS}}, \left(w_j^{\mathrm{GS}}\right)^{\mathsf{T}}\right)\, \mathbf{G}_j = \mathbf{G}_j^{\mathsf{T}} \mathbf{C}_{j+1}^{\mathrm{GS}}\, \mathbf{G}_j \tag{5.99}$$

Chapter 6

Error Estimation and Adaptivity with Operator-Customized Wavelets

"You know we are on a wrong track altogether.
We must not think of the things we could do with,
but only of the things that we can't do without."
– Harry in Jerome K. Jerome's Three Men in a Boat.

6.1 Overview and chapter outline

In this chapter, we propose a multiresolution technique for efficiently and adaptively generating the solution to a given PDE (described using its weak form, Eq (4.4)) such that a given bounded linear functional of the solution is well-predicted (this is the problem of *goal-oriented* adaptivity [12, 27, 28, 33, 32, 38]). Our multiresolution error-estimation and adaptive refinement framework is based on the use of operator-customized wavelet that were described in Chapter 5. The use of scale-orthogonal wavelets possessing the Riesz stability property in the energy norm allows us to (a) efficiently estimate the details at each level of resolution, based on which the details to be preserved are determined and (b) to solve a system of equations corresponding only to details chosen to be preserved in step (a), enabling the implementation of *incremental* rather than *cumulative* refinement schemes. The key point of departure of our technique from the methods currently in vogue

in finite element analysis is that instead of estimating the *true* error at each step of refinement, we aim at efficiently computing and representing only its projection at the next level of resolution (defined in Section 6.2.1 as the *two-level* error). As can be expected, this process is much more accurate than estimating the error itself and is almost independent of the coarsest mesh. Further, as demonstrated in Section 6.2.1, the true solution can be represented in terms of these two-level errors and hence efficiently representing these error components automatically leads to an efficient, but accurate representation of the true solution itself.

Our procedure for estimating the contribution of the two-level errors to the functional of interest, step (a) in the previous paragraph, can be seen as a variation of both the error-estimation procedure of Bank and Smith [9] and the dual-weighted residual technique of Rannacher and collaborators (see for example, Becker and Rannacher [12], Grätsch and Bathe [32, 33] and references therein). By directly estimating the contribution of the wavelets at each level of resolution, our approach avoids many of the pitfalls (such as lack of error cancellation) associated with techniques based on element-wise energy norms (such as the method originally proposed by Becker and Rannacher [12]). Moreover, unlike the approach of Prudhomme and Oden [38], which requires the estimation of the error in both the primal and the dual solution on each mesh, our approach requires the estimation of the detail components of only the primal solution at a given level of resolution.

In contrast to the adaptive wavelet-Galerkin approach proposed by Cohen, Dahmen and their collaborators based on the use of biorthogonal spline wavelets on the interval (see for example, [18, 20] and references therein), our approach is based on the use of wavelets constructed from finite element interpolation functions. This allows our techniques to be generalized more easily to complex meshes and higher-order differential operators. Further, all computations (assembly, inverse transform, etc.) can be done at the element level and computing the inner-products of the orthogonalized wavelets does not require special quadrature techniques and may instead be computed using a simple scheme based on Gauss elimination that were proposed in Section 5.7.1. Finally, adaptive approaches based on the wavelet-Galerkin method currently drive adaptivity based solely on the magnitude of the wavelet coefficients. While this approach is suitable for adaptivity based on the energy

norm (provided of course that the wavelets are Riesz stable in the energy norm, as considered by Cohen et al. [18]), this strategy alone is not sufficient in general to drive goal-oriented adaptivity. A distinguishing feature of our wavelet approach is that we consider the more general case of goal-oriented adaptivity and our refinement procedure is based on how much a wavelet contributes to the quantity of interest rather than just the magnitude of the corresponding coefficient.

6.2 Error estimation and adaptivity in classical finite element analysis

Consider again the virtual work equation, Eq (4.4) and let $u_j \in V_j$ be the Galerkin projection of the true solution u satisfying the finite dimensional virtual work equation, Eq (4.6). Further, define

$$\varepsilon_j \stackrel{\text{def}}{=} u - u_j$$

to be the error in the solution and let

$$\mathcal{R}_j(v) \stackrel{\text{def}}{=} l(v) - a\left(u_j, v\right) \quad (v \in V)$$

be the corresponding residual. The true solution can then be written as

$$u = u_j + \varepsilon_j \tag{6.1}$$

where the error ε_j satisfies the residual equation

$$a\left(\varepsilon_j, v\right) = \mathcal{R}_j\left(v\right) \quad (v \in V)$$

and is a-orthogonal to the space V_j

$$a\left(\varepsilon_j, v_j\right) = 0 \quad (v_j \in V_j)$$

In principle therefore, given the solution at level j, it is possible to obtain the true solution provided the error is known. Unfortunately, the error belongs to an infinite dimensional Hilbert space, V and solving for it is often as expensive as obtaining the true solution itself. Therefore, one instead computes an inexpensive approximation to the error, $\varepsilon_j^{\text{est}}$ using various *a posteriori* error estimators such as implicit, explicit or recovery based error estimators [1, 33]. Then, if the estimated error is larger than a given error tolerance ϵ, a refined mesh is constructed by subdividing elements based on the principle of *equidistribution of error*, i.e., we sudivide those elements $S_{j,v},\ v = \{1, 2, \ldots, N_j\}$ satisfying

$$\left\|\varepsilon_{j,v}^{\text{est}}\right\|_{\text{E}} > \frac{\epsilon}{N_j} \tag{6.2}$$

where $\left\|\varepsilon_{j,v}^{\text{est}}\right\|_{\text{E}}$ is the energy norm of the contribution of each element to the error estimate and N_j is the number of elements at level j. Based on this criterion, we can therefore establish a refined space of functions $V_{j+1}^{\text{Adapt}} \subset V_{j+1}$ on which the improved solution, $\overline{u}_{j+1}$ is computed. This process is repeated until the estimated error is less than the prescribed error tolerance.

There are a number of disadvantages associated with the canonical error-estimation and adaptive refinement procedure described above. For example, the quality of the estimated error often depends very closely on the quality of the initial mesh. In the case of recovery-based error estimation procedures such as the Zienkiewicz-Zhu technique [54] a lack of oscillation in the solution is indicative of a more accurate solution. Hence on very coarse meshes, misleading estimates for the error could be obtained (see for example Grätsch and Bathe [33], Section 4.3). Another disadvantage with classical error estimators in finite element analysis is that many of them, particularly the explicit error estimators (see [1, 33]) are based on the element-wise application of the Cauchy-Schwarz inequality to lead to error-estimates of the form

$$\|\varepsilon_j\|_{\text{E}}^2 \leq \left\|\varepsilon_j^{\text{est}}\right\|_{\text{E}}^2 \stackrel{\text{def}}{=} \sum_{v=1}^{N_j} \left\|\varepsilon_{j,v}^{\text{est}}\right\|_{\text{E}}^2 \tag{6.3}$$

Hence, while the individual element-wise error indicators, $\left\|\varepsilon_{j,v}^{\text{est}}\right\|_{\text{E}}$ can serve as good indi-

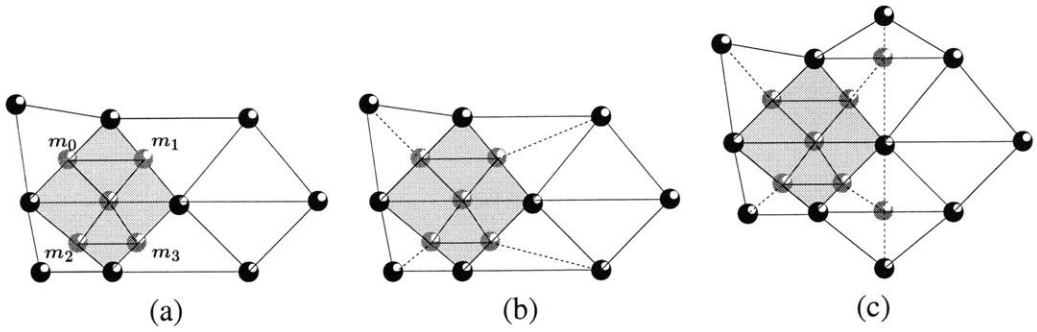

Figure 6-1: Handling of irregular vertices using (a) Imposition of multi-point constraints on vertices $m_0, \ldots, m_3$ (b) Green refinement (c) Refinement by successive bisection of longest edges

cators for driving adaptive mesh refinement, the estimated error $\left\|\varepsilon_j^{\text{est}}\right\|_{\text{E}}$ often produces an overestimation of the true error [33] and can lead to suboptimally-refined meshes. A standard technique for overcoming this problem is to actually refine only a certain fraction of the elements marked for refinement based on Eq (6.2). However, there is usually no means for choosing this fraction in a systematic, *a priori* manner.

Apart for the problems due to inaccurate error-estimation on coarse meshes, classical adaptive refinement procedures themselves have several disadvantages. For instance, refinement schemes based on subdivision of individual elements often have to contend with hanging or irregular vertices either using transition elements and multi-point constraints, Figure 6-1 (a) or with specialized techniques such as green refinement of Bank [7] (that requires heuristics to prevent triangles with poor aspect ratios), Figure 6-1 (b) or successive longest edge bisection technique of Rivara [39], Figure 6-1 (c). However, most of these techniques work reliably only for certain special cases (such as piecewise linear interpolation on triangular meshes) and extensions to more general elements (such as the Bogner-Fox-Schmidt element) are normally extremely tedious to implement and may not result in displacement fields with sufficient continuity.

There is therefore a lot of scope for the construction of reliable, efficient and easy-to-implement error estimation and adaptive refinement procedures in practical finite element analysis (see also the conclusions in [33]).

6.2.1 A point of departure

Instead of using Eq (6.1) to represent the solution, the multilevel error estimation and adaptive refinement algorithms that we propose in this chapter are based the decomposition of the error ε_j belonging to an infinite-dimensional space Hilbert space V into a convergent sequence of errors belonging to successively richer finite-dimensional spaces. The estimation procedure aims at cheaply computing approximations to these components of the error and the adaptive refinement procedure aims at developing a compact representation of these components. Unlike standard finite element analysis where the choice of a particular error-estimation technique (explicit, implicit or recovery-based) is often completely independent of the choice of a refinement procedure (transition elements, multi-point constraints, remeshing, etc.), the estimation and refinement steps in our multilevel technique are tightly integrated. This allows us, for example, to predict in an *a priori* manner (i.e., before actually computing the details exactly), how much the solution will improve upon mesh refinement.

Observe that for an estimation technique based on predicting certain *components* of the error there is no implicit assumption that if a particular component of the error is negligible, the total error itself is small. Such techniques can therefore expected to perform in a robust manner on coarse meshes.

Further, the adaptive refinement procedures themselves are based on the notion of *space refinement* [18, 20] where the new approximation spaces, V_{j+1}^{Adapt} are created by selectively augmenting an existing approximation space V_j^{Adapt} with a set of wavelet basis functions. This form of enrichment does not have to explicitly deal with irregular vertices since the wavelet coefficients corresponding to these vertices do not enter the system of equations at all.

The basic principle behind the multiresolution error-estimation and adaptive refinement algorithm is the following: Since for conforming finite element approximations clos $\bigcup_{j=0}^{\infty} V_j = V$ (see Section 3.2), we have $\lim_{j\to\infty} u_j = u$. Hence, the sequence of *two-level errors*

$$e_j \stackrel{\text{def}}{=} u_{j+1} - u_j$$

belonging to the space V_{j+1} is itself a convergent sequence tending to 0. Given the solution u_0 corresponding to the space V_0 of finite element interpolation functions on the coarsest level mesh, we can therefore decompose the solution u in terms of a telescopic sum as

$$u = u_0 + \sum_{j=0}^{\infty} (u_{j+1} - u_j) \tag{6.4a}$$

$$= u_0 + \sum_{j=0}^{\infty} e_j \tag{6.4b}$$

From the above decomposition, it follows that the error at a certain level j can be written as

$$\varepsilon_j = \sum_{i=j}^{\infty} e_i \tag{6.5}$$

The key properties of the two-level error are summarized in the following lemma.

Lemma 6.1. *The two-level error e_i, $i \geq j$ corresponds to the projection of the true error, ε_j onto the space V_{i+1},*

$$\|\varepsilon_j - e_i\|_E = \inf_{v_{i+1} \in V_{i+1}} \|\varepsilon_j - v_{i+1}\|_E$$

Further, the two-level errors are scale-orthogonal, i.e.,

$$a(u_j, e_i) = 0 \quad (i \geq j) \tag{6.6a}$$

$$a(e_i, e_{i'}) = 0 \quad (i \neq i') \tag{6.6b}$$

Proof. To prove the first part of the lemma, observe from that the true error at level j satisfies

$$a(\varepsilon_j, v_{j+1}) = l(v_{j+1}) - a(u_j, v_{j+1}) \quad (v_{j+1} \in V_{j+1})$$

and the two-level error satisfies

$$a\left(e_j, v_{j+1}\right) = a\left(u_{j+1}, v_{j+1}\right) - a\left(u_j, v_{j+1}\right) \quad \left(v_{j+1} \in V_{j+1}\right) \tag{6.7a}$$

$$= l\left(v_{j+1}\right) - a\left(u_j, v_{j+1}\right) \tag{6.7b}$$

$$= a\left(\varepsilon_j, v_{j+1}\right) \tag{6.7c}$$

and therefore, the proof follows by definition [24].

Further, from the Galerkin orthogonality condition we have

$$a\left(e_i, v_i\right) = 0 \quad \left(v_i \in V_i\right) \tag{6.8}$$

and since the two level error $e_{i'} \in V_{i'+1} \subset V_i$ for $i > i'$ the second result follows trivially.

□

A direct consequence of the above lemma that forms the basis of our multiresolution method is the following result:

Lemma 6.2. *The two level error e_j corresponds to the projection of the true solution u onto the space $W_j \stackrel{\text{def}}{=} V_{j+1} \bigcap V_j^{\perp_a}$ where $V_j^{\perp_a}$ is the orthogonal complement [24] of V_j with respect to the $a(\cdot,\cdot)$ inner-product,*

$$\|u - e_j\|_E = \inf_{\eta_j \in W_j} \|u - \eta_j\|_E \tag{6.9}$$

Proof. By definition

$$a(u_j, \eta_j) = 0 \quad \left(\eta_j \in W_j\right) \tag{6.10}$$

and hence

$$a(e_j, \eta_j) = a(u_{j+1}, \eta_j) = a(u, \eta_j) \tag{6.11}$$

since $\eta_j \in V_{j+1}$. □

Given the solution u_j at a certain level, the task at hand in this chapter is to construct a compact representation for the two-level errors e_j, $j = 0, \ldots, \infty$ that is much less computationally expensive to compute than the solution u_{j+1}. A straightforward technique

to achieve this is to augment the existing space of functions V_j using basis functions belonging to a subspace satisfying the direct-sum property, Eq (2.4b) such as the space of hierarchical basis functions W_j^{HB}. A compact representation of the two-level error can then be obtained by choosing only the set of hierarchical basis functions belonging to an index set $\mathcal{M}'(j) \subset \mathcal{M}(j)$. As discussed in Section 4.4, a disadvantage of this approach is that the adaptative refinement procedure is *cumulative* rather than *incremental* - each time a new space of functions is added, the components of the two-level error along the existing space of functions must be updated due to the coupling between the spaces V_j and W_j^{HB}.

This problem can however be overcome using Lemma 6.2: We determine the two-level errors by projecting the solution onto the spaces W_j (which are precisely the spaces spanned by the scale-orthogonal wavelets constructed in Chapter 5). Due to the scale-orthogonality of the two-level errors, Lemma 6.1, these error components do not have to be updated upon the enrichment of the spaces. As for the case of the hierarchical basis functions, a compact representation of e_j can be obtained by projecting the true error on to a subspace W_j^{Adapt} of W_j consisting only of a few of the scale-orthogonal wavelets. In the next subsection, we describe why it is important for the scale-orthogonal wavelets to be Riesz stable in the energy norm in order to obtain a compact representation of the two-level errors.

6.2.2 On the significance of Riesz stability of scale-orthogonal wavelets

Expanding the two-level error function e_j in terms of the scale-orthogonal wavelets spanning the space W_j we have:

$$e_j = \sum_{m \in \mathcal{M}(j)} r_{j,m}^{\mathsf{T}} w_{j,m}$$

Assuming that the adapted solution $\overline{u}_{j+1}$ is computed by retaining only a few wavelets belonging to the set $m \in \mathcal{M}'(j)$,

$$\overline{u}_{j+1} = u_j + \sum_{m \in \mathcal{M}'(j)} r_{j,m}^{\mathsf{T}} w_{j,m} \tag{6.12}$$

the error incurred due to the adaptive refinement process (denoted henceforth as the *adaptation error*) can be given as

$$u_{j+1} - \overline{u}_{j+1} = \sum_{m \in \mathcal{M}''(j)} r_{j,m}^{\mathsf{T}} w_{j,m}$$

where $\mathcal{M}''(j) \stackrel{\text{def}}{=} \mathcal{M}(j) \setminus \mathcal{M}'(j)$. We therefore need a strategy for selecting the set of wavelets to discard such that the error due to adaptive refinement, $u_{j+1} - \overline{u}_{j+1}$ remains small in some metric, typically the energy norm.

If the wavelets form an a-orthogonal basis for the spaces W_j, the adaptation error in the energy norm can be written directly using the Pythagorous theorem [24] as

$$\|u_{j+1} - \overline{u}_{j+1}\|_{\mathrm{E}}^2 = \sum_{m \in \mathcal{M}''(j)} \left\|r_{j,m}^{\mathsf{T}} w_{j,m}\right\|_{\mathrm{E}}^2 \tag{6.13}$$

Hence given a certain accuracy threshold τ_j for the adaptation error $u_{j+1} - \overline{u}_{j+1}$ in the energy norm, it suffices to choose the set of wavelets to discard such that

$$\sum_{m \in \mathcal{M}''(j)} \left\|r_{j,m}^{\mathsf{T}} w_{j,m}\right\|_{\mathrm{E}}^2 \leq \tau_j^2 \tag{6.14}$$

In practice, it is much easier to discard wavelets with extremely small contributions to the energy norm, i.e., given a threshold $\tilde{\tau}_j$ we select the set of wavelets to discard such that

$$\left\|r_{j,m''}^{\mathsf{T}} w_{j,m''}\right\|_{\mathrm{E}} \leq \tilde{\tau}_j \max_{m \in \mathcal{M}(j)} \left\|r_{j,m}^{\mathsf{T}} w_{j,m}\right\|_{\mathrm{E}} \quad m'' \in \mathcal{M}''(j) \tag{6.15}$$

In the absence of an a-orthogonal basis, the next best alternative is a basis that is Riesz stable in the energy norm (see Eq (5.52)). Here, instead of the equality, Eq (6.13), we have the following *equivalence* between the energy norm squared of the adaptation error and the energy-norm squared of the discarded wavelets

$$c_1 \sum_{m \in \mathcal{M}''(j)} \left\|r_{j,m}^{\mathsf{T}} w_{j,m}\right\|_{\mathrm{E}}^2 \leq \|u_{j+1} - \overline{u}_{j+1}\|_{\mathrm{E}}^2 \leq c_2 \sum_{m \in \mathcal{M}''(j)} \left\|r_{j,m}^{\mathsf{T}} w_{j,m}\right\|_{\mathrm{E}}^2 \tag{6.16}$$

where the constants $0 < c_1 \leq c_2 < \infty$ are independent of j. Provided the stability ratio c_2/c_1 is not very large, in this case too, an adaptation process based on discarding coefficients with small energy-norm contributions as in Eq (6.15) is theoretically justified.

The procedure discussed above assumes that the wavelet coefficients $r_{j,m},\ m \in \mathcal{M}(j)$ are known. However, this is rarely the case and computing the wavelet coefficients exactly is usually at least as expensive as computing the solution at the higher resolution. In practice therefore, one needs an efficient technique for *estimating* the wavelet coefficients that is much less expensive than computing them exactly. A technique relying closely on the Riesz stability property of the wavelets is presented later in this chapter. The essential principle behind this approach is that the detail matrices $\mathbf{C}_{j+1}$ corresponding to Riesz stable wavelets are equivalent to their diagonals irrespective of the levels and a good estimate for the details can be obtained simply by diagonally scaling the corresponding right-hand sides.

6.2.3 Goal-oriented error estimation and adaptivity

The procedure discussed in the previous subsection was primarily concerned with constructing an adapted solution $\overline{u}$ that is close to the true solution u in the energy norm. However, this form of adaptivity does not ensure that certain other properties of the solution (such as the average values of the solution or gradient along a section of the domain) are also predicted with sufficient accuracy (see for example Becker and Rannacher [12]). There has therefore been much interest in recent years towards the development of more general, *goal-oriented* [12, 27, 28, 33, 32, 38] error-estimation and adaptive refinement techniques that aim at predicting certain linear functionals of the solution in a reliable and computationally efficient manner. In this section, we give a brief overview of the problem of goal-oriented finite element analysis; more details, including the classical solution approaches can be found in the original papers by Eriksson, et al. [27], Becker and Rannacher [12], Prudhomme and Oden [38], the review article by Grätsch and Bathe [33] and the monograph by Ainsworth and Oden [1].

Given a bounded linear functional $Q : V \rightarrow \mathbb{R}$ (the quantity of interest), the prob-

lem of goal-oriented error estimation and adaptivity is to determine the quantity $Q(u)$ in an efficient, yet accurate manner. This is done by considering an error tolerance, ϵ, and constructing a computationally inexpensive approximation $\overline{u} \in V$ such that

$$d(u, \overline{u}) \stackrel{\text{def}}{=} |Q(u) - Q(\overline{u})| \leq \epsilon \tag{6.17}$$

Since $Q \in V'$, the dual space of V, by the Lax-Milgram lemma, there exists a unique solution $z \in V$ to the *dual* or *adjoint* problem (called the *influence function*), $z \in V$, satisfying

$$a(z, v) = Q(v) \quad (v \in V) \tag{6.18}$$

From the symmetry of the bilinear form $a(\cdot, \cdot)$, there are therefore two ways of computing the quantity of interest

$$Q(u) = a(z, u) = l(z) \tag{6.19}$$

that is a powerful generalization of the Maxwell-Betti reciprocity principle.

For the particular case of the output functional $Q \equiv l$ we have

$$d(u, \overline{u}) = |l(u) - l(\overline{u})| = \|u\|_{\mathrm{E}}^2 - \|\overline{u}\|_{\mathrm{E}}^2 = \|u - \overline{u}\|_{\mathrm{E}}^2 \tag{6.20}$$

where the adapted solution $\overline{u}$ is the projection of u onto a subspace $V^{\text{Adapt}} \subset V$. Hence, the problem of goal-oriented adaptivity, Eq (6.17) is more general than adaptivity based on the energy norm. In the rest of this chapter, we threfore propose a simple strategy for the solution of the problem of goal-oriented analysis based on the use of Riesz-stable scale-orthogonal wavelets with the implicit understanding that the same principles can be applied for more traditional forms of adaptivity based on the energy norm.

6.3 Multiresolution goal-oriented error estimation and adaptive refinement

As in Eq (6.4a) we can write the decompose the solutions to the primal and dual problems in terms of their respective two-level error components as:

$$u = u_0 + \sum_{j=0}^{\infty} e_j \quad \text{and} \quad z = z_0 + \sum_{j=0}^{\infty} \eta_j \tag{6.21}$$

where $u_0, z_0 \in V_0$ are, respectively, the the finite element solutions of the primal and dual problem on the coarsest mesh and $e_j, \eta_j \in V_{j+1}$ are the respective two-level errors. Moreover, from Eq (6.8) we have

$$a(e_i, \eta_{i'}) = 0 \quad (i \neq i') \tag{6.22}$$

and hence the quantity of interest $Q(u)$ can be further decomposed (using the continuity of $Q(\cdot)$ and $a(\cdot,\cdot)$ as)

$$Q(u) = Q(u_0) + \sum_{j=0}^{\infty} Q(e_j) \tag{6.23a}$$

$$= a(u_0, z_0) + \sum_{j=0}^{\infty} a(e_j, \eta_j) \tag{6.23b}$$

Further, using the Cauchy-Schwarz inequality,

$$|Q(e_j)| = |a(e_j, \eta_j)| \leq \|e_j\|_{\mathrm{E}} \|\eta_j\|_{\mathrm{E}} \tag{6.24}$$

While the adaptive refinement procedure will be based on the use of Eq (6.23a), Eq (6.24) will be used to provide *a priori* upper-bounds for the error-estimation procedures presented later in this section.

6.3.1 Construction of adapted complementary spaces

As for adaptivity based on the energy-norm metric, we can expand the two-level error function at level j in terms of the scale-orthogonal wavelets at that level as

$$e_j = \sum_{m \in \mathcal{M}(j)} r_{j,m}^{\mathsf{T}} w_{j,m} \tag{6.25}$$

Then, as in Eq (6.12) by computing the adapted solution $\overline{u}_{j+1}$ by preserving only the set of wavelets belonging to the set $\mathcal{M}'(j)$ the error incurred in the quantity of interest can be expressed as

$$\left|Q\left(u_{j+1} - \overline{u}_{j+1}\right)\right| = \left|\sum_{m \in \mathcal{M}''(j)} Q\left(r_{j,m}^{\mathsf{T}} w_{j,m}\right)\right| \quad \leq \sum_{m \in \mathcal{M}''(j)} \left|Q\left(r_{j,m}^{\mathsf{T}} w_{j,m}\right)\right| \tag{6.26}$$

Therefore, for an accurate approximation of $Q\left(u_{j+1}\right)$ by $Q\left(\overline{u}_{j+1}\right)$ up to an accuracy τ_j, we select the set $\mathcal{M}''(j)$ such that

$$\frac{\left|\sum_{m \in \mathcal{M}''(j)} Q\left(r_{j,m}^{\mathsf{T}} w_{j,m}\right)\right|}{\max_{m \in \mathcal{M}(j)} Q\left(r_{j,m}^{\mathsf{T}} w_{j,m}\right)} \leq \tau_j \tag{6.27}$$

or more conveniently, select a threshold $\tilde{\tau}_j$ and choose $\mathcal{M}'(j)$ such that

$$\frac{\left|Q\left(r_{j,m'}^{\mathsf{T}} w_{j,m'}\right)\right|}{\max_{m \in \mathcal{M}(j)} Q\left(r_{j,m}^{\mathsf{T}} w_{j,m}\right)} \geq \tilde{\tau}_j \quad (m' \in \mathcal{M}'(j)) \tag{6.28}$$

Let W_j^{Adapt} be the subspace of W_j spanned by the set of wavelets in $\mathcal{M}'(j)$ and let $V_{j+1}^{\text{Adapt}} = {}^{\text{def}} V_j^{\text{Adapt}} \oplus W_j^{\text{Adapt}}$. Finally, let the adapted solution $\overline{u}$ in Eq (6.17) be given as the limit of the adapted solution at each level,

$$\overline{u} \stackrel{\text{def}}{=} \lim_{j \to \infty} \overline{u}_j$$

To see how the error in the quantity of interest due to adaptive refinement at each level j, $\left|Q\left(u_j - \overline{u}_j\right)\right|$ affects the final error $\left|Q\left(u - \overline{u}\right)\right|$, observe that Q is bounded and linear, and hence it is also uniformly continuous [24]. We therefore conclude that the final error is

simply the limit of the error incurred at each step since

$$d(u,\overline{u}) = |Q(u-\overline{u})| = \left|Q\left(\lim_{j\to\infty} u_j\right) - Q\left(\lim_{j\to\infty} \overline{u}_j\right)\right| = \left|\lim_{j\to\infty} Q\left(u_j - \overline{u}_j\right)\right| = \lim_{j\to\infty} d\left(u_j - \overline{u}_j\right) \tag{6.29}$$

The next section describes the details of our error-estimation and adaptive refinement scheme for goal-oriented analysis. The section following that provides an *a priori* analysis of the approximations made for computational efficiency (such as partial orthogonalization, of the wavelets, approximate computation of the detail coefficients, etc.).

6.3.2 Multiresolution error estimation and adaptive refinement algorithm

In this section, we describe an efficient technique for the estimation of the two-level errors, e_j and propose an adaptive refinement algorithm that selects the set of wavelets to be retained such that the final adapted solution predicts a certain quantity of interest in an accurate and efficient manner. Observe that steps 1 and 2 below are the estimation steps while steps 3 and 4 are the adaptive refinement steps.

1. Given solution at level j, u_j, estimate the details r_j. The details are computed by solving a system of equations of the form:

$$\mathbf{C}_{j+1} r_j = g_j \tag{6.30}$$

where $\mathbf{C}_{j+1} = a\left(w_j, w_j^{\mathrm{T}}\right)$ is the detail matrix corresponding to the addition of scale-orthogonal wavelets at level j and $g_j = l\left(w_j\right)$ is the corresponding load vector. For scale-orthogonal wavelets constructed using Gram-Schmidt orthogonalization of the hierarchical basis, $\mathbf{C}_{j+1}$ is the Schur's complement of the hierarchical basis detail matrix and the right-hand side is the corresponds to the residual in the space V_{j+1}, see Lemma 5.2.

Obviously computing all the detail coefficients at level j by inverting $\mathbf{C}_{j+1}$ is extremely expensive since it is normally a dense matrix. However, from Lemma 5.8

$\mathbf{C}_{j+1}$ and $\mathbf{C}_{j+1}^{\mathrm{HB}}$ (a sparse matrix) are equivalent in the sense that for any vector of detail coefficients, r_j,

$$\left(1-\gamma^2\right) r_j^{\mathsf{T}} \mathbf{C}_{j+1}^{\mathrm{HB}} r_j \leq r_j^{\mathsf{T}} \mathbf{C}_{j+1} r_j \leq r_j^{\mathsf{T}} \mathbf{C}_{j+1}^{\mathrm{HB}} r_j, \quad \gamma \in [0,1)$$

The matrix $\mathbf{C}_{j+1}^{\mathrm{HB}}$ is therefore a good approximation to the matrix $\mathbf{C}_{j+1}$. Hence, let

$$\tilde{r}_j = \left(\mathbf{C}_{j+1}^{\mathrm{HB}}\right)^{-1} g_j = \left(\mathbf{C}_{j+1}^{\mathrm{HB}}\right)^{-1} \left(g_j^{\mathrm{HB}} - \left(\mathbf{B}_{j+1}^{\mathrm{HB}}\right)^{\mathsf{T}} u_j\right) \tag{6.31}$$

be an estimate for r_j.

In order to compute the estimates $\tilde{r}_j$ more efficiently, we use the property that the hierarchical basis functions form corresponding to interpolating wavelets form a Riesz stable basis for their span, see Lemma 5.12 and Yserentant [51] and therefore the condition number, κ of $\mathbf{C}_{j+1}^{\mathrm{HB}}$ is uniformly bounded . Hence we can approximately invert $\mathbf{C}_{j+1}^{\mathrm{HB}}$ using only a few conjugate gradient iterations with block diagonal scaling. In our numerical experiments, the number of iterations required was usually between 5 and 7.

2. Compute contribution of the detail coefficients at each node to the linear functional as

$$Q\left(\tilde{r}_{j,m}^{\mathsf{T}} w_{j,m}\right) = \tilde{r}_{j,m}^{\mathsf{T}} Q\left(w_{j,m}\right) = \tilde{r}_{j,m}^{\mathsf{T}} Q_{j,m} \tag{6.32}$$

where from Lemma 5.2, the dual load vector, Q_j is computed in exactly the same manner as the primal load vector as

$$Q_j = Q_j^{\mathrm{HB}} - \left(\mathbf{B}_{j+1}^{\mathrm{HB}}\right)^{\mathsf{T}} z_j \tag{6.33}$$

with z_j being the influence function at level j.

3. Given a threshold τ_j, select the set $\mathcal{M}'(j)$ of wavelets to be retained according to Eq (6.28):

$$\left|Q\left(\tilde{r}_{j,m'}^{\mathsf{T}} w_{j,m'}\right)\right| \geq \tau_j \max_{m \in \mathcal{M}(j)} \left|Q\left(\tilde{r}_{j,m}^{\mathsf{T}} w_{j,m}\right)\right| \quad \left(m' \in \mathcal{M}'(j)\right) \tag{6.34}$$

In our numerical experiments, the thresholds were determined by constructing a histogram of the quantities $\left|Q\left(\tilde{r}_{j,m}^{\mathsf{T}} w_{j,m}\right)\right|$ (normalized with respect to $\max_{m \in \mathcal{M}(j)} \left|Q\left(\tilde{r}_{j,m}^{\mathsf{T}} w_{j,m}\right)\right|$) with a bin size of 0.02 and discarding only the coefficients belonging to the last few bins.

4. Construct scale-orthogonal wavelets corresponding to the set $\mathcal{M}'(j)$ using the Gram-Schmidt orthogonalization procedure, Eq (5.30) and solve for the corresponding detail coefficients exactly.

5. Compute the contribution of retained details to the influence function by performing one back-solve on the factorized detail matrix (needed for step 2 at level $j+1$).

6. Finally, we can estimate the contribution of the discarded detail coefficients as

$$d\left(u_{j+1}, \overline{u}_{j+1}\right) \approx \left| \sum_{m \in \mathcal{M}''(j)} Q\left(\tilde{r}_{j,m}^{\mathsf{T}} w_{j,m}\right) \right| \tag{6.35}$$

Remark. For symmetric problems, the estimation steps, 1 and 2 in the algorithm above can be easily shown to be a variation of the dual weighted residual (DWR) approach by Rannacher, et al. [12]. The key difference however, is that in the DWR method the error in the quantity of interest is typically estimated by constructing an improved approximation to the influence function (as done for instance in by Estep et al. [28] and Grätsch and Bathe [32]), whereas in the present approach, the error in the quantity of interest is estimated by efficiently constructing an improved approximation to the solution itself (by adding details at level j) and using the influence function at the current level. Both these approaches have the advantage that one needs to estimate the errors only in the solution or the influence function. An additional advantage of our approach is that as in [28, 32], the estimates are computed directly using the weak-form residuals instead of applying integration by parts over each element of patch of elements defining a basis function. Hence it is ideally suited for problems such as the deformation of thin plates and shells where computing the strong-form residuals is very inconvenient.

6.4 Analysis of the multiresolution goal-oriented error estimation method

In the goal-oriented error-estimation and adaptive refinement algorithm presented in the previous section, there were three main approximations made: (a) The detail matrix $\mathbf{C}_{j+1}$ was replaced by the hierarchical basis detail matrix $\mathbf{C}_{j+1}^{\mathrm{HB}}$, (b) the approximate detail coefficients $\tilde{r}_j$ were computed using a few iterations of the conjugate-gradient method and finally (c) the scale-orthogonal wavelets were constructed using a Gram-Schmidt orthogonalization approach that only ensures partial scale-orthogonality of the wavelets. This simplification is independent of the other two approximations and has an impact on how accurately the details (and consequently, the functional of interest) are computed.

6.4.1 Replacement of $\mathbf{C}_{j+1}$ with $\mathbf{C}_{j+1}^{\mathrm{HB}}$

We first analyze the effect of replacing the stiffness matrix corresponding to the orthogonalized wavelets, $\mathbf{C}_{j+1}$ with that corresponding to the hierarchical basis functions, $\mathbf{C}_{j+1}^{\mathrm{HB}}$

Theorem 6.3. *If e_j are the exact details and $\tilde{e}_j$ are the details computed by approximating $\mathbf{C}_{j+1}$ with $\mathbf{C}_{j+1}^{HB}$ then*

$$|Q\left(e_j - \tilde{e}_j\right)| \leq \frac{\gamma^2}{\sqrt{1-\gamma^2}} \left\|e_j\right\|_E \left\|\eta_j\right\|_E \tag{6.36}$$

Proof. Since the approximate two-level error functions $\tilde{e}_j$ correspond to the estimated detail coefficients $\tilde{r}_j$, we first have

$$\mathbf{C}_{j+1}^{\mathrm{HB}}\left(r_j - \tilde{r}_j\right) = \left(\mathbf{B}_{j+1}^{\mathrm{HB}}\right)^{\mathsf{T}} \mathbf{K}_j^{-1} \mathbf{B}_{j+1}^{\mathrm{HB}} r_j \tag{6.37}$$

and hence

$$\begin{aligned}
\frac{\|e_j - \tilde{e}_j\|_{\mathrm{E}}^2}{\|e_j\|_{\mathrm{E}}^2} &= \frac{(r_j - \tilde{r}_j)^{\mathsf{T}} \mathbf{C}_{j+1} (r_j - \tilde{r}_j)}{r_j^{\mathsf{T}} \mathbf{C}_{j+1} r_j} \\
&= \frac{r_j^{\mathsf{T}} \left((\mathbf{B}_{j+1}^{\mathrm{HB}})^{\mathsf{T}} \mathbf{K}_j^{-1} \mathbf{B}_{j+1}^{\mathrm{HB}} (\mathbf{C}_{j+1}^{\mathrm{HB}})^{-1} \mathbf{C}_{j+1} (\mathbf{C}_{j+1}^{\mathrm{HB}})^{-1} (\mathbf{B}_{j+1}^{\mathrm{HB}})^{\mathsf{T}} \mathbf{K}_j^{-1} \mathbf{B}_{j+1}^{\mathrm{HB}} \right) r_j}{r_j^{\mathsf{T}} \mathbf{C}_{j+1} r_j} \\
&= \frac{(r'_j)^{\mathsf{T}} \mathbf{X}_{j+1}^{\mathsf{T}} \mathbf{X}_{j+1} (\mathbf{I} - \mathbf{X}_{j+1}^{\mathsf{T}} \mathbf{X}_{j+1}) \mathbf{X}_{j+1}^{\mathsf{T}} \mathbf{X}_{j+1} r'_j}{(r'_j)^{\mathsf{T}} (\mathbf{I} - \mathbf{X}_{j+1}^{\mathsf{T}} \mathbf{X}_{j+1}) r'_j},
\end{aligned}$$

on substituting $\mathbf{C}_{j+1} = \mathbf{C}_{j+1}^{\mathrm{HB}} - (\mathbf{B}_{j+1}^{\mathrm{HB}})^{\mathsf{T}} \mathbf{K}_j \mathbf{B}_{j+1}^{\mathrm{HB}}$ and setting $r'_j = (\mathbf{C}_{j+1}^{\mathrm{HB}})^{\frac{1}{2}} r_j$. We therefore have,

$$\begin{aligned}
\frac{\|e_j - \tilde{e}_j\|_{\mathrm{E}}}{\|e_j\|_{\mathrm{E}}} &\leq \left\| (\mathbf{I} - \mathbf{X}_{j+1}^{\mathsf{T}} \mathbf{X}_{j+1})^{\frac{1}{2}} \mathbf{X}_{j+1}^{\mathsf{T}} \mathbf{X}_{j+1} \right\| \left\| (\mathbf{I} - \mathbf{X}_{j+1}^{\mathsf{T}} \mathbf{X}_{j+1})^{-\frac{1}{2}} \right\| \\
&\leq \left\| (\mathbf{I} - \mathbf{X}_{j+1}^{\mathsf{T}} \mathbf{X}_{j+1})^{\frac{1}{2}} \right\| \|\mathbf{X}_{j+1}^{\mathsf{T}} \mathbf{X}\| \left\| (\mathbf{I} - \mathbf{X}_{j+1}^{\mathsf{T}} \mathbf{X}_{j+1})^{-\frac{1}{2}} \right\| \\
&\leq \frac{\gamma^2}{\sqrt{1-\gamma^2}} \quad \text{by Lemma 4.4} \qquad (6.38)
\end{aligned}$$

Observe that since $\gamma < 1$, $\gamma^2 < \gamma$. Further,

$$\begin{aligned}
|Q(e_j - \tilde{e}_j)| &= |a(\eta_j, e_j - \tilde{e}_j)| \\
&\leq \|e_j - \tilde{e}_j\|_{\mathrm{E}} \|\eta_j\|_{\mathrm{E}} \\
&\leq \frac{\gamma^2}{\sqrt{1-\gamma^2}} \|e_j\|_{\mathrm{E}} \|\eta_j\|_{\mathrm{E}}
\end{aligned}$$

□

6.4.2 Computation of $\tilde{r}_j$ via conjugate gradient iterations

We next analyze the effect of computing the approximate two-level errors $\tilde{e}_j$ using k conjugate-gradient iterations with block-diagonal scaling. The estimates follow in a straightforward manner from conjugate gradient convergence theory (see for example Golub and van Loan [31]).

Theorem 6.4. *If $\tilde{e}_j^{(k)}$ is an approximation of $\tilde{e}_j$ computed by k conjugate gradient iterations with block-diagonal scaling, then*

$$\left|Q\left(\tilde{e}_j - \tilde{e}_j^{(k)}\right)\right| \leq \frac{2}{\sqrt{1-\gamma^2}} \left\|\tilde{e}_j\right\|_E \left\|\eta_j\right\|_E \left(\frac{\sqrt{\kappa}-1}{\sqrt{\kappa}+1}\right)^k \tag{6.39}$$

Proof. Let $\mathbf{D}_{j+1}$ denote a block-diagonal approximation to $\mathbf{C}_{j+1}^{\mathrm{HB}}$. Then, using standard conjugate gradient convergence estimates, we have

$$\left\| \mathbf{D}_{j+1}^{\frac{1}{2}} \underbrace{\left(\tilde{r}_j - \tilde{r}_j^{(k)}\right)}_{\tilde{\varepsilon}_j^{(k)}} \right\|^2_{\mathbf{D}_{j+1}^{-\frac{1}{2}} \mathbf{C}_{j+1}^{\mathrm{HB}} \mathbf{D}_{j+1}^{-\frac{1}{2}}} \leq 4 \left\| \mathbf{D}_{j+1}^{\frac{1}{2}} \tilde{r}_{j+1} \right\|^2_{\mathbf{D}_{j+1}^{-\frac{1}{2}} \mathbf{C}_{j+1}^{\mathrm{HB}} \mathbf{D}_{j+1}^{-\frac{1}{2}}} \left(\frac{\sqrt{\kappa}-1}{\sqrt{\kappa}+1}\right)^{2k} \tag{6.40}$$

where $\|x\|_{\mathbf{A}} \stackrel{\mathrm{def}}{=} \left(x^{\mathsf{T}} \mathbf{A} x\right)^{\frac{1}{2}}$ is the $\mathbf{A}$-norm of a vector and $\kappa = \kappa\left(\mathbf{D}_{j+1}^{-\frac{1}{2}} \mathbf{C}_{j+1}^{\mathrm{HB}} \mathbf{D}_{j+1}^{-\frac{1}{2}}\right) = \mathcal{O}(1)$ by the Riesz stability property of the hierarchical basis functions, Lemma 5.12. Hence,

$$\left(\tilde{\varepsilon}_j^{(k)}\right)^{\mathsf{T}} \mathbf{C}_{j+1}^{\mathrm{HB}} \tilde{\varepsilon}_j^{(k)} \leq 4\, \tilde{r}_j^{\mathsf{T}} \mathbf{C}_{j+1}^{\mathrm{HB}} \tilde{r}_j \left(\frac{\sqrt{\kappa}-1}{\sqrt{\kappa}+1}\right)^{2k} \tag{6.41}$$

Further, by equivalence of the Gram-Schmidt orthogonalized wavelets and hierarchical bases, Lemma 5.8,

$$\left\|\tilde{e}_j - \tilde{e}_j^{(k)}\right\|_{\mathrm{E}}^2 \leq \left(\tilde{\varepsilon}_j^{(k)}\right)^{\mathsf{T}} \mathbf{C}_{j+1}^{\mathrm{HB}} \tilde{\varepsilon}_j^{(k)} \leq \frac{4}{1-\gamma^2} \left\|\tilde{e}_j\right\|_{\mathrm{E}}^2 \left(\frac{\sqrt{\kappa}-1}{\sqrt{\kappa}+1}\right)^{2k} \tag{6.42}$$

We therefore have from Eq (6.24),

$$\begin{aligned} \left|Q\left(\tilde{e}_j - \tilde{e}_j^{(k)}\right)\right| &\leq \left\|\tilde{e}_j - \tilde{e}_j^{(k)}\right\|_{\mathrm{E}} \left\|\eta_j\right\|_{\mathrm{E}} \\ &\leq \frac{2}{\sqrt{1-\gamma^2}} \left\|\tilde{e}_j\right\|_{\mathrm{E}} \left\|\eta_j\right\|_{\mathrm{E}} \left(\frac{\sqrt{\kappa}-1}{\sqrt{\kappa}+1}\right)^k \end{aligned}$$

exactly as desired. □

6.4.3 Partial scale-orthogonalization of the wavelets

We finally analyze the influence of constructing partially orthogonal wavelets by Gram-Schmidt orthogonalization. Let W_{j-1}^{Res} be the space spanned by discarded hierarchical basis functions up to level $j-1$, i.e.,

$$W_{j-1}^{\text{Res}} \stackrel{\text{def}}{=} \bigcup_{i=0}^{j-1} \text{span}\left\{w_{i,m''}^{\text{HB}},\ m'' \in \mathcal{M}''(i)\right\} \tag{6.43}$$

Observe that $V_j = V_j^{\text{Adapt}} \oplus W_{j-1}^{\text{Res}}$. We can then define three pairs of strengthened Cauchy-Schwarz inequalities, between elements of V_j^{Adapt} and W_j^{HB}, V_j^{Adapt} and W_{j-1}^{Res} and W_j^{HB} and W_j^{Res} as:

$$\theta_1 = \sup \frac{|a(u,v)|}{\|u\|_{\text{E}} \|v\|_{\text{E}}} \qquad \forall u \in V_j^{\text{Adapt}}\ v \in W_j^{\text{HB}} \tag{6.44a}$$

$$\theta_2 = \sup \frac{|a(u,v)|}{\|u\|_{\text{E}} \|v\|_{\text{E}}} \qquad \forall u \in V_j^{\text{Adapt}}\ v \in W_{j-1}^{\text{Res}} \tag{6.44b}$$

$$\theta_3 = \sup \frac{|a(u,v)|}{\|u\|_{\text{E}} \|v\|_{\text{E}}} \qquad \forall u \in W_{j-1}^{\text{Res}}\ v \in W_j^{\text{HB}} \tag{6.44c}$$

Note that since $V_j^{\text{Adapt}} \subset V_j$ and $W_{j-1}^{\text{Res}} \subset V_j$, $\theta_1, \theta_3 \leq \gamma$.

Theorem 6.5. *Let $\tilde{u}_{Adapt,\,j}$ and $\tilde{u}_{Res,\,j-1}$ be the components of u_{j+1} on V_j^{Adapt} and W_{j-1}^{Res} respectively. Then,*

$$|Q\left(e_j - \overline{e}_j\right)| \leq \frac{\gamma\left(1+\theta_2\right)}{1-\gamma^2} \|\tilde{u}_{Res,j-1}\|_E \|\eta_j\|_E \tag{6.45}$$

Proof. First consider the multilevel system of equations to determine the details e_j at level j:

$$\begin{bmatrix} \mathbf{K}_{\text{Adapt},j} & \mathbf{B}_{\text{Adapt},j+1}^{\text{HB}} & \overline{\mathbf{B}}_{\text{Res},j} \\ \left(\mathbf{B}_{\text{Adapt},j+1}^{\text{HB}}\right)^{\mathsf{T}} & \mathbf{C}_{j+1}^{\text{HB}} & \mathbf{B}_{\text{Res},j+1}^{\text{HB}} \\ \left(\overline{\mathbf{B}}_{\text{Res},j}\right)^{\mathsf{T}} & \left(\mathbf{B}_{\text{Res},j+1}^{\text{HB}}\right)^{\mathsf{T}} & \mathbf{C}_{\text{Res},\,j}^{\text{HB}} \end{bmatrix} \begin{bmatrix} \tilde{u}_{\text{Adapt},j} \\ r_j \\ \tilde{u}_{\text{Res},j-1} \end{bmatrix} = \begin{bmatrix} f_{\text{Adapt},j} \\ g_j^{\text{HB}} \\ g_{\text{Res},j-1} \end{bmatrix} \tag{6.46}$$

where the interaction matrices $\mathbf{B}_{\text{Adapt},j+1}^{\text{HB}}$, $\mathbf{B}_{\text{Res},j+1}^{\text{HB}}$ and $\overline{\mathbf{B}}_{\text{Res},j}$ contain the inner-products of basis functions in V_j^{Adapt} and W_j^{HB}, W_{j-1}^{Res} and W_j^{HB} and V_j^{Adapt} and W_{j-1}^{Res} respectively. Now,

on substituting $\tilde{u}'_{\text{Adapt},j} = (\mathbf{K}_{\text{Adapt},j})^{\frac{1}{2}}\, \tilde{u}_{\text{Adapt},j}$, $r'_j = \left(\mathbf{C}^{\text{HB}}_{j+1}\right)^{\frac{1}{2}} r_j$ and $\tilde{u}'_{\text{Res},j-1} = \left(\mathbf{C}^{\text{HB}}_{\text{Res},\,j}\right)^{\frac{1}{2}} \tilde{u}_{\text{Res},j-1}$ and suitably normalizing the system of equations we have:

$$\begin{bmatrix} \mathbf{I} & \mathbf{X}_{j+1} & \mathbf{Y}_{j+1} \\ \mathbf{X}^{\mathsf{T}}_{j+1} & \mathbf{I} & \mathbf{Z}_{j+1} \\ \mathbf{Y}^{\mathsf{T}}_{j+1} & \mathbf{Z}^{\mathsf{T}}_{j+1} & \mathbf{I} \end{bmatrix} \begin{bmatrix} \tilde{u}'_{\text{Adapt},j} \\ r'_j \\ \tilde{u}'_{\text{Res},j-1} \end{bmatrix} = \begin{bmatrix} f'_{\text{Adapt},j} \\ g'_j \\ g'_{\text{Res},j-1} \end{bmatrix} \tag{6.47}$$

where from Lemma 4.3, $\|\mathbf{X}_{j+1}\| = \theta_1$, $\|\mathbf{Y}_{j+1}\| = \theta_2$ and $\|\mathbf{Z}_{j+1}\| = \theta_3$. In the case of adaptive refinement, we neglect the contribution of the solution on the space of discarded basis functions, $\tilde{u}_{\text{Res},j}$ giving rise to a normalized system of equations of the form:

$$\begin{bmatrix} \mathbf{I} & \mathbf{X}_{j+1} \\ \mathbf{X}^{\mathsf{T}}_{j+1} & \mathbf{I} \end{bmatrix} \begin{bmatrix} \overline{u}'_j \\ \overline{r}'_j \end{bmatrix} = \begin{bmatrix} f'_{\text{Adapt},j} \\ g'_j \end{bmatrix} \tag{6.48}$$

Hence

$$\left(\mathbf{I} - \mathbf{X}^{\mathsf{T}}_{j+1}\mathbf{X}_{j+1}\right)\left(r'_j - \overline{r}'_j\right) = \left(-\mathbf{Z}_{j+1} + \mathbf{X}^{\mathsf{T}}_{j+1}\mathbf{Y}_{j+1}\right)\tilde{u}'_{\text{Res},j-1} \tag{6.49}$$

Let

$$\tilde{\mathbf{X}}_{j+1} \;=\; \begin{bmatrix} \mathbf{I} & \mathbf{Y}_{j+1} \\ \mathbf{Y}^{\mathsf{T}}_{j+1} & \mathbf{I} \end{bmatrix}^{-\frac{1}{2}} \begin{bmatrix} \mathbf{X}_{j+1} \\ \mathbf{Z}_{j+1} \end{bmatrix} \tag{6.50}$$

Then we have,

$$\begin{aligned} \left\|e'_j - \overline{e}'_j\right\|_{\text{E}} &= \left(\left(r'_j - \overline{r}'_j\right)^{\mathsf{T}}\left(\mathbf{I} - \tilde{\mathbf{X}}^{\mathsf{T}}_{j+1}\tilde{\mathbf{X}}_{j+1}\right)\left(r'_j - \overline{r}'_j\right)\right)^{\frac{1}{2}} \\ &\leq \left\|\mathbf{I} - \tilde{\mathbf{X}}^{\mathsf{T}}_{j+1}\tilde{\mathbf{X}}_{j+1}\right\| \left\|r'_j - \overline{r}'_j\right\| \\ &\leq \left\|\mathbf{I} - \tilde{\mathbf{X}}^{\mathsf{T}}_{j+1}\tilde{\mathbf{X}}_{j+1}\right\| \left\|\left(\mathbf{I} - \mathbf{X}^{\mathsf{T}}_{j+1}\mathbf{X}_{j+1}\right)^{-1}\left(-\mathbf{Z}_{j+1} + \mathbf{X}^{\mathsf{T}}_{j+1}\mathbf{Y}_{j+1}\right)\right\| \left\|\tilde{u}'_{\text{Res},j-1}\right\| \\ &\leq \frac{1}{1-\theta_1^2}\left(\|\mathbf{Z}_{j+1}\| + \|\mathbf{X}_{j+1}\|\,\|\mathbf{Y}_{j+1}\|\right)\left\|\tilde{u}_{\text{Res},j-1}\right\|_{\text{E}} \\ &= \frac{1}{1-\theta_1^2}\left(\theta_3 + \theta_1\theta_2\right)\left\|\tilde{u}_{\text{Res},j-1}\right\|_{\text{E}} \\ &\leq \frac{\gamma}{1-\gamma^2}\left(1 + \theta_2\right)\left\|\tilde{u}_{\text{Res},j-1}\right\|_{\text{E}} \end{aligned} \tag{6.51}$$

Observe that $\left\|e'_j - \overline{e}'_j\right\|_{\text{E}} = 0$ either if $\theta_3 = 0$ and $\theta_2 = 0$ (i.e. if $W^{\text{Res}}_{j-1} \perp V^{\text{Adapt}}_j$ and

$W_{j-1}^{\text{Res}} \perp W_j^{\text{HB}}$) or if $\theta_3 = 0$ and $\theta_1 = 0$ (i.e. scales are fully decoupled).

Further as in the previous two results we can bound the error in the quantity of interest due to partial orthogonalization as:

$$\begin{aligned} |Q(e_j - \overline{e}_j)| &\leq \|e_j - \overline{e}_j\|_{\text{E}} \|\eta_j\|_{\text{E}} \\ &\leq \frac{\gamma(1+\theta_2)}{1-\gamma^2} \|\tilde{u}_{\text{Res},j-1}\|_{\text{E}} \|\eta_j\|_{\text{E}} \end{aligned}$$

□

6.5 Closure

In this chapter we described a multiresolution approach towards error-estimation and adaptivity in finite element analysis based on the use of operator-customized wavelets. Our proposed approach hinged on two important results. The first was the decomposition of the solution error belonging to an infinite dimensional Hilbert space into a sequence of two-level error components belonging to finite dimensional spaces. By Lemma 6.2, these components could then be determined by projecting the solution u onto the wavelet spaces spanned by the scale-orthogonal wavelets that were constructed in Chapter 5. Moreover, due to the scale-orthogonal nature of the assumed decomposition, these components do not change on the addition of more levels of details. The second key result was the existence of a Riesz stable basis in the energy norm for the complementary spaces W_j. This property provided a theoretical justification for an adaptive refinement process based on discarding wavelet coefficients with small energy norms. We then proposed an error estimation and adaptive refinement scheme based on the use of our operator-customized, Riesz stable wavelets for solving the problem of goal-oriented adaptivity. We then derived *a priori* error bounds on the accuracy of our estimation technique by considering the effect of various approximations such as partial orthogonalization of the wavelets.

In the next chapter, we present several numerical examples in error estimation and adaptive mesh refinement for both energy-norm and goal-oriented adaptivity problems to validate the effectiveness of the techniques proposed in this chapter.

Chapter 7

Numerical Experiments

Those who can, do. Those who cannot, simulate.
– /usr/games/fortune

7.1 Chapter overview

In Chapter 5 we described the motivation for the construction of scale-orthogonal wavelets, proposed procedures for the construction of such wavelets and characterized their stability properties; in Chapter 6, we proposed an error-estimation and adaptive refinement algorithm based on the use of such scale-orthogonal wavelets. In this chapter, we illustrate the use of scale-orthogonal wavelets constructed using both stable completion and Gram-Schmidt orthogonalization for the efficient solution of several linear, elliptic partial differential equations and demonstrate the effectiveness of the proposed algorithms.

7.1.1 Measuring the effectiveness of the adaptive refinement algorithms

In adaptive refinement procedures, the fundamental trade-off is between compression and accuracy. As can be observed from the description of the error estimation and adaptive refinement procedure proposed in Chapter 6, by choosing the set $\mathcal{M}'(j)$ to be very small, it is possible to obtain an over-compressed solution which might also be highly inaccurate. One technique to measure this trade off is to define two metrics at each level j, the *compression*

ratio, CR_j and the *accuracy ratio*, AR_j as

$$\mathrm{CR}_j \stackrel{\text{def}}{=} \frac{\text{card } \mathcal{M}'(j)}{\text{card } \mathcal{M}(j)} \tag{7.1a}$$

$$\mathrm{AR}_j \stackrel{\text{def}}{=} \frac{|Q(\overline{u}_j)|}{|Q(u_j)|} \tag{7.1b}$$

Obviously, an effective multiresolution error estimation and adaptive refinement procedure is one that keeps CR_j as small as possible while at the same time ensuring that AR_j are close to 1 as possible. An important property of an effective adaptive refinement algorithm is that if one were to plot the error in the functional of interest vs. the number of levels for both uniform and adaptive refinement cases the two convergence plots will closely coincide. This property will be observed in many of the examples that we present later in this section.

7.2 Prototype problems

We first describe some of the problems that can be solved in an adaptive manner using the multiresolution error-estimation and adaptive refinement approach proposed in Chapter 6. In our numerical experiments we have considered both second and fourth-order linear elliptic PDEs with constant and varying coefficients and where the field variables are both scalars as well as vectors.

7.2.1 Poisson's equation

The simplest example considered is the Poisson's equation (governing problems such as heat transfer), where the strong-form and boundary condition are given as

$$\kappa \nabla^2 u + f = 0 \quad \text{on } \Omega \tag{7.2a}$$

$$u = 0 \quad \text{on } \Gamma_D \tag{7.2b}$$

$$\nabla u \cdot \hat{n} = g \quad \text{on } \Gamma_N \tag{7.2c}$$

The Sobolev space of functions V, the bilinear form and the corresponding linear form are then given as:

$$V = \left\{ v \in H^1(\Omega) \text{ s.t. } v|_{\Gamma_D} = 0 \right\} \tag{7.3a}$$

$$a(u, v) = \int_\Omega \kappa \nabla u \cdot \nabla v \, \mathrm{d}\Omega \tag{7.3b}$$

$$l(v) = \int_\Omega f v \, \mathrm{d}\Omega + \int_{\Gamma_N} g v \, \mathrm{d}\Gamma \tag{7.3c}$$

7.2.2 Two-dimensional linear elasticity

At the next level of complexity we consider the problem of two-dimensional linear elasticity where the field variables are the displacements in the x and y directions. The strong form of the PDE (the "equilibrium equation" [10, 40]) expressed in terms of the Cauchy stress tensor is given as

$$\sigma_{ij,j} + f_i = 0 \quad \text{on } \Omega \tag{7.4a}$$

$$u = 0 \quad \text{on } \Gamma_D \tag{7.4b}$$

$$\sigma_{ij} \cdot \hat{n}_j = \tau_i \quad \text{on } \Gamma_N \tag{7.4c}$$

The stress tensor can in turn be related to the displacement field using the stress-strain and strain-displacement relations as

$$\sigma_{ij} = \mathsf{C}_{ijkl} \varepsilon_{kl} \tag{7.5a}$$

$$\varepsilon_{ij} = \frac{1}{2} (u_{i,j} + u_{j,i}) \tag{7.5b}$$

Using the Voigt notation [40], the 3×3 symmetric stress and strain tensors can be rewritten as 3×1 vectors and the Sobolev space of functions and final weak-form can be expressed

as

$$V = \left\{ v \in H^1(\Omega) \times H^1(\Omega) \text{ s.t. } v|_{\Gamma_D} = 0 \right\} \tag{7.6a}$$

$$a(u, v) = \int_\Omega v^\mathsf{T} \mathsf{B}^\mathsf{T} \mathsf{C} \mathsf{B}^\mathsf{T} u \, \mathrm{d}\Omega \tag{7.6b}$$

$$l(v) = \int_\Omega v^\mathsf{T} f \, \mathrm{d}\Omega + \int_{\Gamma_N} v^\mathsf{T} \tau \, \mathrm{d}\Gamma \tag{7.6c}$$

where the matrices B and C contain the strain-displacement and stress-strain relations respectively. For the precise expressions, see Bathe [10] or Slaughter [40].

7.2.3 Kirchhoff plate

At the final level of complexity, we consider the problem of deformation of a thin (Kirchhoff) plate, where the only field variable is the normal displacement. In this case, plane sections that are straight and normal before deformation remain straight and normal after deformation and hence all the strain components normal to the surface of the plate are identically 0. The strong-form (a fourth-order PDE) and a few typical boundary conditions are given as [26, 47]

$$\mathsf{D} \nabla^4 u = q \quad \text{on } \Omega \tag{7.7a}$$

$$u = 0 \quad \text{on } \Gamma_{D;\text{Simply-supported}} \tag{7.7b}$$

$$u \text{ and } \nabla u \cdot \hat{n} = 0 \quad \text{on } \Gamma_{D;\text{Clamped}} \tag{7.7c}$$

The Sobolev space of functions and the bilinear form can then be given as

$$V_{\text{Simply-supported}} = \left\{ v \in H^2(\Omega) \text{ s.t. } v|_{\Gamma_D} = 0 \right\} \tag{7.8a}$$

$$V_{\text{Clamped}} = \left\{ v \in H^2(\Omega) \text{ s.t. } v|_{\Gamma_D} = 0,\ \nabla v \cdot \hat{n}|_{\Gamma_D} = 0 \right\} \tag{7.8b}$$

$$a(u,v) = \mathsf{D} \int_{\Omega} \nabla^2 u \nabla^2 v + (1-\nu)\left\{ 2u_{12}v_{12} - u_{11}v_{22} - u_{22}v_{11} \right\} \, \mathrm{d}\Omega \tag{7.8c}$$

$$l(v) = \int_{\Omega} qv \, \mathrm{d}\Omega \tag{7.8d}$$

7.3 Application of locally-supported scale-orthogonal wavelets

In this section, we give several examples of scale-orthogonal wavelets constructed using the stable completion procedure described in Section 5.5. The construction of scale-orthogonal wavelets for second-order problems is rather well-established and therefore in this section we exclusively consider examples of wavelets customized to the thin-plate bending problem with the bilinear form given by Eq (7.8c).

For simplicity, we consider the case of polygonal domains with either clamped or simply-supported boundary conditions. The bilinear form Eq (7.8c) can then be simplified as [26]:

$$a(u,v) = \int_{\Omega} \nabla^2 u \, \nabla^2 v \, \mathrm{d}\Omega, \quad (u, v \in V) \tag{7.9}$$

Assume that Eq (7.9) is discretized using Bogner-Fox-Schmidt interpolating polynomials and that the basis functions are normalized such that they all have the same dimension (for example, the basis function interpolating rotations are multiplied by the mesh width).

The minimum support over which a set of non-trivial solutions to Eq (5.21a) exists in the interior of the domain is shown in Figure 7-1(a): There are 36 orthogonality constraints to satisfy (four constraints corresponding to each of the nine vertices $k_0, \ldots, k_8$) and 36 degrees of freedom (four degrees of freedom corresponding to each of the vertices $m_0, \ldots, m_7$ and k_4).

The 36×36 local interaction matrix, $\mathbf{K}^{\text{loc}}_{G,j}$ may be decomposed as:

$$\mathbf{K}^{\text{loc}}_{G,j} = \left[\begin{array}{c|c|c|c} \mathbf{K}^{\text{loc}}_{B,j,1} & \mathbf{K}^{\text{loc}}_{B,j,2} & \mathbf{K}^{\text{loc}}_{B,j,3} & \mathbf{K}^{\text{loc}}_{A,j} \end{array}\right]$$

where $\mathbf{K}^{\text{loc}}_{B,j,1}$ (resp. $\mathbf{K}^{\text{loc}}_{B,j,2}$ and $\mathbf{K}^{\text{loc}}_{B,j,3}$) contain the columns corresponding to the vertices m_0, m_1, m_2 (resp. m_3, m_4 and m_5, m_6, m_7) and are given in the next few pages.

$$\mathbf{K}^{\text{loc}}_{B,j,1} = \left(\begin{array}{cccc|cccc|cccc}
0 & 0 & 0 & -\frac{2}{25} & -3 & 3 & -\frac{121}{175} & \frac{58}{175} & 0 & 0 & 0 & 0 \\
0 & 0 & \frac{1}{5} & -\frac{1}{25} & -\frac{3}{2} & 1 & -\frac{43}{175} & \frac{109}{1050} & 0 & 0 & 0 & 0 \\
0 & \frac{1}{5} & 0 & \frac{1}{25} & \frac{17}{10} & -\frac{4}{5} & \frac{43}{175} & -\frac{23}{350} & 0 & 0 & 0 & 0 \\
-\frac{1}{2} & \frac{1}{10} & -\frac{1}{10} & \frac{1}{50} & \frac{3}{5} & -\frac{1}{4} & \frac{51}{700} & -\frac{13}{700} & 0 & 0 & 0 & 0 \\
\hline
0 & 0 & 0 & \frac{2}{25} & 6 & 0 & \frac{242}{175} & 0 & 0 & 0 & 0 & -\frac{2}{25} \\
0 & 0 & -\frac{1}{5} & -\frac{1}{25} & 0 & 4 & 0 & \frac{239}{525} & 0 & 0 & \frac{1}{5} & -\frac{1}{25} \\
0 & -\frac{1}{5} & 0 & -\frac{1}{25} & -\frac{17}{5} & 0 & -\frac{86}{175} & 0 & 0 & \frac{1}{5} & 0 & \frac{1}{25} \\
\frac{1}{2} & \frac{1}{10} & \frac{1}{10} & \frac{1}{50} & 0 & -\frac{11}{10} & 0 & -\frac{33}{350} & -\frac{1}{2} & \frac{1}{10} & -\frac{1}{10} & \frac{1}{50} \\
\hline
0 & 0 & 0 & 0 & -3 & -3 & -\frac{121}{175} & -\frac{58}{175} & 0 & 0 & 0 & \frac{2}{25} \\
0 & 0 & 0 & 0 & \frac{3}{2} & 1 & \frac{43}{175} & \frac{109}{1050} & 0 & 0 & -\frac{1}{5} & -\frac{1}{25} \\
0 & 0 & 0 & 0 & \frac{17}{10} & \frac{4}{5} & \frac{43}{175} & \frac{23}{350} & 0 & -\frac{1}{5} & 0 & -\frac{1}{25} \\
0 & 0 & 0 & 0 & -\frac{3}{5} & -\frac{1}{4} & -\frac{51}{700} & -\frac{13}{700} & \frac{1}{2} & \frac{1}{10} & \frac{1}{10} & \frac{1}{50} \\
\hline
0 & 0 & 0 & \frac{2}{25} & -3 & 3 & \frac{121}{175} & -\frac{58}{175} & 0 & 0 & 0 & 0 \\
0 & 0 & -\frac{1}{5} & \frac{1}{25} & -\frac{3}{2} & 1 & \frac{43}{175} & -\frac{109}{1050} & 0 & 0 & 0 & 0 \\
0 & -\frac{1}{5} & 0 & \frac{1}{25} & -\frac{17}{10} & \frac{4}{5} & \frac{43}{175} & -\frac{23}{350} & 0 & 0 & 0 & 0 \\
\frac{1}{2} & -\frac{1}{10} & -\frac{1}{10} & \frac{1}{50} & -\frac{3}{5} & \frac{1}{4} & \frac{51}{700} & -\frac{13}{700} & 0 & 0 & 0 & 0 \\
\hline
0 & 0 & 0 & -\frac{2}{25} & 6 & 0 & -\frac{242}{175} & 0 & 0 & 0 & 0 & \frac{2}{25} \\
0 & 0 & \frac{1}{5} & \frac{1}{25} & 0 & 4 & 0 & -\frac{239}{525} & 0 & 0 & -\frac{1}{5} & \frac{1}{25} \\
0 & \frac{1}{5} & 0 & -\frac{1}{25} & \frac{17}{5} & 0 & -\frac{86}{175} & 0 & 0 & -\frac{1}{5} & 0 & \frac{1}{25} \\
-\frac{1}{2} & -\frac{1}{10} & \frac{1}{10} & \frac{1}{50} & 0 & \frac{11}{10} & 0 & -\frac{33}{350} & \frac{1}{2} & -\frac{1}{10} & -\frac{1}{10} & \frac{1}{50} \\
\hline
0 & 0 & 0 & 0 & -3 & -3 & \frac{121}{175} & \frac{58}{175} & 0 & 0 & 0 & -\frac{2}{25} \\
0 & 0 & 0 & 0 & \frac{3}{2} & 1 & -\frac{43}{175} & -\frac{109}{1050} & 0 & 0 & \frac{1}{5} & \frac{1}{25} \\
0 & 0 & 0 & 0 & -\frac{17}{10} & -\frac{4}{5} & \frac{43}{175} & \frac{23}{350} & 0 & \frac{1}{5} & 0 & -\frac{1}{25} \\
0 & 0 & 0 & 0 & \frac{3}{5} & \frac{1}{4} & -\frac{51}{700} & -\frac{13}{700} & -\frac{1}{2} & -\frac{1}{10} & \frac{1}{10} & \frac{1}{50} \\
\hline
0 & 0 & 0 & 0 & 0 & 0 & 0 & 0 & 0 & 0 & 0 & 0 \\
0 & 0 & 0 & 0 & 0 & 0 & 0 & 0 & 0 & 0 & 0 & 0 \\
0 & 0 & 0 & 0 & 0 & 0 & 0 & 0 & 0 & 0 & 0 & 0 \\
0 & 0 & 0 & 0 & 0 & 0 & 0 & 0 & 0 & 0 & 0 & 0 \\
\hline
0 & 0 & 0 & 0 & 0 & 0 & 0 & 0 & 0 & 0 & 0 & 0 \\
0 & 0 & 0 & 0 & 0 & 0 & 0 & 0 & 0 & 0 & 0 & 0 \\
0 & 0 & 0 & 0 & 0 & 0 & 0 & 0 & 0 & 0 & 0 & 0 \\
0 & 0 & 0 & 0 & 0 & 0 & 0 & 0 & 0 & 0 & 0 & 0 \\
\hline
0 & 0 & 0 & 0 & 0 & 0 & 0 & 0 & 0 & 0 & 0 & 0 \\
0 & 0 & 0 & 0 & 0 & 0 & 0 & 0 & 0 & 0 & 0 & 0 \\
0 & 0 & 0 & 0 & 0 & 0 & 0 & 0 & 0 & 0 & 0 & 0 \\
0 & 0 & 0 & 0 & 0 & 0 & 0 & 0 & 0 & 0 & 0 & 0
\end{array}\right)$$

$$
\mathbf{K}^{\mathrm{loc}}_{B,j,2} = \left(\begin{array}{cccc|cccc}
-3 & \frac{121}{175} & -3 & \frac{58}{175} & 0 & 0 & 0 & 0 \\
-\frac{17}{10} & \frac{43}{175} & -\frac{4}{5} & \frac{23}{350} & 0 & 0 & 0 & 0 \\
\frac{3}{2} & -\frac{43}{175} & 1 & -\frac{109}{1050} & 0 & 0 & 0 & 0 \\
\frac{3}{5} & -\frac{51}{700} & \frac{1}{4} & -\frac{13}{700} & 0 & 0 & 0 & 0 \\
\hline
-3 & -\frac{121}{175} & -3 & -\frac{58}{175} & -3 & \frac{121}{175} & -3 & \frac{58}{175} \\
\frac{17}{10} & \frac{43}{175} & \frac{4}{5} & \frac{23}{350} & -\frac{17}{10} & \frac{43}{175} & -\frac{4}{5} & \frac{23}{350} \\
\frac{3}{2} & \frac{43}{175} & 1 & \frac{109}{1050} & \frac{3}{2} & -\frac{43}{175} & 1 & -\frac{109}{1050} \\
-\frac{3}{5} & -\frac{51}{700} & -\frac{1}{4} & -\frac{13}{700} & \frac{3}{5} & -\frac{51}{700} & \frac{1}{4} & -\frac{13}{700} \\
\hline
0 & 0 & 0 & 0 & -3 & -\frac{121}{175} & -3 & -\frac{58}{175} \\
0 & 0 & 0 & 0 & \frac{17}{10} & \frac{43}{175} & \frac{4}{5} & \frac{23}{350} \\
0 & 0 & 0 & 0 & \frac{3}{2} & \frac{43}{175} & 1 & \frac{109}{1050} \\
0 & 0 & 0 & 0 & -\frac{3}{5} & -\frac{51}{700} & -\frac{1}{4} & -\frac{13}{700} \\
\hline
6 & -\frac{242}{175} & 0 & 0 & 0 & 0 & 0 & 0 \\
\frac{17}{5} & -\frac{86}{175} & 0 & 0 & 0 & 0 & 0 & 0 \\
0 & 0 & 4 & -\frac{239}{525} & 0 & 0 & 0 & 0 \\
0 & 0 & \frac{11}{10} & -\frac{33}{350} & 0 & 0 & 0 & 0 \\
\hline
6 & \frac{242}{175} & 0 & 0 & 6 & -\frac{242}{175} & 0 & 0 \\
-\frac{17}{5} & -\frac{86}{175} & 0 & 0 & \frac{17}{5} & -\frac{86}{175} & 0 & 0 \\
0 & 0 & 4 & \frac{239}{525} & 0 & 0 & 4 & -\frac{239}{525} \\
0 & 0 & -\frac{11}{10} & -\frac{33}{350} & 0 & 0 & \frac{11}{10} & -\frac{33}{350} \\
\hline
0 & 0 & 0 & 0 & 6 & \frac{242}{175} & 0 & 0 \\
0 & 0 & 0 & 0 & -\frac{17}{5} & -\frac{86}{175} & 0 & 0 \\
0 & 0 & 0 & 0 & 0 & 0 & 4 & \frac{239}{525} \\
0 & 0 & 0 & 0 & 0 & 0 & -\frac{11}{10} & -\frac{33}{350} \\
\hline
-3 & \frac{121}{175} & 3 & -\frac{58}{175} & 0 & 0 & 0 & 0 \\
-\frac{17}{10} & \frac{43}{175} & \frac{4}{5} & -\frac{23}{350} & 0 & 0 & 0 & 0 \\
-\frac{3}{2} & \frac{43}{175} & 1 & -\frac{109}{1050} & 0 & 0 & 0 & 0 \\
-\frac{3}{5} & \frac{51}{700} & \frac{1}{4} & -\frac{13}{700} & 0 & 0 & 0 & 0 \\
\hline
-3 & -\frac{121}{175} & 3 & \frac{58}{175} & -3 & \frac{121}{175} & 3 & -\frac{58}{175} \\
\frac{17}{10} & \frac{43}{175} & -\frac{4}{5} & -\frac{23}{350} & -\frac{17}{10} & \frac{43}{175} & \frac{4}{5} & -\frac{23}{350} \\
-\frac{3}{2} & -\frac{43}{175} & 1 & \frac{109}{1050} & -\frac{3}{2} & \frac{43}{175} & 1 & -\frac{109}{1050} \\
\frac{3}{5} & \frac{51}{700} & -\frac{1}{4} & -\frac{13}{700} & -\frac{3}{5} & \frac{51}{700} & \frac{1}{4} & -\frac{13}{700} \\
\hline
0 & 0 & 0 & 0 & -3 & -\frac{121}{175} & 3 & \frac{58}{175} \\
0 & 0 & 0 & 0 & \frac{17}{10} & \frac{43}{175} & -\frac{4}{5} & -\frac{23}{350} \\
0 & 0 & 0 & 0 & -\frac{3}{2} & -\frac{43}{175} & 1 & \frac{109}{1050} \\
0 & 0 & 0 & 0 & \frac{3}{5} & \frac{51}{700} & -\frac{1}{4} & -\frac{13}{700}
\end{array}\right)
$$

$$
\mathbf{K}^{\mathrm{loc}}_{B,j,3} = \left(\begin{array}{cccc|cccc|cccc}
0 & 0 & 0 & 0 & 0 & 0 & 0 & 0 & 0 & 0 & 0 & 0 \\
0 & 0 & 0 & 0 & 0 & 0 & 0 & 0 & 0 & 0 & 0 & 0 \\
0 & 0 & 0 & 0 & 0 & 0 & 0 & 0 & 0 & 0 & 0 & 0 \\
0 & 0 & 0 & 0 & 0 & 0 & 0 & 0 & 0 & 0 & 0 & 0 \\
\hline
0 & 0 & 0 & 0 & 0 & 0 & 0 & 0 & 0 & 0 & 0 & 0 \\
0 & 0 & 0 & 0 & 0 & 0 & 0 & 0 & 0 & 0 & 0 & 0 \\
0 & 0 & 0 & 0 & 0 & 0 & 0 & 0 & 0 & 0 & 0 & 0 \\
0 & 0 & 0 & 0 & 0 & 0 & 0 & 0 & 0 & 0 & 0 & 0 \\
\hline
0 & 0 & 0 & 0 & 0 & 0 & 0 & 0 & 0 & 0 & 0 & 0 \\
0 & 0 & 0 & 0 & 0 & 0 & 0 & 0 & 0 & 0 & 0 & 0 \\
0 & 0 & 0 & 0 & 0 & 0 & 0 & 0 & 0 & 0 & 0 & 0 \\
0 & 0 & 0 & 0 & 0 & 0 & 0 & 0 & 0 & 0 & 0 & 0 \\
\hline
0 & 0 & 0 & -\frac{2}{25} & -3 & 3 & -\frac{121}{175} & \frac{58}{175} & 0 & 0 & 0 & 0 \\
0 & 0 & \frac{1}{5} & -\frac{1}{25} & -\frac{3}{2} & 1 & -\frac{43}{175} & \frac{109}{1050} & 0 & 0 & 0 & 0 \\
0 & \frac{1}{5} & 0 & \frac{1}{25} & \frac{17}{10} & -\frac{4}{5} & \frac{43}{175} & -\frac{23}{350} & 0 & 0 & 0 & 0 \\
-\frac{1}{2} & \frac{1}{10} & -\frac{1}{10} & \frac{1}{50} & \frac{3}{5} & -\frac{1}{4} & \frac{51}{700} & -\frac{13}{700} & 0 & 0 & 0 & 0 \\
\hline
0 & 0 & 0 & \frac{2}{25} & 6 & 0 & \frac{242}{175} & 0 & 0 & 0 & 0 & -\frac{2}{25} \\
0 & 0 & -\frac{1}{5} & -\frac{1}{25} & 0 & 4 & 0 & \frac{239}{525} & 0 & 0 & \frac{1}{5} & -\frac{1}{25} \\
0 & -\frac{1}{5} & 0 & -\frac{1}{25} & -\frac{17}{5} & 0 & -\frac{86}{175} & 0 & 0 & \frac{1}{5} & 0 & \frac{1}{25} \\
\frac{1}{2} & \frac{1}{10} & \frac{1}{10} & \frac{1}{50} & 0 & -\frac{11}{10} & 0 & -\frac{33}{350} & -\frac{1}{2} & \frac{1}{10} & -\frac{1}{10} & \frac{1}{50} \\
\hline
0 & 0 & 0 & 0 & -3 & -3 & -\frac{121}{175} & -\frac{58}{175} & 0 & 0 & 0 & \frac{2}{25} \\
0 & 0 & 0 & 0 & \frac{3}{2} & 1 & \frac{43}{175} & \frac{109}{1050} & 0 & 0 & -\frac{1}{5} & -\frac{1}{25} \\
0 & 0 & 0 & 0 & \frac{17}{10} & \frac{4}{5} & \frac{43}{175} & \frac{23}{350} & 0 & -\frac{1}{5} & 0 & -\frac{1}{25} \\
0 & 0 & 0 & 0 & -\frac{3}{5} & -\frac{1}{4} & -\frac{51}{700} & -\frac{13}{700} & \frac{1}{2} & \frac{1}{10} & \frac{1}{10} & \frac{1}{50} \\
\hline
0 & 0 & 0 & \frac{2}{25} & -3 & 3 & \frac{121}{175} & -\frac{58}{175} & 0 & 0 & 0 & 0 \\
0 & 0 & -\frac{1}{5} & \frac{1}{25} & -\frac{3}{2} & 1 & \frac{43}{175} & -\frac{109}{1050} & 0 & 0 & 0 & 0 \\
0 & -\frac{1}{5} & 0 & \frac{1}{25} & -\frac{17}{10} & \frac{4}{5} & \frac{43}{175} & -\frac{23}{350} & 0 & 0 & 0 & 0 \\
\frac{1}{2} & -\frac{1}{10} & -\frac{1}{10} & \frac{1}{50} & -\frac{3}{5} & \frac{1}{4} & \frac{51}{700} & -\frac{13}{700} & 0 & 0 & 0 & 0 \\
\hline
0 & 0 & 0 & -\frac{2}{25} & 6 & 0 & -\frac{242}{175} & 0 & 0 & 0 & 0 & \frac{2}{25} \\
0 & 0 & \frac{1}{5} & \frac{1}{25} & 0 & 4 & 0 & -\frac{239}{525} & 0 & 0 & -\frac{1}{5} & \frac{1}{25} \\
0 & \frac{1}{5} & 0 & -\frac{1}{25} & \frac{17}{5} & 0 & -\frac{86}{175} & 0 & 0 & -\frac{1}{5} & 0 & \frac{1}{25} \\
-\frac{1}{2} & -\frac{1}{10} & \frac{1}{10} & \frac{1}{50} & 0 & \frac{11}{10} & 0 & -\frac{33}{350} & \frac{1}{2} & -\frac{1}{10} & -\frac{1}{10} & \frac{1}{50} \\
\hline
0 & 0 & 0 & 0 & -3 & -3 & \frac{121}{175} & \frac{58}{175} & 0 & 0 & 0 & -\frac{2}{25} \\
0 & 0 & 0 & 0 & \frac{3}{2} & 1 & -\frac{43}{175} & -\frac{109}{1050} & 0 & 0 & \frac{1}{5} & \frac{1}{25} \\
0 & 0 & 0 & 0 & -\frac{17}{10} & -\frac{4}{5} & \frac{43}{175} & \frac{23}{350} & 0 & \frac{1}{5} & 0 & -\frac{1}{25} \\
0 & 0 & 0 & 0 & \frac{3}{5} & \frac{1}{4} & -\frac{51}{700} & -\frac{13}{700} & -\frac{1}{2} & -\frac{1}{10} & \frac{1}{10} & \frac{1}{50}
\end{array}\right)
$$

$$
\mathbf{K}^{\mathrm{loc}}_{A,j} = \left(\begin{array}{cccc}
-\frac{36}{175} & \frac{158}{175} & -\frac{158}{175} & \frac{123}{350} \\
-\frac{158}{175} & \frac{74}{175} & -\frac{123}{350} & \frac{39}{350} \\
\frac{158}{175} & -\frac{123}{350} & \frac{74}{175} & -\frac{39}{350} \\
\frac{123}{350} & -\frac{39}{350} & \frac{39}{350} & -\frac{83}{3150} \\
\hline
-\frac{2028}{175} & 0 & -\frac{734}{175} & 0 \\
0 & \frac{4}{25} & 0 & \frac{2}{25} \\
\frac{734}{175} & 0 & \frac{202}{175} & 0 \\
0 & -\frac{2}{25} & 0 & -\frac{58}{1575} \\
\hline
-\frac{36}{175} & -\frac{158}{175} & -\frac{158}{175} & -\frac{123}{350} \\
\frac{158}{175} & \frac{74}{175} & \frac{123}{350} & \frac{39}{350} \\
\frac{158}{175} & \frac{123}{350} & \frac{74}{175} & \frac{39}{350} \\
-\frac{123}{350} & -\frac{39}{350} & -\frac{39}{350} & -\frac{83}{3150} \\
\hline
-\frac{2028}{175} & \frac{734}{175} & 0 & 0 \\
-\frac{734}{175} & \frac{202}{175} & 0 & 0 \\
0 & 0 & \frac{4}{25} & -\frac{2}{25} \\
0 & 0 & \frac{2}{25} & -\frac{58}{1575} \\
\hline
\frac{8256}{175} & 0 & 0 & 0 \\
0 & \frac{192}{25} & 0 & 0 \\
0 & 0 & \frac{192}{25} & 0 \\
0 & 0 & 0 & \frac{704}{1575} \\
\hline
-\frac{2028}{175} & -\frac{734}{175} & 0 & 0 \\
\frac{734}{175} & \frac{202}{175} & 0 & 0 \\
0 & 0 & \frac{4}{25} & \frac{2}{25} \\
0 & 0 & -\frac{2}{25} & -\frac{58}{1575} \\
\hline
-\frac{36}{175} & \frac{158}{175} & \frac{158}{175} & -\frac{123}{350} \\
-\frac{158}{175} & \frac{74}{175} & \frac{123}{350} & -\frac{39}{350} \\
-\frac{158}{175} & \frac{123}{350} & \frac{74}{175} & -\frac{39}{350} \\
-\frac{123}{350} & \frac{39}{350} & \frac{39}{350} & -\frac{83}{3150} \\
\hline
-\frac{2028}{175} & 0 & \frac{734}{175} & 0 \\
0 & \frac{4}{25} & 0 & -\frac{2}{25} \\
-\frac{734}{175} & 0 & \frac{202}{175} & 0 \\
0 & \frac{2}{25} & 0 & -\frac{58}{1575} \\
\hline
-\frac{36}{175} & -\frac{158}{175} & \frac{158}{175} & \frac{123}{350} \\
\frac{158}{175} & \frac{74}{175} & -\frac{123}{350} & -\frac{39}{350} \\
-\frac{158}{175} & -\frac{123}{350} & \frac{74}{175} & \frac{39}{350} \\
\frac{123}{350} & \frac{39}{350} & -\frac{39}{350} & -\frac{83}{3150}
\end{array}\right)
$$

It can be verified that the columns of the 36×12 matrix, $\mathbf{G}_j^{\text{loc}} =$

$$\left(\begin{array}{cccc|cccc|cccc}
-1 & 1 & 0 & 0 & -1 & 1 & 0 & 0 & 0 & \frac{1596190585}{28606955693} & -\frac{1596190585}{28606955693} & \frac{287765}{20072196} \\
-32 & \frac{85}{6} & \frac{5}{6} & -1 & -30 & \frac{115}{14} & \frac{15}{14} & 1 & \frac{17277}{14788} & \frac{9950568021}{114427822772} & \frac{10891748189}{114427822772} & \frac{61637}{6690732} \\
30 & -\frac{115}{14} & -\frac{15}{14} & 1 & 32 & -\frac{85}{6} & -\frac{5}{6} & -1 & -\frac{17277}{14788} & \frac{10891748189}{114427822772} & \frac{9950568021}{114427822772} & -\frac{61637}{6690732} \\
\frac{3105}{7} & -\frac{1445}{14} & -\frac{295}{14} & \frac{121}{7} & \frac{3105}{7} & -\frac{1445}{14} & -\frac{295}{14} & -\frac{121}{7} & \frac{5565}{14788} & -\frac{12940758243}{114427822772} & \frac{12940758243}{114427822772} & -\frac{112977}{2230244} \\
\hline
2 & 0 & 0 & 0 & 0 & 0 & 0 & 0 & -1 & 0 & -\frac{12805564431}{57213911386} & 0 \\
0 & \frac{5}{3} & -\frac{5}{3} & 0 & 0 & 0 & 0 & 0 & 0 & -\frac{1}{2} & 0 & -\frac{260797}{3345366} \\
-60 & 0 & 0 & -2 & 0 & 0 & 0 & 0 & \frac{61641}{14788} & 0 & \frac{77655643693}{57213911386} & 0 \\
0 & -40 & 10 & 0 & 0 & 0 & 0 & 0 & 0 & \frac{55428566751}{57213911386} & 0 & \frac{188863}{1115122} \\
\hline
-1 & -1 & 0 & 0 & 1 & 0 & 1 & 0 & 0 & -\frac{1596190585}{28606955693} & -\frac{1596190585}{28606955693} & -\frac{287765}{20072196} \\
32 & \frac{85}{6} & \frac{5}{6} & 1 & 0 & -\frac{15}{14} & -\frac{115}{14} & -1 & -\frac{17277}{14788} & \frac{9950568021}{114427822772} & -\frac{10891748189}{114427822772} & \frac{61637}{6690732} \\
30 & \frac{115}{14} & \frac{15}{14} & 1 & -2 & -\frac{5}{6} & -\frac{85}{6} & -1 & -\frac{17277}{14788} & -\frac{10891748189}{114427822772} & \frac{9950568021}{114427822772} & \frac{61637}{6690732} \\
-\frac{3105}{7} & -\frac{1445}{14} & -\frac{295}{14} & -\frac{121}{7} & -75 & \frac{295}{14} & \frac{1445}{14} & \frac{121}{7} & -\frac{5565}{14788} & -\frac{12940758243}{114427822772} & -\frac{12940758243}{114427822772} & -\frac{112977}{2230244} \\
\hline
0 & 0 & 0 & 0 & 2 & 0 & 0 & 0 & -1 & \frac{12805564431}{57213911386} & 0 & 0 \\
0 & 0 & 0 & 0 & 60 & 0 & 0 & -2 & -\frac{61641}{14788} & \frac{77655643693}{57213911386} & 0 & 0 \\
0 & 0 & 0 & 0 & 0 & -\frac{5}{3} & \frac{5}{3} & 0 & 0 & 0 & -\frac{1}{2} & \frac{260797}{3345366} \\
0 & 0 & 0 & 0 & 0 & -40 & 10 & 0 & 0 & 0 & -\frac{55428566751}{57213911386} & \frac{188863}{1115122} \\
\hline
0 & 0 & 0 & 0 & -2 & 0 & 0 & 0 & -1 & -\frac{12805564431}{57213911386} & 0 & 0 \\
0 & 0 & 0 & 0 & 0 & 0 & 0 & 2 & \frac{61641}{14788} & \frac{77655643693}{57213911386} & 0 & 0 \\
0 & 0 & 0 & 0 & 0 & \frac{5}{3} & -\frac{5}{3} & 0 & 0 & 0 & -\frac{1}{2} & -\frac{260797}{3345366} \\
0 & 0 & 0 & 0 & 0 & -10 & 40 & 0 & 0 & 0 & \frac{55428566751}{57213911386} & \frac{188863}{1115122} \\
\hline
1 & 0 & 1 & 0 & -1 & -1 & 0 & 0 & 0 & \frac{1596190585}{28606955693} & \frac{1596190585}{28606955693} & -\frac{287765}{20072196} \\
2 & \frac{5}{6} & \frac{85}{6} & -1 & -30 & -\frac{115}{14} & -\frac{15}{14} & 1 & \frac{17277}{14788} & \frac{9950568021}{114427822772} & -\frac{10891748189}{114427822772} & -\frac{61637}{6690732} \\
0 & \frac{15}{14} & \frac{115}{14} & -1 & -32 & -\frac{85}{6} & -\frac{5}{6} & 1 & \frac{17277}{14788} & -\frac{10891748189}{114427822772} & \frac{9950568021}{114427822772} & -\frac{61637}{6690732} \\
-75 & \frac{295}{14} & \frac{1445}{14} & -\frac{121}{7} & -\frac{3105}{7} & -\frac{1445}{14} & -\frac{295}{14} & \frac{121}{7} & -\frac{5565}{14788} & \frac{12940758243}{114427822772} & \frac{12940758243}{114427822772} & -\frac{112977}{2230244} \\
\hline
-2 & 0 & 0 & 0 & 0 & 0 & 0 & 0 & -1 & 0 & \frac{12805564431}{57213911386} & 0 \\
0 & -\frac{5}{3} & \frac{5}{3} & 0 & 0 & 0 & 0 & 0 & 0 & -\frac{1}{2} & 0 & \frac{260797}{3345366} \\
0 & 0 & 0 & 2 & 0 & 0 & 0 & 0 & -\frac{61641}{14788} & 0 & \frac{77655643693}{57213911386} & 0 \\
0 & -10 & 40 & 0 & 0 & 0 & 0 & 0 & 0 & -\frac{55428566751}{57213911386} & 0 & \frac{188863}{1115122} \\
\hline
1 & 0 & -1 & 0 & 1 & 0 & -1 & 0 & 0 & -\frac{1596190585}{28606955693} & \frac{1596190585}{28606955693} & \frac{287765}{20072196} \\
-2 & \frac{5}{6} & \frac{85}{6} & 1 & 0 & \frac{15}{14} & \frac{115}{14} & -1 & -\frac{17277}{14788} & \frac{9950568021}{114427822772} & \frac{10891748189}{114427822772} & -\frac{61637}{6690732} \\
0 & -\frac{15}{14} & -\frac{115}{14} & -1 & 2 & -\frac{5}{6} & -\frac{85}{6} & 1 & \frac{17277}{14788} & \frac{10891748189}{114427822772} & \frac{9950568021}{114427822772} & \frac{61637}{6690732} \\
75 & \frac{295}{14} & \frac{1445}{14} & \frac{121}{7} & 75 & \frac{295}{14} & \frac{1445}{14} & -\frac{121}{7} & \frac{5565}{14788} & \frac{12940758243}{114427822772} & -\frac{12940758243}{114427822772} & -\frac{112977}{2230244} \\
\hline
0 & 0 & 0 & 0 & 0 & 0 & 0 & 0 & 1 & 0 & 0 & 0 \\
0 & 0 & 0 & 0 & 0 & 0 & 0 & 0 & 0 & 1 & 0 & 0 \\
0 & 0 & 0 & 0 & 0 & 0 & 0 & 0 & 0 & 0 & 1 & 0 \\
0 & 0 & 0 & 0 & 0 & 0 & 0 & 0 & 0 & 0 & 0 & 1
\end{array}\right)$$

form a basis for the null space of the local interaction matrix $\mathbf{K}_{G,j}^{\text{loc}}$. The 12 wavelets corresponding to these filters are illustrated in Figure7-1(b)–(m).

It can be shown via enumeration that it is not possible to span the space of scale-orthogonal wavelets using only the wavelets in the interior. We therefore need to construct additional wavelets adjacent to the boundary. For example, near a clamped boundary, such

as the one illustrated in Figure 7-2(a), we still have 36 degrees of freedom, but only 24 constraints corresponding to the vertices $k_0, \ldots, k_5$. The local interaction matrix near the boundary can now be verified to have a 16 dimensional null space. It can be further verified that 12 of the resulting wavelets correspond exactly to the ones in the interior, Figure 7-1(b)–(m). The four additional wavelets near the boundary are illustrated in Figure 7-2(b)–(e).

Figure 7-3 illustrates the use of scale-orthogonal wavelets for incremental solution of the bending displacements of a clamped square plate. By considering the wavelets in the interior and those next to the boundary, illustrated in Figures 7-1 and 7-2 respectively, we can construct a scale-orthogonal basis for the wavelet space W_j that preserves the direct-sum property of the hierarchical basis functions. This is confirmed by the fact that the resulting block-diagonal matrix is non-singular and upon adding all the wavelets at a particular level, the reconstructed solution converges at exactly the same rate as the underlying finite element approximation. Note that for the bilinear form considered, Eq (7.8c), a discretization based on classical hierarchical basis functions *does not* lead to a decoupled stiffness matrix as evident from Figure 7-3 (d).

The construction of scale-orthogonal wavelets is of course not restricted to square domains with clamped boundary conditions. To emphasize this, in Figures 7-4 and 7-5 we illustrate the scale-decoupled nature of stiffness matrices arising from for the multilevel discretization of a simply-supported plate and a L-shaped plate using wavelets that are customized to the operator.

While incremental computation can be beneficial in the case of uniform refinement, it becomes even more effective for problems that require adaptive mesh refinement. However, as mentioned in Section 5.9, in addition to the scale-orthogonality of the basis functions, we now require that the basis also be Riesz stable in the energy norm. As discussed in Section 5.9, we have not yet incorporated this constraint into the design of our wavelets and indeed it was observed that the locally-supported scale-orthogonal wavelets illustrated in Figures 7-1 and 7-2 do not satisfy this property. In the next sub-section, we therefore illustrate the use of wavelets constructed using the Gram-Schmidt orthogonalization technique that result in wavelets that are Riesz stable in the energy norm. Even though the construction

of such wavelets is very expensive in a uniform refinement setting, as discussed in Section 5.7, they can be efficiently constructed for the special case of adaptive refinement, where only a small fraction of the wavelets are typically retained at each level.

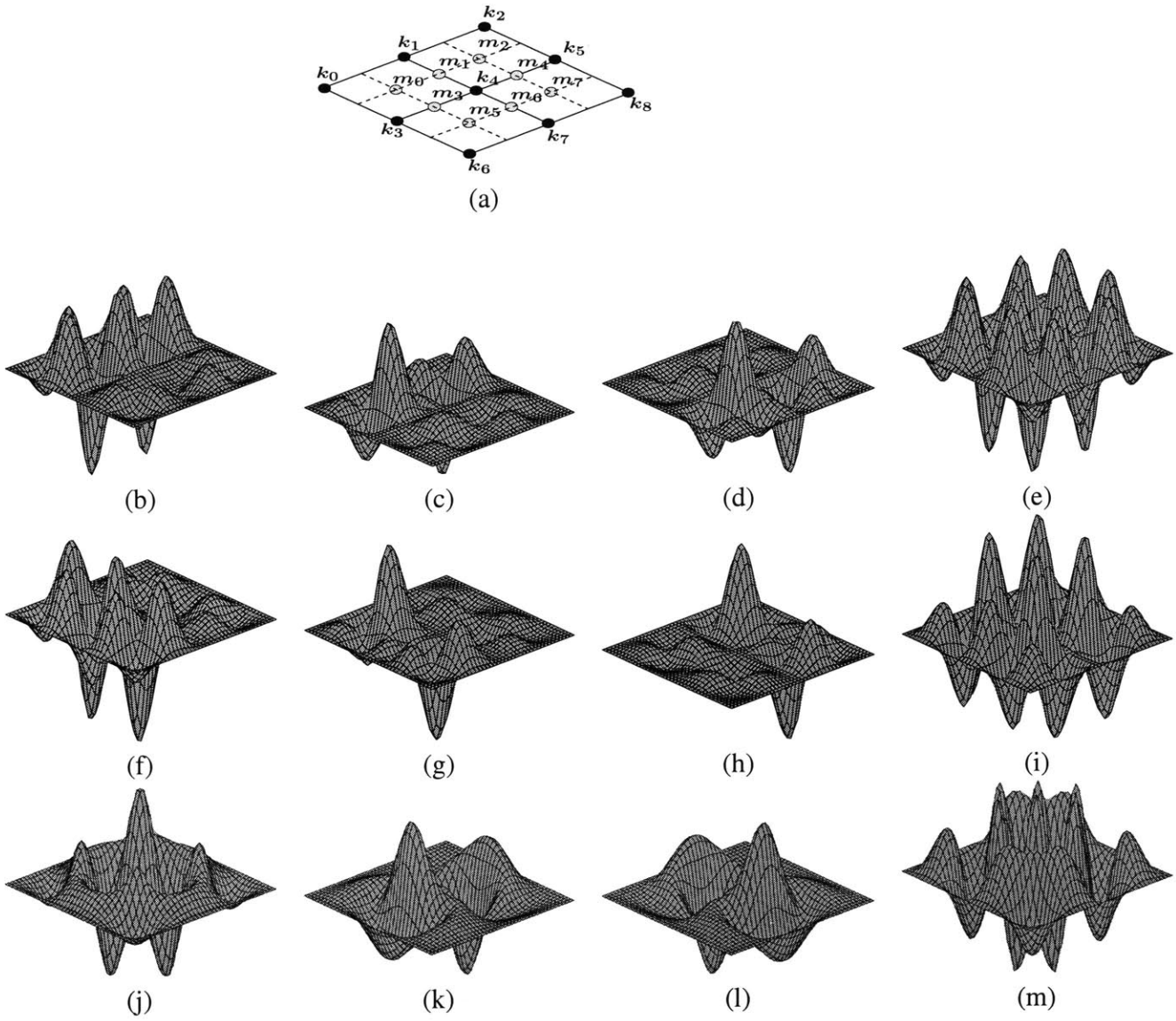

Figure 7-1: Scale-orthogonal on the interior: (a) Support set; (b) – (m) Scale-orthogonal wavelets with assumed support set.

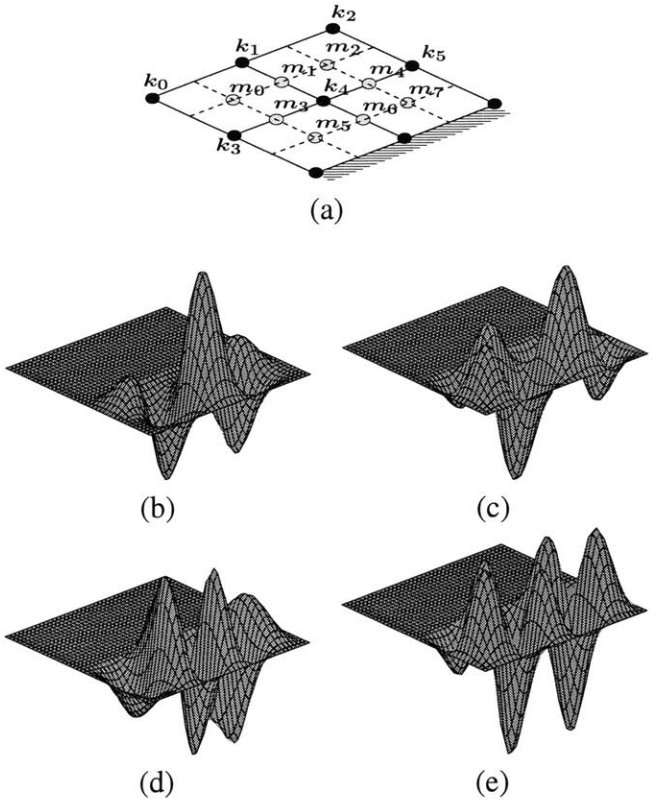

Figure 7-2: Scale-orthogonal wavelets next to a clamped boundary: (a) Support set showing the clamped boundary; (b) – (d) Scale-orthogonal wavelets with assumed support set, in addition to the 12 solutions illustrated in Figure 7-1.

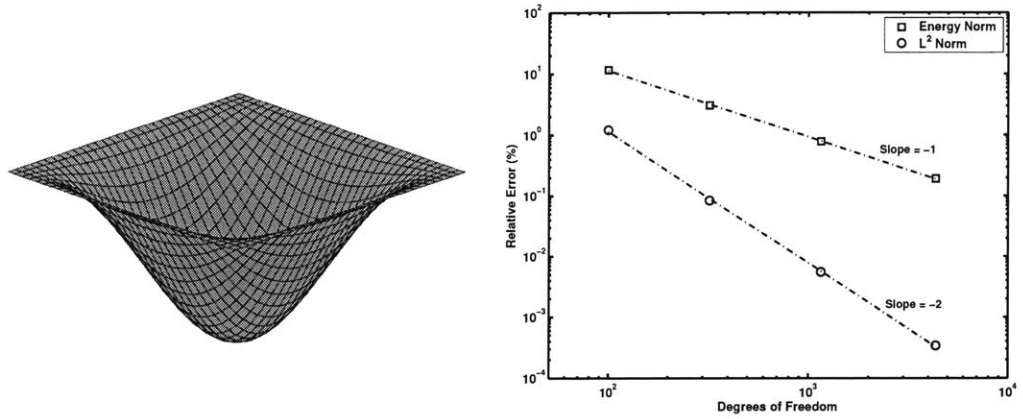

(a) (b)

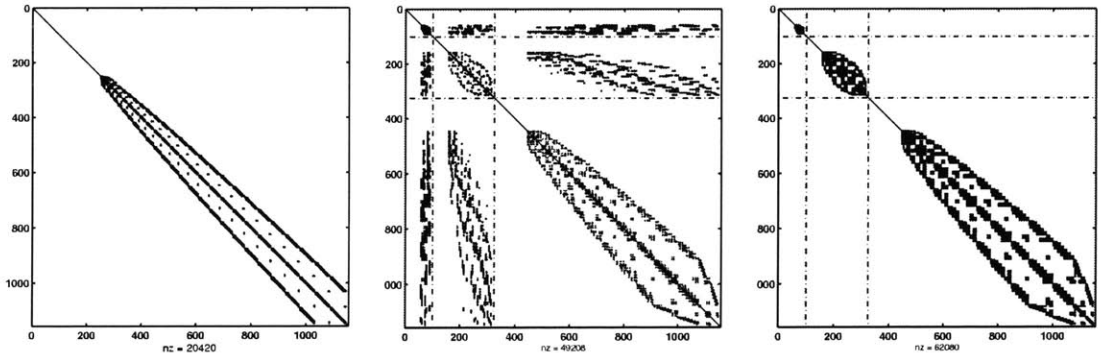

(c) (d) (e)

Figure 7-3: Clamped square plate: (a) Deformed shape; (b) Convergence rates in energy and L^2 norms using customized wavelets; (c) Nodal finite element stiffness matrix; (d) Three-level multiscale representation using hierarchical basis functions and (e) Three-level multiscale representation using customized wavelets.

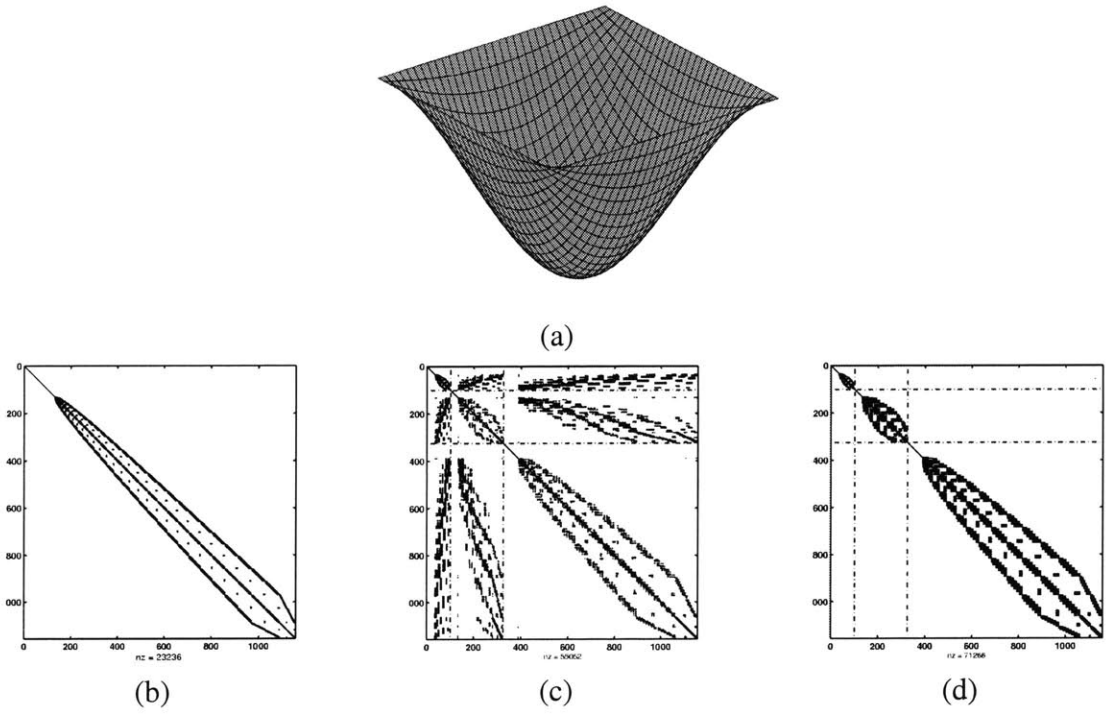

Figure 7-4: Simply-supported square plate: (a) Deformed shape; (b) Nodal finite element stiffness matrix; (c) Three-level multiscale representation using hierarchical basis functions and (d) Three-level multiscale representation using customized wavelets.

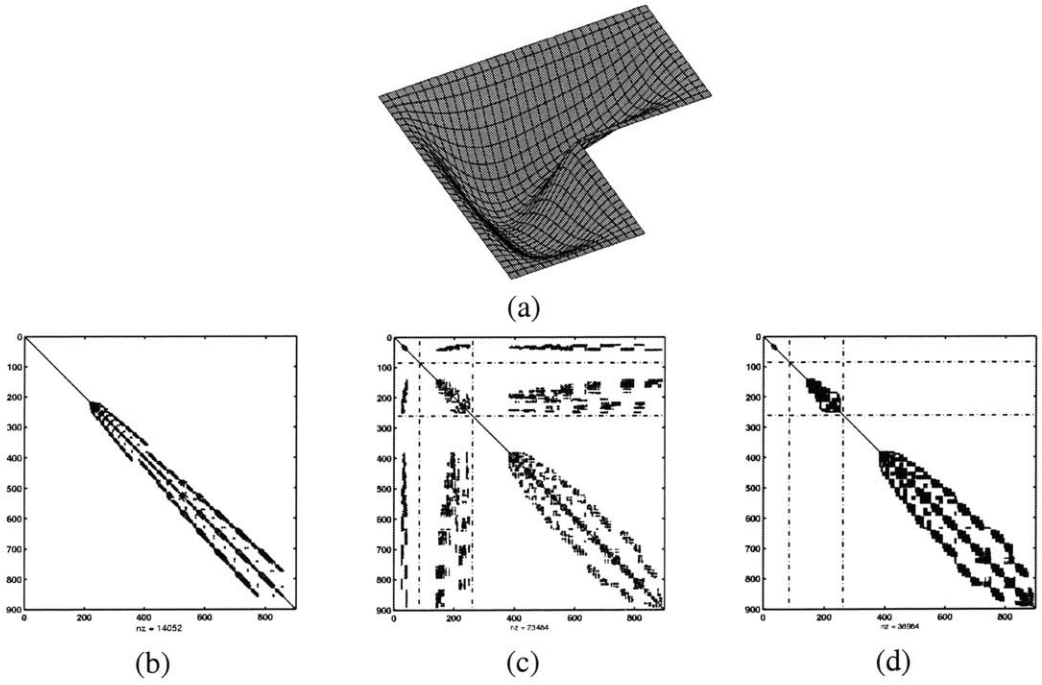

Figure 7-5: Clamped L-shaped plate. (a) Deformed shape; (b) Nodal finite element stiffness matrix; (c) Three-level multiscale representation using hierarchical basis functions and (d) Three-level multiscale representation using customized wavelets.

7.4 Application of wavelets constructed using Gram-Schmidt orthogonalization

In this section, we demonstrate the application of wavelets constructed via Gram-Schmidt orthogonalization to the adaptive solution of the prototype problems considered in Section 7.2. A typical set of scale-orthogonal wavelets constructed out of the Bogner-Fox-Schmidt interpolating functions using Gram-Schmidt orthogonalization is shown in Figure 7-6. Observe that even though the wavelets are globally supported, they decay rapidly outside the support of the original hierarchical basis functions and the rate of decay is in turn governed by the rate of decay of the Green's function for the corresponding operator.

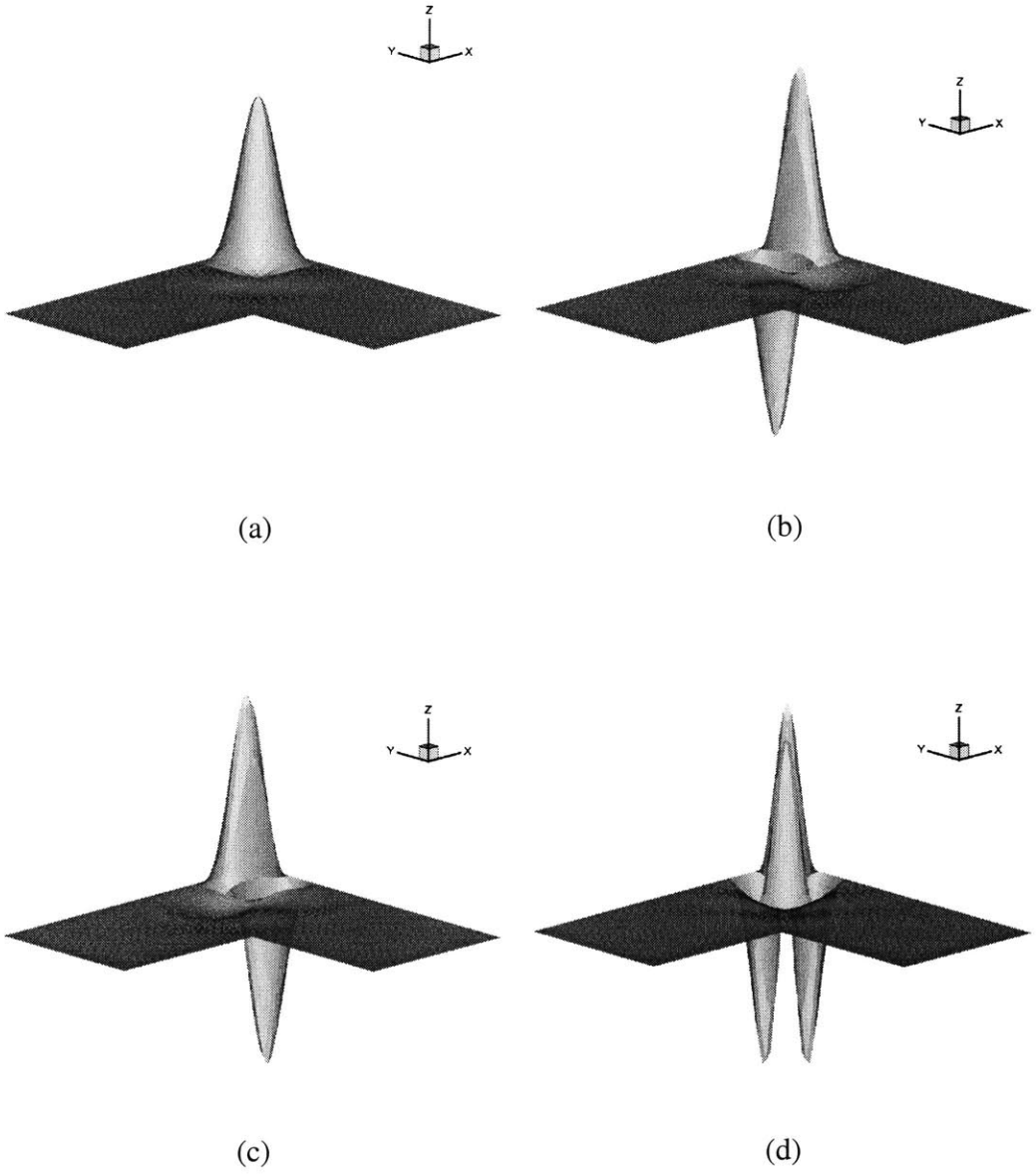

Figure 7-6: Scale-orthogonal wavelets constructed using Gram-Schmidt orthogonalization: (a) $w_{j,m}^{(0,0)}$; (b) $w_{j,m}^{(1,0)}$; (c) $w_{j,m}^{(0,1)}$; (d) $w_{j,m}^{(1,1)}$.

7.4.1 Integrated heat flux for a L-shaped domain

We first consider the adaptive solution of the steady-state heat conduction problem over the L-shaped domain with varying conductance, κ shown in Figure 7-7. The top boundary is subjected to homogeneous Dirichlet boundary conditions and the interior of the domain is subjected to uniform heating. The functional of interest is the integrated heat flux over the section $X - X$ corresponding to $y = -25$,

$$Q(u) = \int_{x=0}^{50} \nabla u \cdot \hat{n} \, \mathrm{d}x \Big|_{y=-25} \tag{7.10}$$

The reference solution, u_{ref} is taken to be the finite element solution at level 7 with 12545 degrees of freedom.

The set of wavelets retained at three consecutive levels 3, 4 and 5 are shown respectively in Figures 7-7(b), (c) and (d). Observe that to resolve the heat flux accurately, one needs to add wavelets only near the section of interest. The convergence of the functional for uniform and adaptive refinement is numerically shown in Table 7.1 and plotted with respect to the levels in Figure 7-8. As can be observed, the adaptive refinement technique gives almost exactly the same value of the functional as uniform refinement for each level although it is computed with much fewer degrees of freedom.

j	Uniform Refinement			Adaptive Refinement			Effectivity	
	DoF	$\lvert Q(u_j)\rvert$	$\frac{Q(u_j-u_{\text{Ref}})}{Q(u_{\text{Ref}})}$ %	DoF	$\lvert Q(\overline{u}_j)\rvert$	$\frac{Q(\overline{u}_j-u_{\text{Ref}})}{Q(u_{\text{Ref}})}$ %	CR_j	AR_j
3	65	156.2500	23.077	65	156.2500	23.077	1.00	1.00
4	225	140.6250	10.769	82	140.6250	10.769	0.36	1.00
5	833	132.8125	4.615	115	132.8125	4.615	0.14	1.00
6	3201	128.9063	1.539	180	128.9063	1.539	0.06	1.00
7	12545	126.9531		309	126.9532	0.000	0.02	1.00

Table 7.1: Convergence of the integrated heat flux for uniform and adaptive refinement.

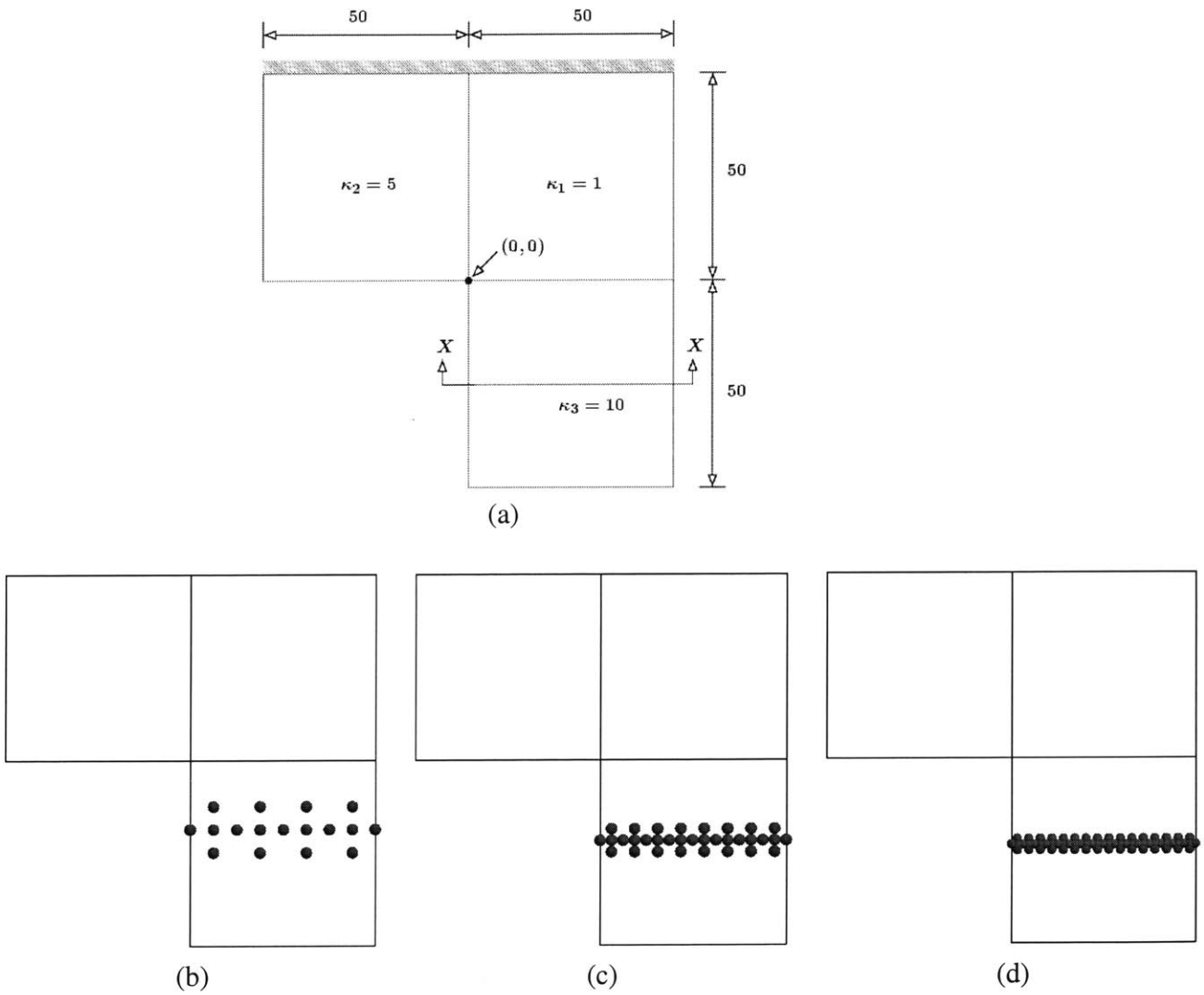

Figure 7-7: (a) Problem definition and retained wavelets at levels (b) 4 (c) 5 and (d) 6.

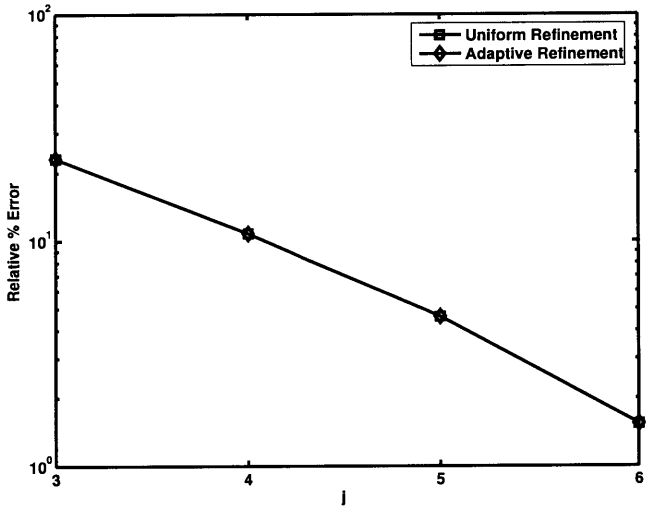

Figure 7-8: Convergence of integrated heat flux with number of levels for uniform and adaptive refinement.

7.4.2 Integrated shear stresses on a portal frame

We now consider the portal frame structure in plane stress described in Section 9.2 in [33] and illustrated in Figure 7-9. The thickness, Young's modulus and Poisson's ratio are assumed to be $h = 1$, $\mathsf{E} = 3 \times 10^7$ and $\nu = 0.16$. The frame is subjected to a uniform, horizontal body load of unit magnitude and the output functional of interest is the integrated shear stress across a horizontal section at a height of 4 units above the support,

$$Q(u) = \left(\int_0^2 \sigma_{12} \, \mathrm{d}x + \int_{14}^{16} \sigma_{12} \, \mathrm{d}x \right) \Bigg|_{y=4}$$

From elementary force balance, the exact shear force across the cross section is 144 units, which corresponds to the volume above the cross section. Figures 7-9 (b), (c) and (d) show the adapted meshes at levels 2, 3 and 4. Notice that in this case, to resolve the integrated shear stresses, one needs to add wavelets *both* near the singularities as well as near the section of interest. Table 7.2 shows the convergence in the quantity of interest with increasing levels of resolution and in Figure 7-10 we illustrate the convergence rates for the cases of uniform and adaptive refinement with increasing number of levels. Observe that the adapted solution is quite close to the solution obtained by uniform refinement and hence the adaptation process indeed does not lead to over compression.

j	Uniform Refinement			Adaptive Refinement			Effectivity	
	DoF	$\lvert Q(u_j)\rvert$	$\frac{Q(u_j - u_{\mathrm{Ref}})}{Q(u_{\mathrm{Ref}})}$ %	DoF	$\lvert Q(\overline{u}_j)\rvert$	$\frac{Q(\overline{u}_j - u_{\mathrm{Ref}})}{Q(u_{\mathrm{Ref}})}$ %	CR_j	AR_j
1	122	72.7377	49.488	122	72.7377	49.488	1.00	1.000
2	402	137.3411	4.625	202	136.4227	5.262	0.50	0.993
3	1442	152.7357	6.067	270	150.5721	4.564	0.19	0.986
4	5442	151.7893	5.409	318	149.6154	3.900	0.06	0.986
5	21122	148.7684	3.311	378	148.8423	3.363	0.02	1.000

Table 7.2: Convergence of integrated shear stresses at the section of interest for uniform and adaptive refinement

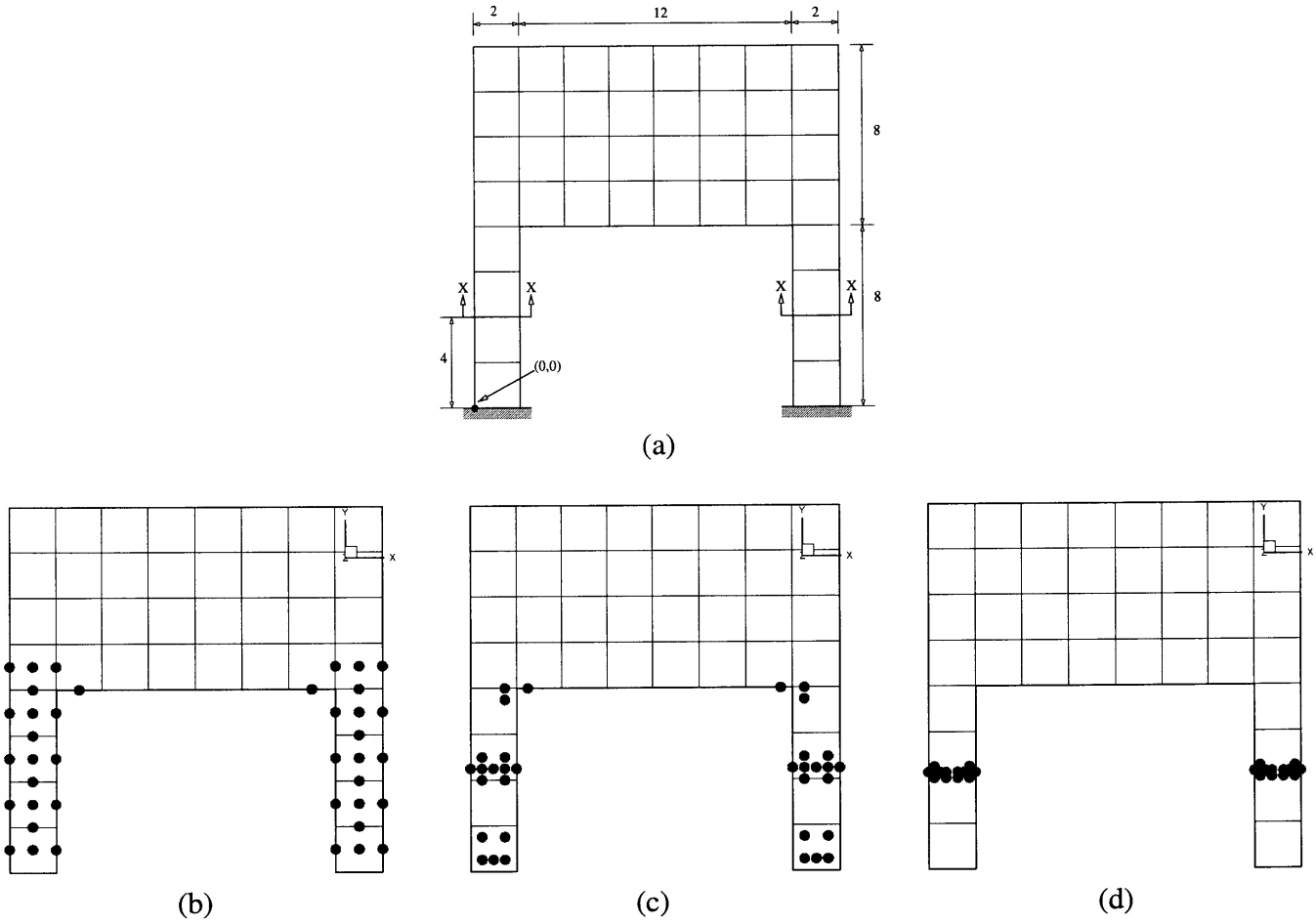

Figure 7-9: (a) Problem definition and retained wavelets at levels (b) 2 (c) 3 and (d) 4.

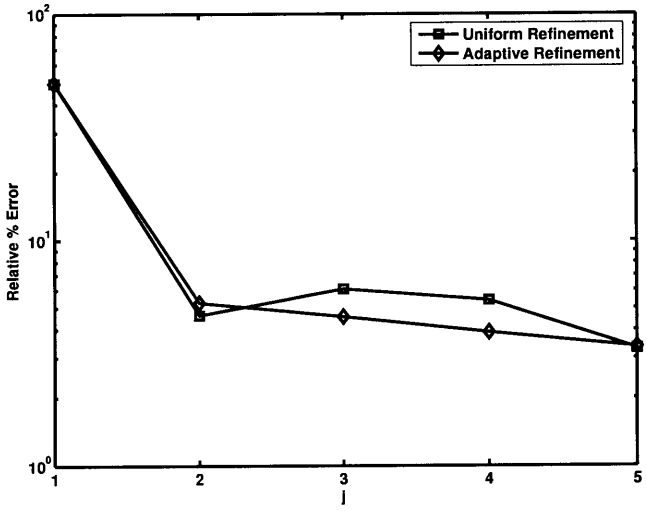

Figure 7-10: Convergence of integrated shear stress with number of levels for uniform and adaptive refinement.

7.4.3 Integrated normal stresses over the section of a MIT-shaped domain

We consider the MIT-shaped domain in plane stress illustrated in Figure 7-11 (a). The thickness and Poisson's ratio over the whole domain is taken as $h = 1$ and $\nu = 0.16$ and the Young's modulus over the "M" and "T" portions of the domain is $E = 1 \times 10^7$ and over the "I" portion of the domain is $E = 2 \times 10^7$. The body forces are applied as follows: the "M" and "T" portions of the domain have a horizontal body forces of magnitude 100 and -200 respectively whereas the "I" portion of the domain has a vertical body force of magnitude -400. Finally, the section $y = 0$ is subjected to homogeneous Dirichlet boundary conditions. The functional of interest is the integrated normal stress σ_{yy} over the support. Figure 7-11 (b) shows the deformed shape and the distribution of the normal stress over the domain.

Figures 7-12 (a), (b) and (c) illustrate the set of wavelets retained at levels 2, 3 and 4 while Table 7.3 and Figure 7-13 show the convergence of the integrated normal stress for the uniform and adaptive refinement cases.

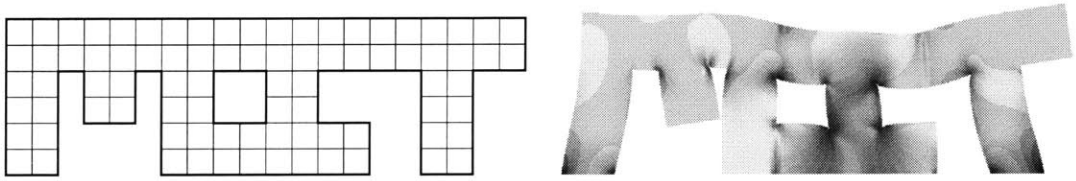

(a) (b)

Figure 7-11: (a) Undeformed initial mesh and (b) Deformed shape showing normal stress distribution.

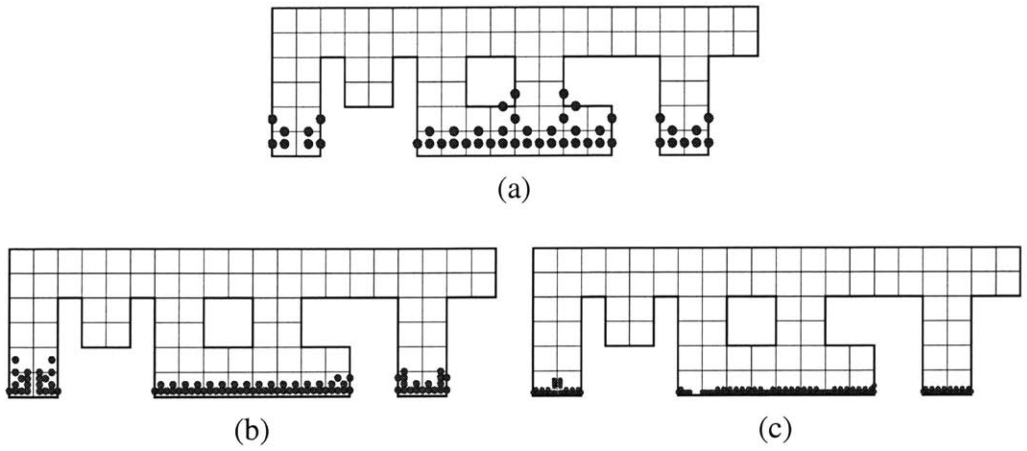

Figure 7-12: Retained wavelets over the MIT domain at levels (a) 2; (b) 3 and (c) 4.

j	Uniform Refinement			Adaptive Refinement			Effectivity	
	DoF	$\lvert Q(u_j)\rvert$	$\frac{Q(u_j-u_{\text{Ref}})}{Q(u_{\text{Ref}})}$ %	DoF	$\lvert Q(\overline{u}_j)\rvert$	$\frac{Q(\overline{u}_j-u_{\text{Ref}})}{Q(u_{\text{Ref}})}$ %	CR_j	AR_j
1	252	250189.3302	10.089	252	250189.3302	10.089	1.00	1.000
2	840	265498.9751	4.587	350	265477.5437	4.595	0.42	1.000
3	3024	272873.2732	1.937	534	272878.1291	1.935	0.18	1.000
4	11424	276483.5166	0.639	814	276491.5290	0.637	0.07	1.000
5	44352	278262.3455		1206	278278.8867	0.006	0.02	1.000

Table 7.3: Convergence of integrated normal stresses at the support for uniform and adaptive refinement

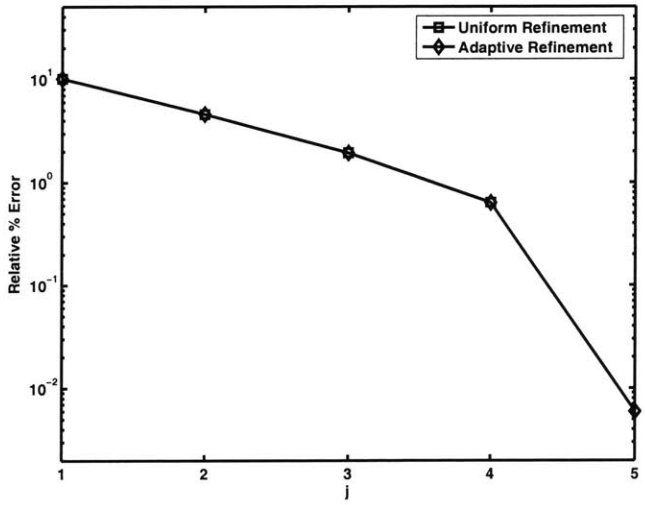

Figure 7-13: Convergence of integrated normal stresses at the support with number of levels for uniform and adaptive refinement.

7.4.4 Energy-norm adaptivity for a L-shaped plate

In this example, we perform energy-norm based adaptivity for a uniformly-loaded L-shaped Kirchhoff plate with length, thickness, Young's modulus and Poisson's ratio taken to be $L = 100.0$, $h = 1.0$, $\mathsf{E} = 1.0 \times 10^7$, and $\nu = 0.3$. Figure 7-14 shows the distribution of the error terms $\left\| r_{j,m}^{\mathsf{T}} w_{j,m} \right\|_{\mathrm{E}}$, $m \in \mathcal{M}(j)$ (normalized with respect to $\max_{m \in \mathcal{M}(j)} \left\| r_{j,m}^{\mathsf{T}} w_{j,m} \right\|_{\mathrm{E}}$) for four levels of adaptive refinement. As expected, wavelets that contribute significantly to the residual norm are localized near the corner, particularly at the higher levels. In Figure 7-15 we compare the displacements and M_{xx} bending moments obtained using mesh adaptivity to the reference solution obtained from a five-level uniform refinement of the base mesh (with 50180 degrees of freedom). The numerical values of the errors in the energy and L^2 norms are summarized in Table 7.4 and the final adapted mesh is illustrated in Figure 7-16. Figure 7-17 illustrates the convergence behavior of the adaptive method with increasing levels of refinement. As can be observed, in the adaptive refinement method, the error (with respect to the reference solution) decays at approximately the same rate as for uniform refinement, except that the solution is represented using far fewer degrees of freedom (see Table 7.4).

j	NonUniform Refinement				Adaptive Refinement				Effectivity	
	DoF	$u_{j,\max}$	$\frac{\|u_j - u_{\mathrm{ref}}\|_{\mathrm{E}}}{\|u_{\mathrm{ref}}\|_{\mathrm{E}}}\%$	$\frac{\|u_j - u_{\mathrm{ref}}\|_{\mathrm{L}^2}}{\|u_{\mathrm{ref}}\|_{\mathrm{L}^2}}\%$	DoF	$\overline{u}_{j,\max}$	$\frac{\|\overline{u}_j - u_{\mathrm{ref}}\|_{\mathrm{E}}}{\|u_{\mathrm{ref}}\|_{\mathrm{E}}}\%$	$\frac{\|\overline{u}_j - u_{\mathrm{ref}}\|_{\mathrm{L}^2}}{\|u_{\mathrm{ref}}\|_{\mathrm{L}^2}}\%$	CR_j	$\frac{\|\overline{u}_j\|_{\mathrm{E}}}{\|u_j\|_{\mathrm{E}}}$
1	260	0.02468	18.24	4.13	260	0.02468	18.24	4.13	1.00	1.0000
2	900	0.02536	11.53	1.76	600	0.02536	11.69	1.79	0.67	0.9998
3	3332	0.02565	7.36	0.72	652	0.02565	7.79	0.78	0.20	0.9997
4	12804	0.02579	4.17	0.23	704	0.02579	4.93	0.29	0.05	0.9997
5	50180	0.02588			764	0.02585	2.64	0.08	0.02	0.9997

Table 7.4: Comparison of results using uniform and adaptive refinement. The reference solution u_{ref} corresponds to the displacement obtained using the mesh with 50180 degrees of freedom.

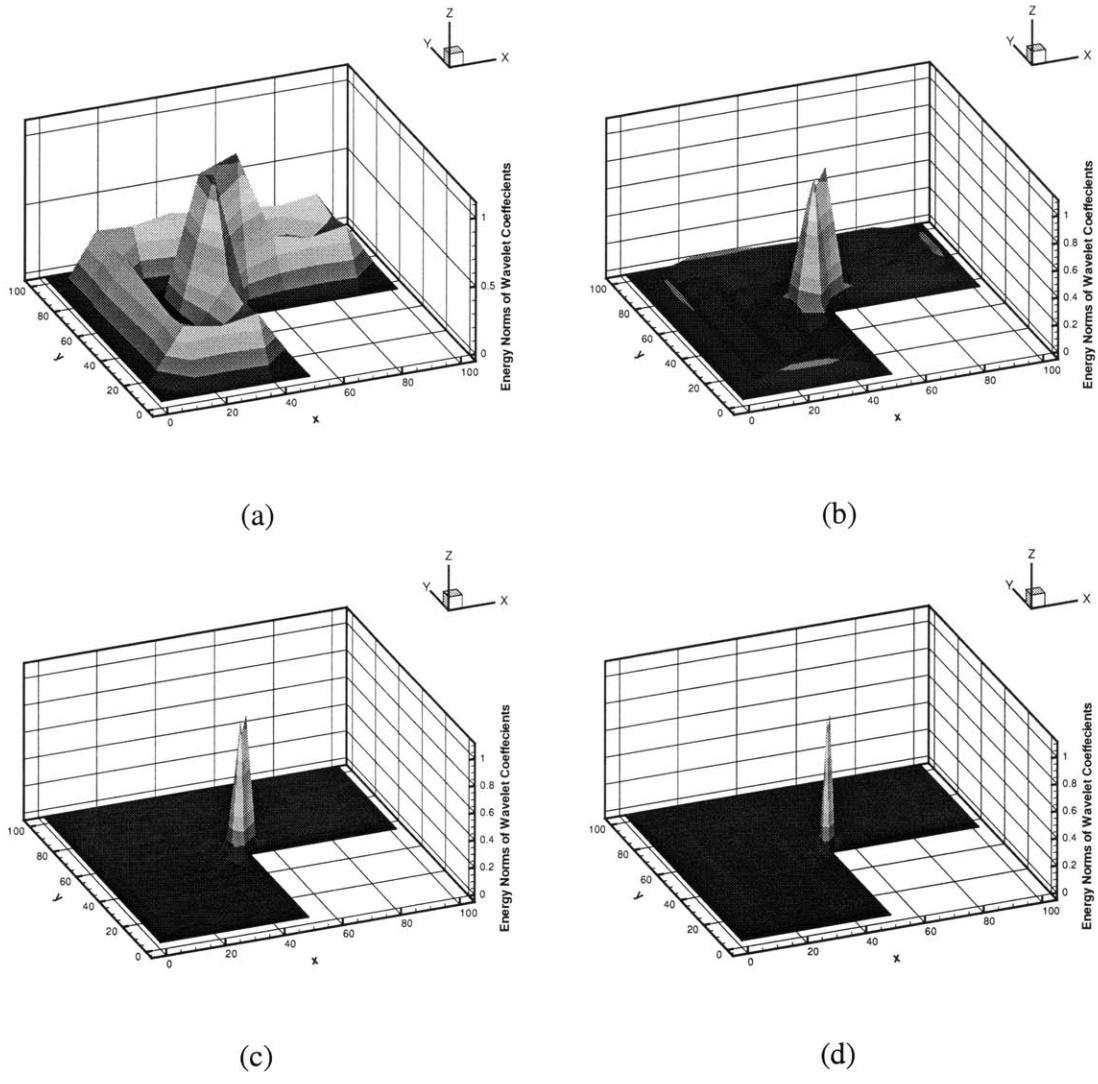

Figure 7-14: Normalized estimated distribution of wavelet coefficients in the energy norm for: (a) $j = 1$ (b) $j = 2$ (c) $j = 3$ and (d) $j = 4$.

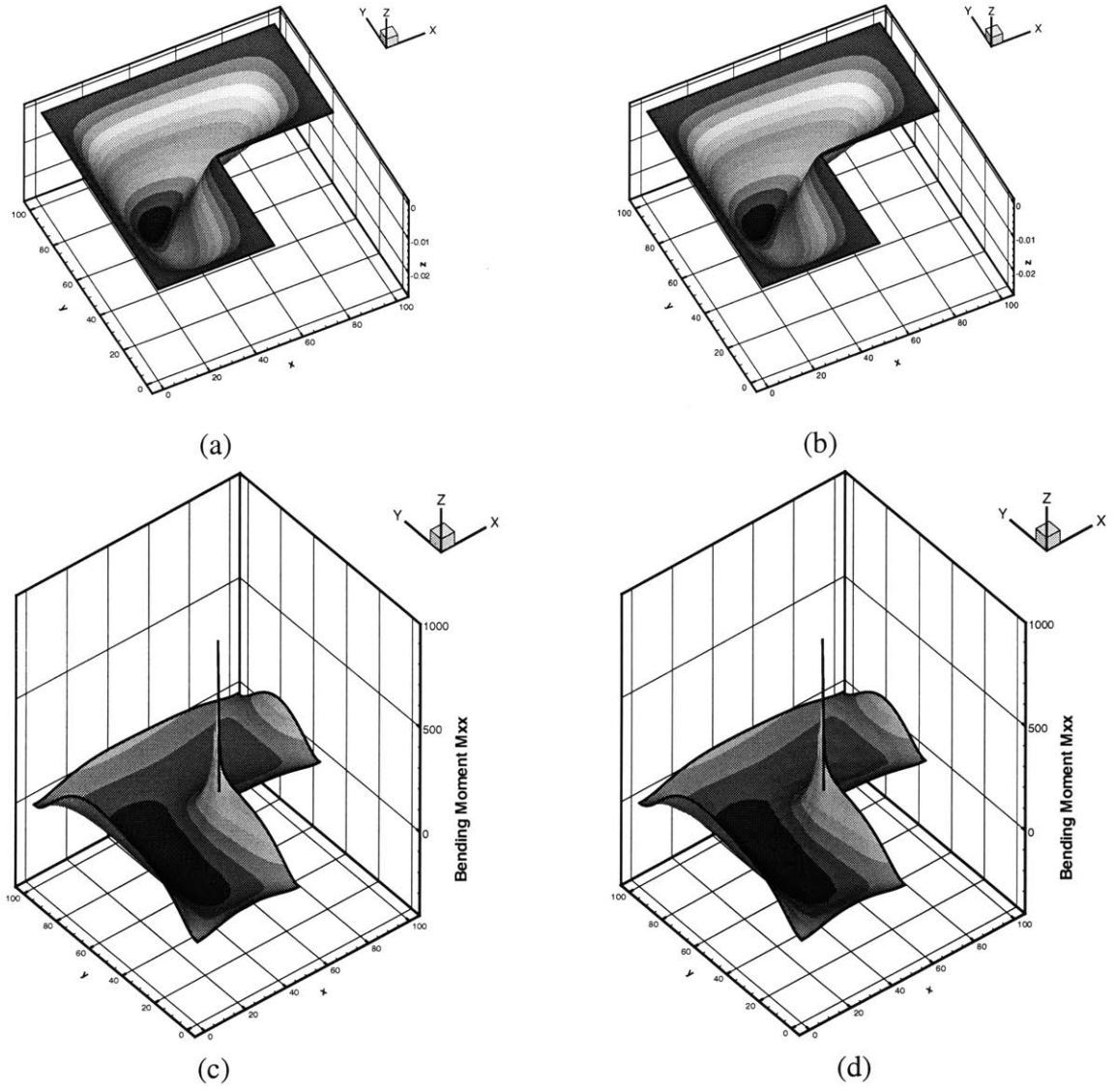

Figure 7-15: Comparison of reference and adapted solutions. (a) Displaced shape of reference solution (50180 DoF); (b) Displaced shape of the adapted solution (764 DoF); (c) M_{xx} bending moment of reference solution and (d) M_{xx} bending moment of the adapted solution.

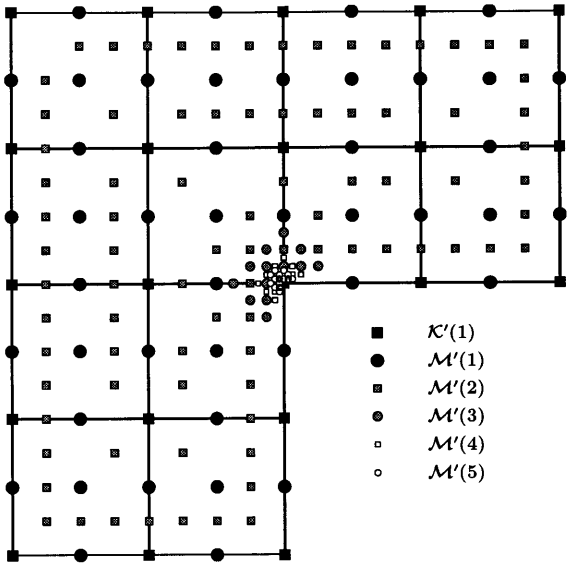

Figure 7-16: Adapted mesh after five refinement levels.

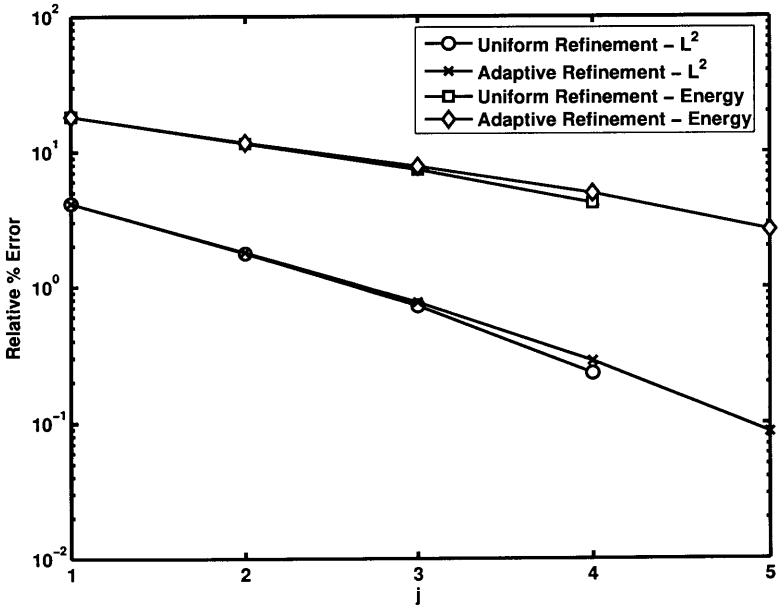

Figure 7-17: Convergence of uniform and adaptive wavelet refinement with increasing number of levels in the energy and L^2 norms.

7.4.5 Tip displacements of a cantilever plate

In this example, we consider the goal of determining the tip displacements of a uniformly-loaded Kirchhoff plate with an overhang as shown in Figure 7-18(a). The functional of interest can therefore be given as

$$Q(u) = \int_{\Omega} u\, \delta(x - x_0)\, \mathrm{d}\Omega \tag{7.11}$$

where $x_0 = (-100, 50)$. The thickness, Young's modulus, and Poisson's ratio of the plate are taken respectively as $h = 2$, $\mathsf{E} = 1.0 \times 10^7$, and $\nu = 0.3$. From symmetry considerations, we choose a half-symmetric model with the section indicated by line X-X being left unconstrained. Figures 7-18(b), (c), and (d) illustrate the adapted meshes at levels $j = 3$, 4, and 5 respectively. The convergence of the tip displacement is shown in Table 7.5. It can be observed that to accurately estimate the point value at the tip, it suffices to refine only near the origin and not near the point of interest. This is because the detail functions r_j and η_j have large contributions from wavelets only near the origin and not near the point of interest as is evident from Figure 7-20.

j	Uniform Refinement			Adaptive Refinement			Effectivity	
	DoF	$\lvert Q(u_{\text{ref}})\rvert$	$\frac{Q(u_j - u_{\text{Ref}})}{Q(u_{\text{Ref}})}$ %	DoF	$\lvert Q(\overline{u}_j)\rvert$	$\frac{Q(\overline{u}_j - u_{\text{Ref}})}{Q(u_{\text{Ref}})}$ %	CR_j	AR_j
2	188	2.81636	17.6993	188	2.81636	17.6993	1.000	1.000
3	628	3.08646	9.8062	212	3.08416	9.8736	0.338	0.999
4	2276	3.25787	4.7973	232	3.25319	4.9338	0.101	0.998
5	8644	3.36129	1.7752	252	3.35341	2.0052	0.029	0.998
6	33668	3.42203		272	3.40989	0.3549	0.008	0.997

Table 7.5: Convergence of tip displacements for uniform and adaptive refinements.

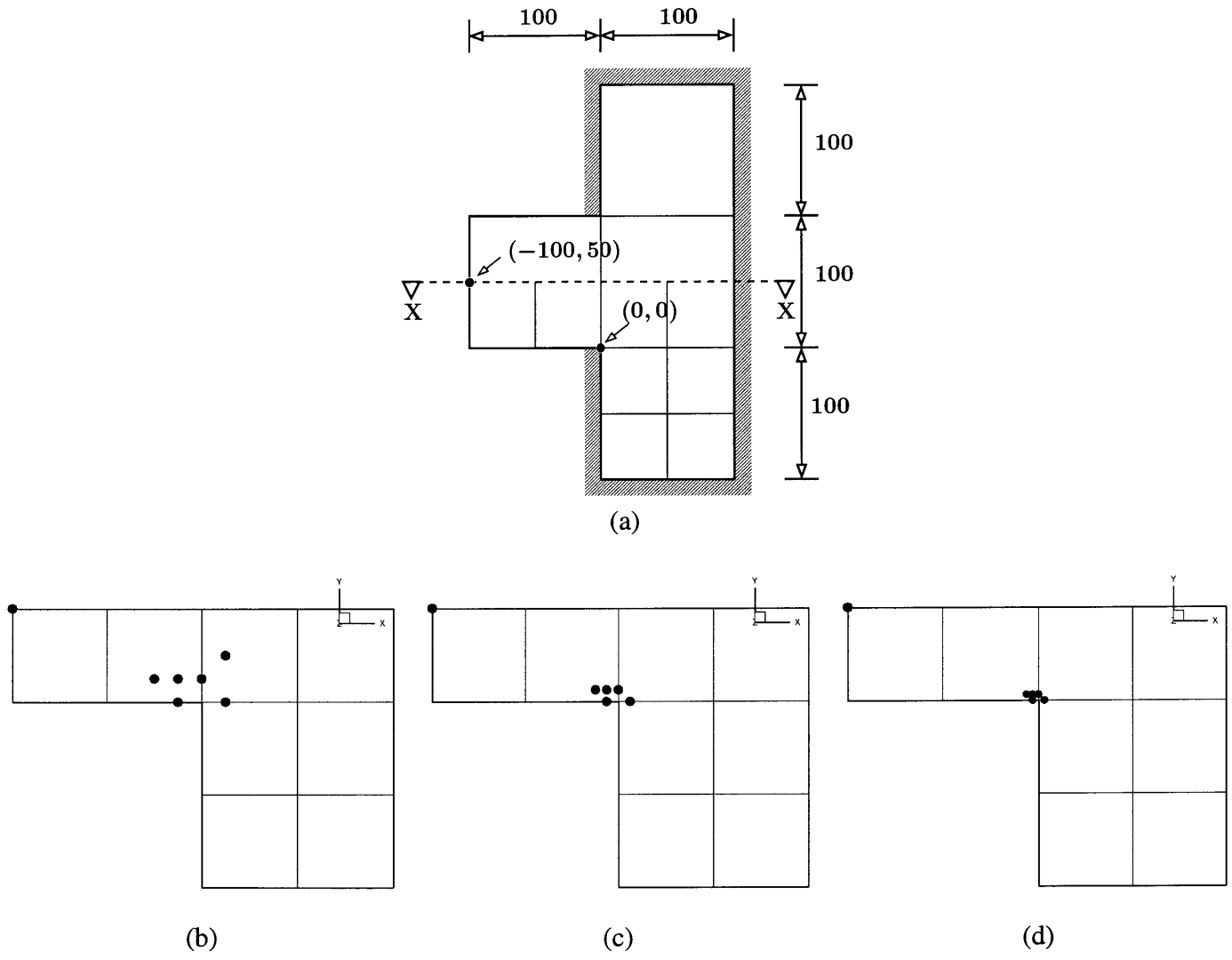

Figure 7-18: Tip displacements of a cantilever overhang. (a) Problem definition and wavelets retainied at levels (b) $j = 3$ (c) $j = 4$; and (d) $j = 5$.

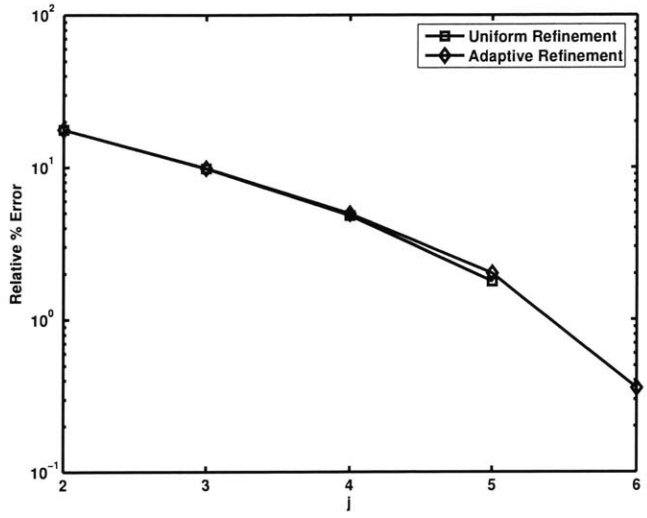

Figure 7-19: Convergence of tip displacements for uniform and adaptive refinement.

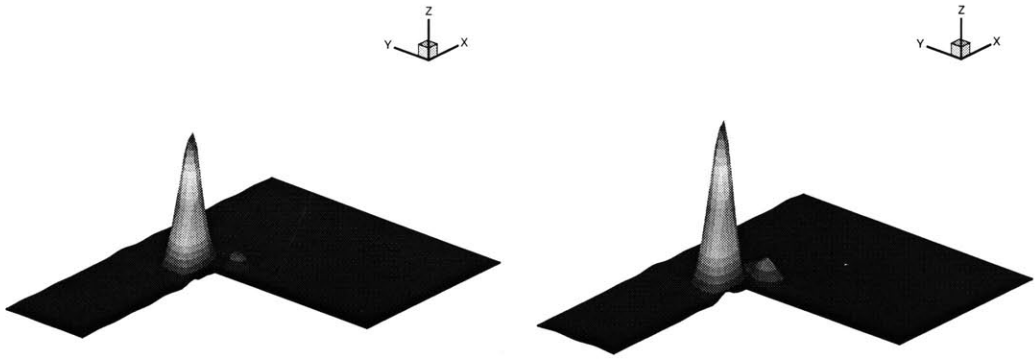

(a) (b)

Figure 7-20: Distribution of (a) the function r_j corresponding to the displacement and (b) the function η_j corresponding to the influence function at level $j = 3$

7.4.6 Support bending moments of a square plate

We finally consider the problem of adaptively computing the M_{xx} bending moment at a point on the support of a uniformly loaded clamped, square plate shown in Figure 7-21(a). The linear functional of interest is then given as

$$Q(u) = \mathsf{D} \int_{\Omega} (\delta_{xx}(x - x_0) + (1 - \nu)\delta_{yy}(x - x_0))\, u \, \mathrm{d}\Omega$$

where δ_{xx}(resp. δ_{yy}) is the second partial distributional derivative of the Dirac distribution in the x (resp. y) direction.

The thickness, Young's modulus, and Poisson's ratio in this problem are taken respectively as $h = 1$, $\mathsf{E} = 1.0 \times 10^7$, and $\nu = 0.3$. Figures 7-18(b), (c), and (d) illustrate the adapted meshes at levels $j = 3,\ 4$, and 5 respectively while the convergence of the support bending moment can be seen in Table 7.6. Figure 7-22 illustrates the convergence of the adaptive refinement procedure with increasing number of levels; once again the convergence properties closely resemble those of the uniform refinement case.

In this example, we observe the wavelets need to be added only near the boundary since the primal solution u is smooth, whereas the dual solution z has large wavelet contributions near the point of interest.

j	Uniform Refinement			Adaptive Refinement			Effectivity	
	DoF	$\lvert Q(u_j)\rvert$	$\frac{Q(u_j - u_{\mathrm{Ref}})}{Q(u_{\mathrm{Ref}})}$ %	DoF	$\lvert Q(\overline{u}_j)\rvert$	$\frac{Q(\overline{u}_j - u_{\mathrm{Ref}})}{Q(u_{\mathrm{Ref}})}$ %	CR_j	AR_j
2	100	434.6900	15.247	100	434.6900	15.247	1.00	1.000
3	324	489.1438	4.630	120	488.9504	4.668	0.37	0.999
4	1156	506.6726	1.212	140	506.6619	1.215	0.12	0.999
5	4356	511.5910	0.253	164	511.7179	0.229	0.04	1.000
6	16900	512.8909		188	513.0806	0.037	0.01	1.000

Table 7.6: Convergence of support bending moments for uniform and adaptive refinement.

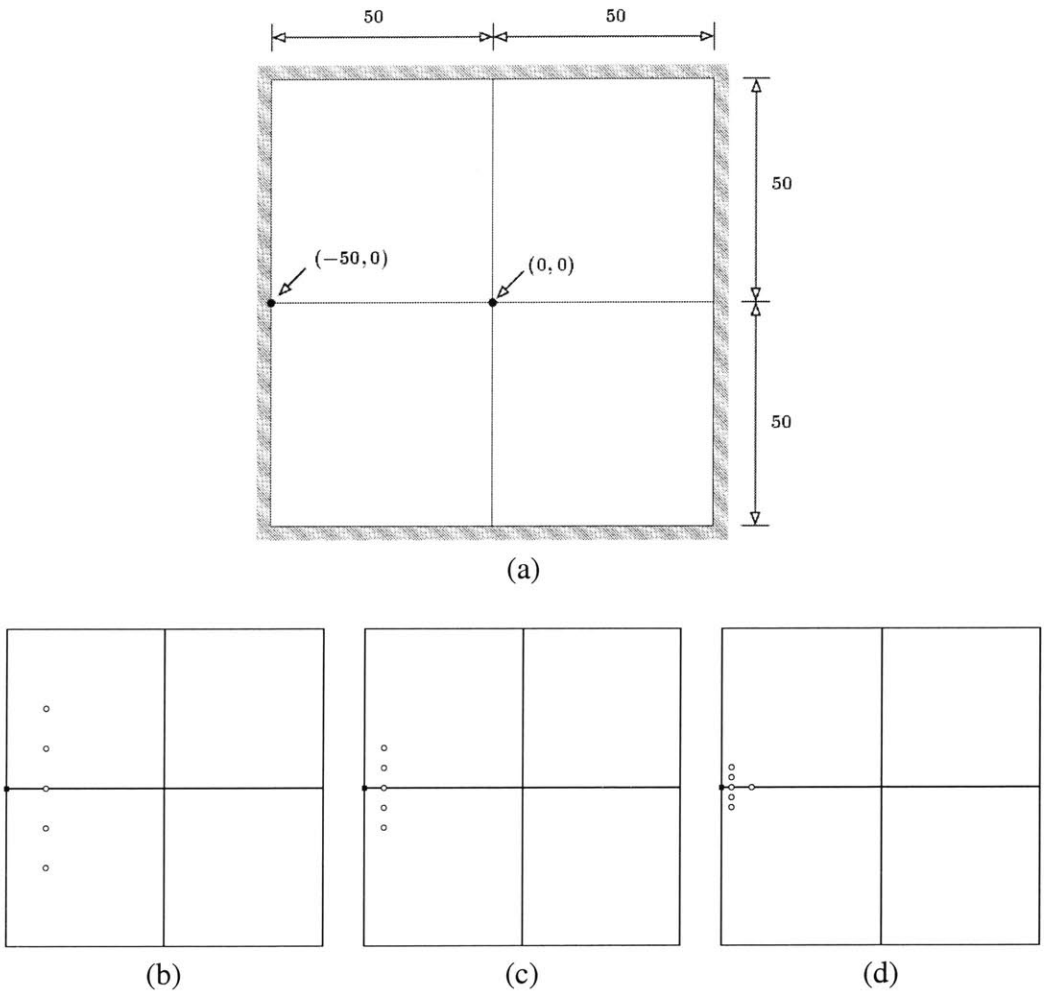

Figure 7-21: Support bending moments for a square, clamped plate. (a) Problem definition and wavelets retained at levels (b) $j = 3$ (c) $j = 4$ and (d) $j = 5$.

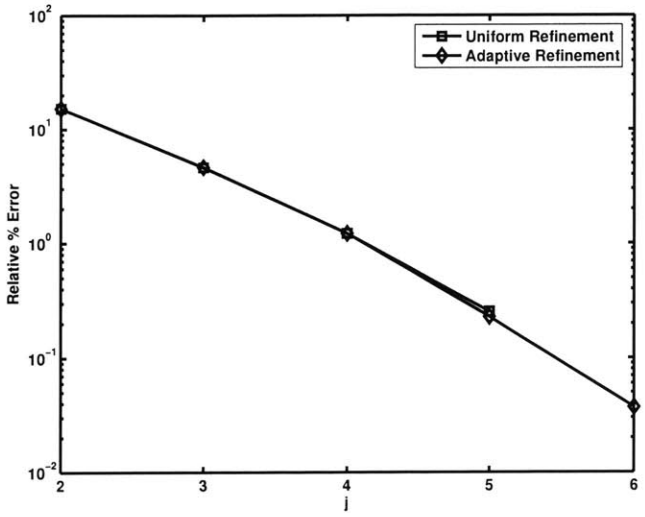

Figure 7-22: Convergence of support bending moment with increasing number of levels.

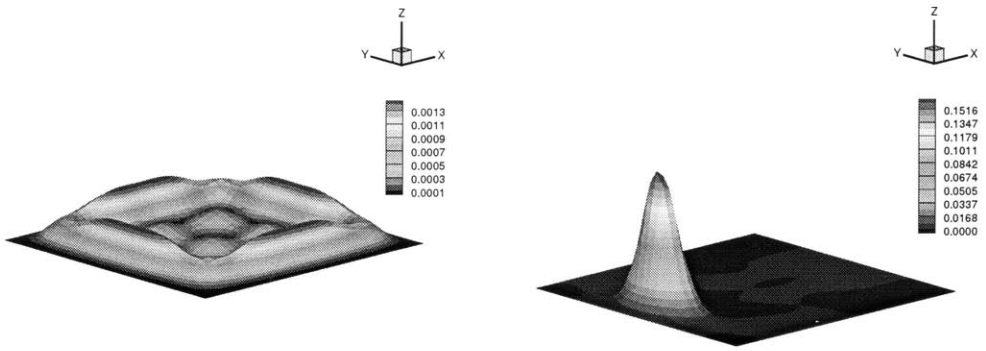

(a) (b)

Figure 7-23: Distribution of (a) the function r_j corresponding to the displacement and (b) the function η_j corresponding to the influence function at level $j = 3$. Note that the two figures are plotted on different scales and the magnitude of the influence function is much larger than that of the solution

7.5 Closure

In this chapter, we demonstrated the application the of error-estimation and adaptive refinement techniques proposed in Chapter 6 for the efficient solution of partial differential equations of second and fourth order. The effectiveness of the proposed techniques was measured using two quantities, the compression ratio (related to how cheaply the adaptively refined solution is computed) and the accuracy ratio (related to how accurate the adapted solution at a particular level is vis-a-vis the solution obtained via uniform refinement).

An interesting observation from the presented results is the clear distinction between goal-oriented adaptivity and adaptivity based solely on the energy norm of the solution error. For example, in the case of the Poisson's equation, adaptivity based on the energy norm would have resulted in a mesh that had a large concentration of wavelets near the re-entrant corner. However, this mesh would not have resulted in an accurate estimate for the heat flux since clearly that requires the addition of wavelets near the section of interest. In contrast, for the case of the cantilever plate, addition of wavelets near the point of interest would not have resulted in a more accurate estimate for the tip displacements since, as can be seen from the presented results, most of the contribution from the wavelets is from those that are localized near the singularity. The presented results also emphasize the importance of an error estimation technique such as the one proposed in Chapter 6 that directly computes the error in the functional of interest in contrast to bounding the error using energy norm of the errors in the solution and the influence function. In the latter case, the resulting adapted meshes can be highly suboptimal due to over-estimation of the error.

Chapter 8

Conclusions and Further Work

The things to do are: the things that need doing, that you see need to be done, and that no one else seems to see need to be done.
– Buckminster Fuller

In this final chapter, we summarize the work presented in this thesis along with our major contributions and present several promising avenues for further research.

8.1 Summary of the thesis

As described in Chapter 1, the primary goal of our research was to cast the problem of adaptive finite element analysis of the solution to the virtual work equation

$$a(u, v) = l(v) \quad (v \in V) \tag{8.1}$$

into the framework of multiresolution signal processing. To this end we considered the solution u as if it were a signal (albeit one that was known only indirectly via the underlying weak-form) and developed computationally efficient techniques to estimate and efficiently represent it at different levels of resolution. There were essentially four "tricks-of-the-trade" that were developed during the course of our research for this to be possible.

The first was to construct a ladder of approximation spaces $V_j,\ j \in \mathbb{N}$ such that they formed a multiresolution analysis of the underlying Sobolev space V. This was made pos-

sible by the use of *conforming* finite element interpolation functions on nested discretizations. Eq (3.4) then ensured that upon mesh refinement by uniform subdivision of elements, the spaces were nested and in the limit, their union was dense in V.

The second trick in our multiresolution finite element framework (which was also a significant point of departure from classical finite element adaptivity) was the decomposition of the true solution into the solution at the coarsest level mesh, u_0 and a telescopic sum consisting of the *two-level* errors. Unlike the true error in a mesh which is often hard to estimate accurately on coarse meshes, the two-level errors lie in succesively richer finite dimensional spaces and lend themselves to highly efficient and accurate estimation. Moreover, we argued in Chapter 6 that error estimation and adaptivity based on the two-level error does not depend on the resolution of the coarsest mesh and hence offers several advantages over contemporary error estimation and adaptivity procedures used in finite element analysis.

The third trick was then to construct a suitable basis for representing the two-level errors. This, it was concluded was most effectively done by the construction of *scale-orthogonal* wavelets that span the orthogonal complements (with respect to the $a(\cdot,\cdot)$ inner-product) of the finite element approximation spaces V_j at each level. It was proven in Lemma 6.2 that the two-level errors were simply the projection of the solution onto these orthogonal spaces and hence the solution could be computed in an entirely scale-decoupled manner. This property in turn permitted efficient *local* and *incremental* refinement of the solution. We also argued that in addition to scale-orthogonality, the wavelets used in our framework must also ideally be compactly supported and Riesz stable in the energy norm. The first property ensured that the coefficients corresponding to the wavelets could be computed in an efficient manner whereas the second property guaranteed that an accurate solution in the energy norm could be obtained simply by discarding wavelets with small energy-norm contributions.

Towards this end, in Chapter 5 we proposed two techniques for the construction of scale-orthogonal wavelets starting from the hierarchical basis framework [51, 52, 53]. The first technique based on the stable completion procedure of Carnicer, et al [16] resulted in the locally supported wavelets that *did not* possess the Riesz stability property in general.

In contrast, the second procedure based on approximate orthogonalization via a Gram-Schmidt process resulted in globally-supported, albeit rapidly decaying wavelets that were provably Riesz stable as shown in Lemma 5.14. We also proposed an efficient implementation technique for the construction of these wavelets based on the connection between Gram-Schmidt orthogonalization and $\mathbf{LDL}^T$ factorization of the Grammian matrix and concluded that it was in fact practical to use these globally supported wavelets *provided* they were used within the framework of an adaptive representation (i.e., only a few of these wavelets were retained at each level).

Once the wavelets were constructed, the final piece of the puzzle was then to decide which wavelets to keep at a certain level and which ones to discard. This is another instance where Riesz stability of the wavelets became invaluable: computing the detail coefficients exactly is as expensive as computing the solution at the next level and we therefore proposed a technique for the efficient estimation of the wavelet coefficients based on the equivalence between the scale-orthogonal wavelets and hierarchical basis functions, Lemma 5.8. The wavelets to be discarded were then determined simply by looking at the contribution of each wavelet to a given functional of interest (i.e., we considered the more general problem of *goal-oriented* adaptivity rather than just adaptivity in the energy norm). We then provided an analysis of the accuracy of the proposed method by estimating the effect of different approximations (such as the replacement of scale-orthogonal wavelets using hierarchical basis functions, the estimation of the details using conjugate gradients and the approximate orthogonalization of the wavelets using Gram-Schmidt orthogonalization).

Finally, we considered several examples of partial differential equations cast in their weak-form, such as the Poisson's equation, two-dimensional linear elasticity and the thin-plate bending equation and demonstrated the effectiveness of our proposed error-estimation and adaptive refinement approaches both for energy norm and goal-oriented adaptivity.

8.2 A look ahead

The following are the possible extensions to the ideas proposed in this thesis:

1. *Construction of Riesz stable locally-supported wavelets.* As mentioned in Chapter 5

the construction procedure for scale-orthogonal wavelets does not, as yet, guarantee that the resulting wavelets will be Riesz stable in the energy norm. However, the locally-supported wavelets with a given support are clearly non-unique (as they arise from the solution of a system of homogenous equations), and it is therefore concievable that appropriate constraints could be imposed during the construction of the filters that can ensure *a priori* Riesz stability of the scale-orthogonal wavelets. What remains to be investigated in this direction is (a) whether it is *always* possible (independent of the operator, the finite element interpolation functions and the domain) to construct locally-supported Riesz stable scale-orthogonal wavelets and (b) exactly what constraints are necessary on the matrices $\mathbf{G}_j$ such that the resulting wavelets are scale-orthogonal, locally supported and Riesz stable in the energy norm and (c) whether such a procedure would be computationally efficient.

2. *Construction of locally-supported, approximately scale-orthogonal wavelets using Gram-Schmidt orthogonalization.* In Chapter 5 it was argued that the exact construction of scale-orthogonal wavelets using Gram-Schmidt orthogonalization was prohibitively expensive; hence an approximate orthogonalization technique based on partial orthogonalization of the wavelets was proposed. Essentially, this procedure constructed wavelets that were scale-orthogonal only to the basis functions in V_j^{Adapt} rather than V_j. We justified this approximation using the estimates derived in Chapter 6: the error incurred in computing the details can be bounded above by the contribution of the discared wavelets to the solution. Since this is typically rather small (as this is the criterion for discarding the wavelets in the first place), the resulting detail coefficients are very close in practice to the true details at a given level.

   An alternative construction procedure for approximately constructing scale-orthogonal wavelets is to use the decay properties of the Green's function for the given inner-product and construct locally-supported wavelets that are only approximately scale-orthogonal. While this procedure can be expected to be computationally efficient, the key questions that one must answer are: (a) how the accuracy of orthogonalization impacts the accuracy of the computed detail coefficients (b) how a suitable

neighborhood for orthogonalization can be determined without *a priori* or with only an approximate knowledge of the Green's function and (c) how much the approximate orthogonalization process impacts the Riesz stability property of the resulting wavelets.

3. *Multiresolution error-estimation and adaptive refinement techniques for mixed interpolation problems.* The main emphasis of this thesis was the development of error estimation and adaptive refinement techniques for single field problems, i.e., where all the components of the solution belong to a single Sobolev space V. However, in many practical problems of interest such as the mechanics of incompressible media or the deformation of shells, the field variables (resp. displacements and pressure or displacements and strains) belong to two or more Sobolev spaces [10]. An interesting extension of our work would be to derive a multiresolution analysis for spaces of the form $V \times W$ where V and W are the individual Sobolev spaces. The open questions in this regard are (a) under what conditions a MRA exist for $V \times W$, i.e., if $V_j \subset V$ and $W_j \subset W$ then is the union of $V_j \times W_j$ always dense in $V \times W$? In particular what is the role of the discrete inf-sup condition [10]? (b) whether the construction techniques for scale-orthogonal wavelets apply equally well to the mixed formulation case and (c) whether the same desirable properties such as Riesz stability can be guaranteed in an *a priori* manner as was possible for the case of a single field formulation.

4. *Adaptive solution of time-dependent problems.* Another natural extension of our work would be to the solution of time-dependent problems where the solution u lies in $V \times [0, T]$. Normally, such problems are solved by carrying out a finite-element discretization of V that result in a system of ODEs in time; this system can be solved using standard time marching methods such as the central-difference method, the trapezoidal rule or the Newmark method [10]. Hence, provided the time stepping scheme is unconditionally stable or the time-step is kept small enough to guarantee stability over all resolutions, spatial adaptivity at each time step can be easily performed using the methods proposed in this thesis. However, in addition to spatial

adaptivity, one also requires time adaptivity in problems such as shock propagation. This is currently an open problem and it is not known at present whether adaptivity in both the spatial and temporal domains can be performed in an efficient, accurate and mathematically rigorous manner.

5. *Extensions to nonlinear problems.* Yet another possible extension of our work would be to the adaptive solution of non-linear problems, particularly those involving geometric non-linearities such as the study of buckling and bifurcation phenomena. In such problems, one would ideally like to take large load steps when the deformations are still in the linear regime and reduce the load increments as well as add details close to the bifurcation points. An obvious manner of coupling the two forms of adaptivity would be to estimate the two-level errors for each load increment as done for the linear problem (this can be again done in a scale-decoupled manner). If a large fraction of details are retained over multiple levels, it would indicate that the system is in turn undergoing inelastic deformations and hence for the next load step, the load increment can be correspondingly reduced.

"So long, and thanks for all the fish."
– Dolphins in Douglas Adams' The Hitchhiker's Guide to the Galaxy

Bibliography

[1] M. Ainsworth and J.T. Oden. *A Posteriori Error Estimation in Finite Element Analysis*. Wiley-Interscience, 2000.

[2] B. Aksoylu and M. Holst. An odyssey into local refinement and multilevel preconditioning II - Stabilizing hierarchical basis methods. *SIAM Journal on Numerical Analysis*, 2002 (Submitted).

[3] B. Alpert, G. Beylkin, R. Coifman, and V. Rokhlin. Wavelet-like bases for the fast solutions of second-kind integral equations. *SIAM Journal on Scientific Computing*, 14(1):159–184, 1993.

[4] K. Amaratunga and J.E. Castrillón-Candás. Surface wavelets: A multiresolution tool for 3D computational modelling. *International Journal for Numerical Methods in Engineering*, 52(3):239–271, 2001.

[5] K. Amaratunga and J.R. Williams. Wavelet-galerkin solution of boundary value problems. *Archives of Computational Methods in Engineering*, 4(3):243–285, 1997.

[6] K. Amaratunga, J.R. Williams, S. Qian, and J. Weiss. Wavelet-galerkin solutions for one dimensional partial differential equations. *International Journal for Numerical Methods in Engineering*, 37:2703–2716, 1994.

[7] R.E. Bank. *PLTMG: A Software for Solving Elliptic Partial Differential Equations. Users' Guide 9.0*. Department of Mathematics, University of California at San Diego, 2004.

[8] R.E. Bank, T.F. Dupont, and H. Yserentant. The hierarchical basis multigrid method. *Numerische Mathematik*, 52(4):427–458, 1988.

[9] R.E. Bank and R.K. Smith. A posteriori error estimates based on hierarchical bases. *SIAM Journal on Numerical Analysis*, 30(4):921–935, 1993.

[10] K.J. Bathe. *Finite Element Procedures*. Prentice Hall, Upper Saddle River, NJ, 1996.

[11] R. Beam and R. Warming. Discrete multiresolution using Hermite interpolation: Biorthogonal multiwavelets. *SIAM Journal on Scientific Computing*, 22(4):1269–1317, 2000.

[12] R. Becker and R. Rannacher. A feed-back approach to error control in finite element analysis: Basis analysis and examples. *East-West Journal on Numerical Mathematics*, 4(4):237–264, 1996.

[13] G. Beylkin, R. Coifman, and V. Rokhlin. The wavelet transform and numerical algorithms. *Communications in Pure and Applied Mathematics*, 44:141–183, 1991.

[14] F.K. Bogner, R.L. Fox, and L.A. Schmit. The generation of interelement-compatible displacement stifness and mass matrices by the use of interpolation formulae. In J.S. Przemienicki, R.M. Bader, W.F. Bozich, J.R. Johnson, and W.J. Mykytow, editors, *Proceedings of the First Conference on Matrix Methods in Structural Mechanics*, volume AFFDITR-66-80, pages 397–443, Air Force Flight Dynamics Labortory, Wright Patterson Air Force Base, OH, October 1966.

[15] S.C. Brenner and L.R. Scott. *The Mathematical Theory of Finite Element Methods*. Springer, 1994.

[16] J. Carnicer, W. Dahmen, and J. Peña. Local decompositions of refinable spaces. *Applied computational and harmonic analysis*, 3:125–153, 1996.

[17] J.E. Castrillón-Candás and K. Amaratunga. Spatially adapted multiwavelets and sparse representation of integral operators on general geometries. *SIAM Journal on Scientific Computing*, 24(5):1530–1566, 2003.

[18] A. Cohen, W. Dahmen, and R. DeVore. Adaptive wavelet methods for elliptic equations: Convergence rates. *Mathematics of Computation*, 70(233):27–75, 2001.

[19] A. Cohen, I. Daubechies, and J.C. Feauveau. Bi- orthogonal bases of compactly supported wavelets. *Communications on Pure Applied Mathematics*, 45:485–560, 1992.

[20] A. Cohen and R. Masson. Wavelet methods for second-order elliptic problems, preconditioning and adaptivity. *SIAM Journal on Scientific Computing*, 21(3):1006–1026, 1999.

[21] S. Dahlke and I. Weinreich. Wavelet-Galerkin-methods: An adapted biorthogonal wavelet basis. *Constructive Approximation*, 9(2):237–262, 1993.

[22] W. Dahmen. Wavelet and multiscale methods for operator equations. *Acta Numerica*, 6:55–228, 1997.

[23] I. Daubechies. Orthonormal bases of compactly supported wavelets. *Communications on Pure Applied Mathematics*, 41:906–996, 1988.

[24] L. Debnath and P. Mikusinski. *An Introduction to Hilbert Spaces with Applications*. Academic Press, Second edition, 1999.

[25] S. D'Heedene, K. Amaratunga, and J.E. Castrillón-Candás. Generalized hierarchical bases: A wavelet-Ritz-Galerkin framework for Lagrangian FEM. *Engineering Computations*, 22:15–37, 2005.

[26] C. Dym and I. Shames. *Energy and Finite Element Methods in Structural Mechanics*. Hemisphere Publishing Corporation, 1985.

[27] K. Eriksson, D. Estep, P. Hansbo, and C. Johnsson. Introduction to adaptive methods for differential equations. *Acta Numerica*, pages 105–158, 1995.

[28] D. Estep, M. Holst, and M. Larson. Generalized Green's functions and the effective domain of influence. *SIAM Journal on Scientific Computing*, To appear, 2004.

[29] I. Fried. The l_2 and l_∞ condition numbers of the finite element stiffness and mass matrices, and the pointwise convergence of the method. In J. R. Whiteman, editor, *The Mathematics of Finite Elements and Applications*, pages 163–174. Academic Press, London, U.K., 1972.

[30] J.S. Geronimo, D.P. Hardin, and P.R. Massopust. Fractal functions and wavelet expansions based on several scaling functions. *Journal of Approximation Theory*, 78(3):373–401, 1994.

[31] G.H. Golub and C.F. Van Loan. *Matrix Computations*. Johns Hopkins University Press, third edition, 1996.

[32] T. Grätsch and K.J. Bathe. Influence functions and goal-oriented error estimation for finite element analysis of shell structures. *International Journal for Numerical Methods in Engineering*, Submitted, 2004.

[33] T. Grätsch and K.J. Bathe. A posteriori error estimation techniques in practical finite element analysis. *Computers and Structures*, 83(4–5):235–265, 2005.

[34] A Latto, H.L. Resnikoff, and E. Tenenbaum. The evaluation of connection coefficients of compactly-supported wavelets. In *Proceedings of the Princeton Conference on Wavelets and Turbulence*, 1991.

[35] M. Lounsbery, T. DeRose, and J. Warren. Multiresolution analysis for surfaces of arbitrary topological type. *ACM Transactions on Graphics*, 16(1):34–73, 1997.

[36] S.G. Mallat. A theory for multiresolution signal decomposition: The wavelet representation. *IEEE Transactions on Pattern Analysis Machine Intelligence*, 11(7):674–693, 1989.

[37] R.H. Melosh. Basis for derivation of matrices by direct stiffness method. *AIAA Journal*, 1(7):1631–1637, 1963.

[38] S. Prudhomme and J.T. Oden. On goal-oriented error estimation for elliptic problems: Application to the control of pointwise errors. *Computer Methods in Applied Mechanics and Engineering*, 176(1-4):313–331, 1999.

[39] M.C. Rivara. Mesh refinement processes based on the generalized bisection of simplices. *SIAM Journal on Numerical Analysis*, 21:603–613, 1984.

[40] W.S. Slaughter. *The Linearized Theory of Elasticity*. Birkhäuser, Boston, 2002.

[41] G. Strang and G. Fix. *An analysis of the finite element method*. Prentice-Hall, 1973.

[42] G. Strang and T. Nguyen. *Wavelets and Filter Banks*. Wellesley-Cambridge Press, Wellesley, MA, Second edition, 1997.

[43] V. Strela and G. Strang. Finite element multiwavelets. In S.P. Singh, editor, *Approximation Theory, Wavelets and Applications*, pages 485–496. Kluwer Academic Publishers, 1995.

[44] R. Sudarshan and S.E. Lee. A parallel hierarchical solver for the Poisson's equation. Technical report, Massachusetts Institute of Technology, 2003.

[45] W. Sweldens. The Lifting Scheme: A construction of second generation wavelets. *SIAM Journal on Mathematical Analysis*, 29(2):511–546, 1998.

[46] B. Szabo and I. Babuska. *Finite Element Analysis*. Interscience, 1991.

[47] S. Timoshenko and S. Woinowsky-Krieger. *Theory of plates and shells*. McGraw-Hill, New York, 1959.

[48] P.S. Vassilevski and J. Wang. Stabilizing the hierarchical basis by approximate wavelets, I: Theory. *Numerical Linear Algebra with Applications*, 4(2):103–126, 1997.

[49] P.S. Vassilevski and J. Wang. Stabilizing the hierarchical basis by approximate wavelets II: Implementation and numerical results. *SIAM Journal on Scientific Computing*, 20(2):490–514, 1998.

[50] J. R. Williams and K. Amaratunga. A multiscale wavelet solver with $\mathcal{O}(n)$ complexity. *Journal of computational physics*, 122:30–38, 1995.

[51] H. Yserentant. On the multilevel splitting of finite element spaces. *Numerische Mathematik*, 49:379–412, 1986.

[52] H. Yserentant. Hierarchical bases. In R. E. O'Malley, editor, *Proceedings ICIAM 91*, pages 256–276. SIAM, Philadelphia, 1992.

[53] O.C. Zienkiewicz, D.W. Kelly, J. Gago, and I. Babuška. Hierarchical finite element approaches, error estimates and adaptive refinement. In J.R.Whitman, editor, *The Mathematics of Finite Elements and Applications - IV*. Academic Press, London, 1982.

[54] O.C. Zienkiewicz and J.Z. Zhu. A simple error estimator and adaptive procedure for practical engineering analysis. *International Journal for Numerical Methods in Engineering*, 24:337–357, 1987.